Doctoral Dissertation

Immunostimulatory properties of CpG oligodeoxynucleotides forming monomeric guanine-quadruplex structure

（単量体グアニン四重鎖構造を形成する

CpG オリゴデオキシヌクレオチドの免疫活性化特性）

TU Thi Tram Anh

Graduate School of Life Science, Hokkaido University
Division of Life Science

2021 03

Content

Chapter 1 Background

1.1. Innate and adaptive immunity

Mammalian bodies are protected against infectious pathogens consisting of bacteria, viruses, fungi, and parasites by innate and adaptive immune systems. The skin, mucosal membrane, and their secretions provide physical and chemical barriers that restrain pathogens from gaining entry to external surfaces of the body. When pathogens break the barriers and access to the soft tissues, they are hunted and destroyed by the immune system.

The innate immune system is the first line of defense, that is fast, and effective in stopping most infections at an early stage. Innate immunity includes four main elements: pathogen receptors that bind noncovalently to the surfaces of pathogens; proteins such as so-called "complement" system that bond covalently to pathogen surfaces, forming ligands for receptors on phagocytes; phagocytic cells that engulf and kill pathogens (neutrophil, eosinophil, basophil, macrophages); and cytotoxic cells that kill virus-infected cells (NK cells). The quick response of the innate immunity can be achieved by mean of a nonspecific protection mechanism through pattern recognition receptors (PRRs), such as Toll-like receptors (TLRs), nucleotide-binding, oligomerization domain (NOD)-like receptors (NLRs), and C-type lectin receptors (CLRs), or by complement system (**Fig. 1.1**).[1]

When pathogens outrun of innate immunity, the adaptive immune system is brought into play to stop the infection. In spite of its slow start, adaptive immunity provides a more powerful response owing to improved specificity in pathogen recognition. The activation of PRRs by their ligands in the innate immune response controls and shapes the subsequent adaptive immune response. An adaptive immune responses involves the T lymphocytes and B lymphocytes, which express receptors of a single and unique pathogen, so it only focuses on termination of infection caused by that pathogen. Effective lymphocytes, such as B cells, αβ T helper and cytotoxic T cells, natural killer T (NKT), and γδ T cells recognize peptides or epitopes presented by classical and

nonclassical major histocompatibility complex (MHC)-I and MHC-II molecules. Amplification of cytokines and antigen-specific immune responses, which can eliminate or inactivate the pathogen, were enabled by the interface activation through interaction of many co-stimulatory molecules, such as clusters of differentiation 40 (CD40)-CD40 ligand (L), CD28-CD80/86, and inducible T cell co-stimulator (ICOS)-ICOSL complexes. An adaptive immune response also provides long-lasting protective immunity against the pathogen that stimulated the response through memory cells (**Fig. 1.1**).[1]

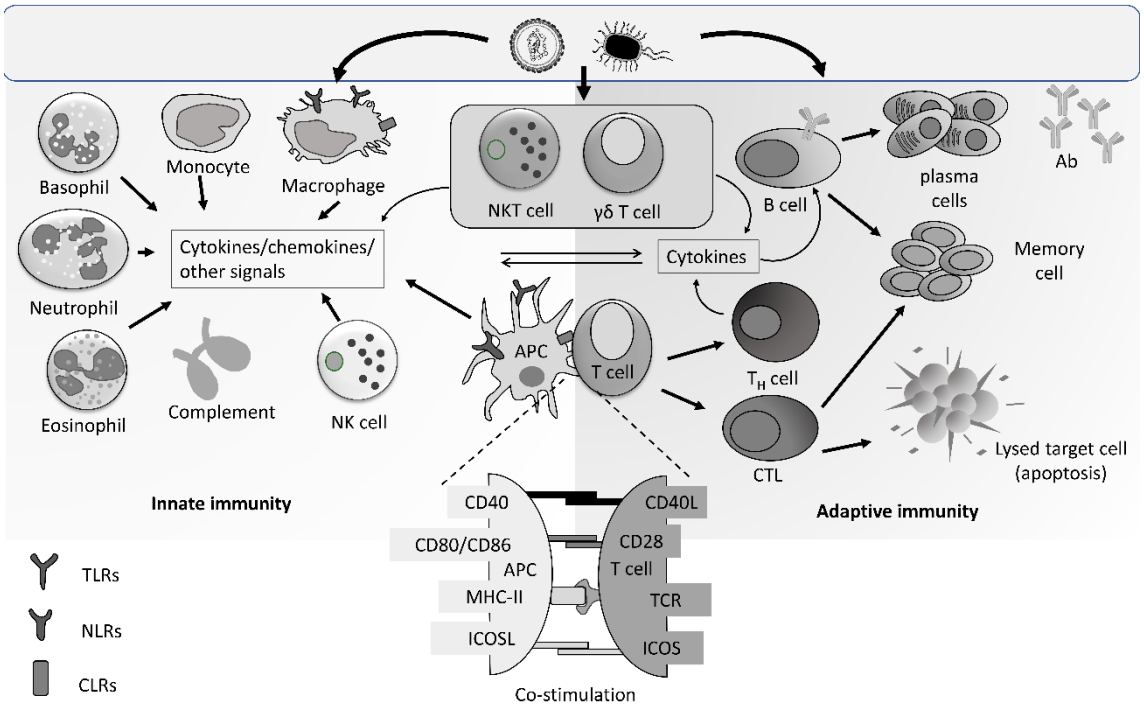

Figure 1.1 Innate and Adaptive Immune Systems. The innate immune system establishes a front line of defense, which responds nonspecifically to invading pathogens. This response is involved to various cells (granulocytes, monocytes, macrophages, dendritic cells, neutrophils, basophils, and natural killer cells, and complement system) and recognition of PAMPs or DAMPs by PRRs. The innate immune response shapes adaptive immunity, leading to the production of antigen-specific T and B lymphocytes. Abbreviations: APCs, antigen-presenting cells; CD, cluster of differentiation; CLRs, C-type lectin receptors; CTL, cytotoxic lymphocytes; DAMPs, damage-associated molecular patterns; ICOS, inducible T cell costimulatory; MHC, major histocompatibility complex; NKT, natural killer T cells; NLRs, nucleotide-binding,

oligomerization domain (NOD)-like receptors; PAMPs, pathogen-associated molecular patterns; PRRs, pathogen recognition receptors; TCR, T cell receptor; TLRs, Toll-like receptors.[1]

1.2. CpG ODNs

The quick response of the innate immunity can be achieved by mean of innate immune receptors, which recognize molecules with conserved motifs associated with pathogen infection, so-called pathogen-associated molecular patterns (PAMPs). Bacterial and viral DNA are PAMPs because they contain abundant cytosine-phosphate-guanine (CpG) dinucleotides, which are present at very low frequencies or methylated in vertebrate DNA.[2] These unmethylated CpG motifs are detected by the innate immune system using Toll-like receptor 9 (TLR9), a member of Toll-like receptors (TLRs).

Synthetic oligodeoxynucleotides containing unmethylated CpG motifs (CpG ODNs) trigger an immune response similarly to bacterial DNA.[3] Therefore, in the absence of invading pathogens, intentional stimulation of TLR9 by synthetic CpG ODNs provides a useful strategy in the development of vaccine adjuvants[3] or in the treatment of some diseases such as cancer and allergies.[4]

1.2.1. TLR9 mediated signaling cascade

PPRs are important components of the innate immune system and are crucial for the recognition of PAMP. Toll-like receptor (TLR) (**Fig. 1.2**) is a typical family of transmembrane-signaling PRRs. There are ten and twelve members of TLRs that have been identified in human and mouse, respectively. In human, TLRs include two subgroups with different localization and ligand recognition. One subset including TLR1, 2, 4, 5, 6, and 10 occupies the plasma membrane and recognizes microbial carbohydrate, lipid, and protein. Another TLR subset including TLR3, 7, 8, and 9 is localized on membranes of endosomes and recognizes derived nucleic acids of pathogens.[5,6]

In humans, TLR9 is expressed in B cells and plasmacytoid dendritic cells (pDCs); in mice, TLR9 is expressed in macrophages and myeloid dendritic cells in addition to B cells and pDCs.[4] Prior to stimulation, TLR9 is localized in the endoplasmic reticulum.[7] Upon treatment with CpG ODN, TLR9 is delivered by an endoplasmic reticulum membrane protein, UNC93B1 to endosomes, and lysosome where it binds directly to CpG ODN.[8] [9] Therefore, internalization of CpG ODNs is necessary for TLR9 activation.

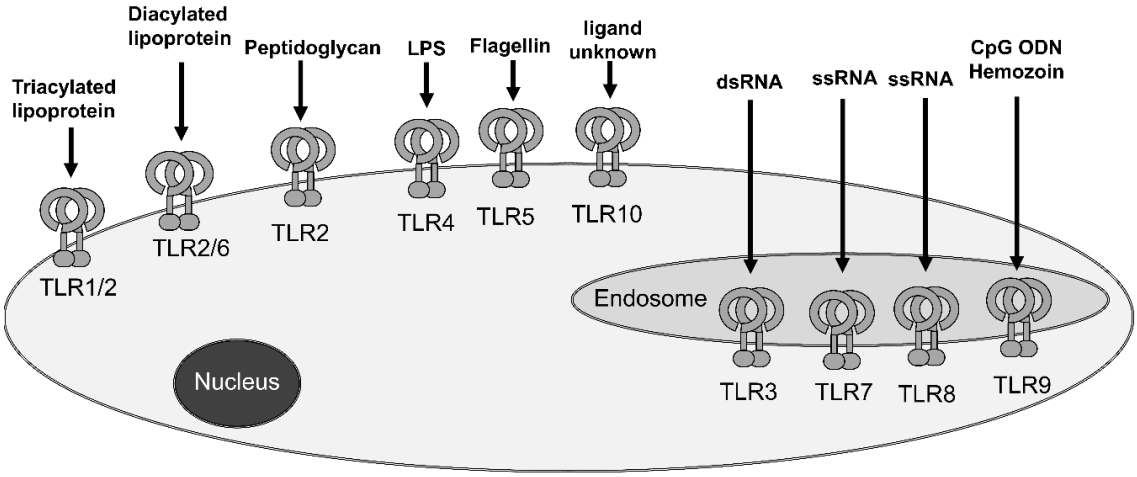

Figure 1.2 Human Toll-like receptors and their pathogen-associated molecular patterns and/or synthetic compounds. TLRs are classified into two groups based on their cellular localization and the type of their ligands. One group consists of TLR 1, 2, and 4–6, which localize to the cell surface (cell surface TLRs) and respond to microbial membrane materials such as lipids, lipoproteins, and proteins. Another one consists of TLR 3 and 7–9, which reside at endosomal compartments (intracellular TLRs) and recognize bacteria- and virus-derived nucleic acids.[10]

CpG oligodeoxynucleotide (ODN) recognition occurs in the endosome[4]. Internalization of CpG ODN into the endo/lysosome of the cell occurs via endocytosis. Following the binding of TLR9 and a CpG ODN, TLR9 dimerized and undergo a conformational change in the TLR9 Toll-interleukin1-resistance (TIR) cytoplasmic domain.[11] This recruits the myeloid differentiation primary response 88 (MyD88) adaptor protein, which triggers a distinct signaling pathway.

TLR9-MyD88 association in B cells recruits interleukin-1R-associated kinases (IRAK1) and IRAK4, which make a complex with tumor necrosis factor receptor-associated factor 6 (TRAF6) to activate kinase inhibitor (IKK) complex. Activation of IKK results in the degradation of inhibitor of kappa B (IkB), which retains the inactivated form of NF-kBp65 (p65)/ NF-kBp50 (p50) heterodimers by sequestrating them in the cytoplasm. Translocation of p50 and p65 into the nucleus enables transcription of proinflammatory cytokine genes such as interleukin (IL)-6, IL-12.[12] Meanwhile, in plasmacytoid dendritic cells, spatiotemporal regulation of MyD88–IRF-7 signaling results in type-I interferon induction.[13] Long-term encounter of CpG ODN and TLR9 in early endosome recruits MyD88, then initiates activation of the IRAK1–TRAF6 complex. In turn, this triggers interferon (IFN) regulatory factor-7 (IRF7) pathways, resulting in production of type I IFN.[9] A summary of the signaling pathway following TLR9 activation is presented in **Figure 1.3**.

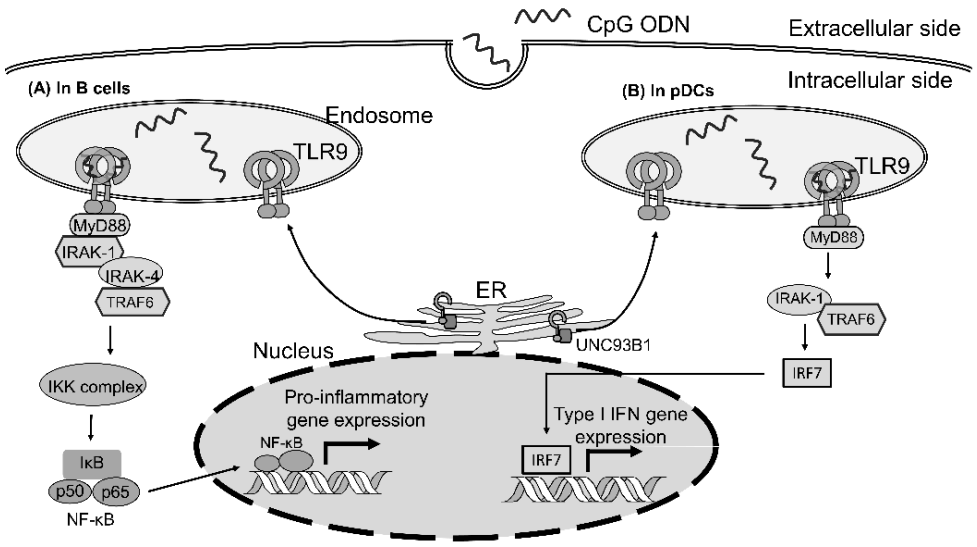

Figure 1.3 Signaling pathway following TLR-9 activation. (A) In B cells, CpG ODNs internalize the cells and quickly are transferred to lysosomal vesicles. Encounter of CpG ODNs with TLR9 activates NF-κB pathway and secretion of inflammatory cytokines. (B) In pDCs, after internalizing in the cells, CpG ODNs, which can retain for long time in early endosomes, activate TLR9 and recruit of the adapter protein MyD88 and initiates IRF7 downstream signaling, resulting in high type I IFN levels. IRAK, interleukin-1R-associated kinase; IRF7, IFN regulatory

factor 7; MyD88, myeloid differentiation primary response 88 adaptor protein; NF-κB, nuclear factor kappa B; pDCs, plasmacytoid dendritic cells; TLR-9, toll-like receptor 9; TRAF, tumor necrosis factor receptor-associated factor.[9,12,14]

1.2.2. Structural aspect of CpG ODN recognition by TLR9

TLR9 is consist of an extracellular ligand-binding domain (ECD), a transmembrane domain, and an intracellular signaling (TIR) domain. (**Fig. 1.4 A**) The ligand binding domain is comprised of N-terminal (LRRNT) and C-terminal (LRRCT) domains at the ends of the protein and 26 leucine-rich repeats (LRRs) between LRRNT and LRRCT. Each LRR forms a loop in which conserved hydrophobic residues point inward. LRRs stack adjacent to each other and form a large horseshoe-like structure. The concave surface is composed of a parallel β-sheet, while the convex surface is formed from α-helices and unstructured loops. These two surfaces are associated by ascending and descending lateral faces.[15] TLR9 also contain an insertion loop ("Z-loop") between LRR14 and 15 (**Fig. 1.4 B**).[16]

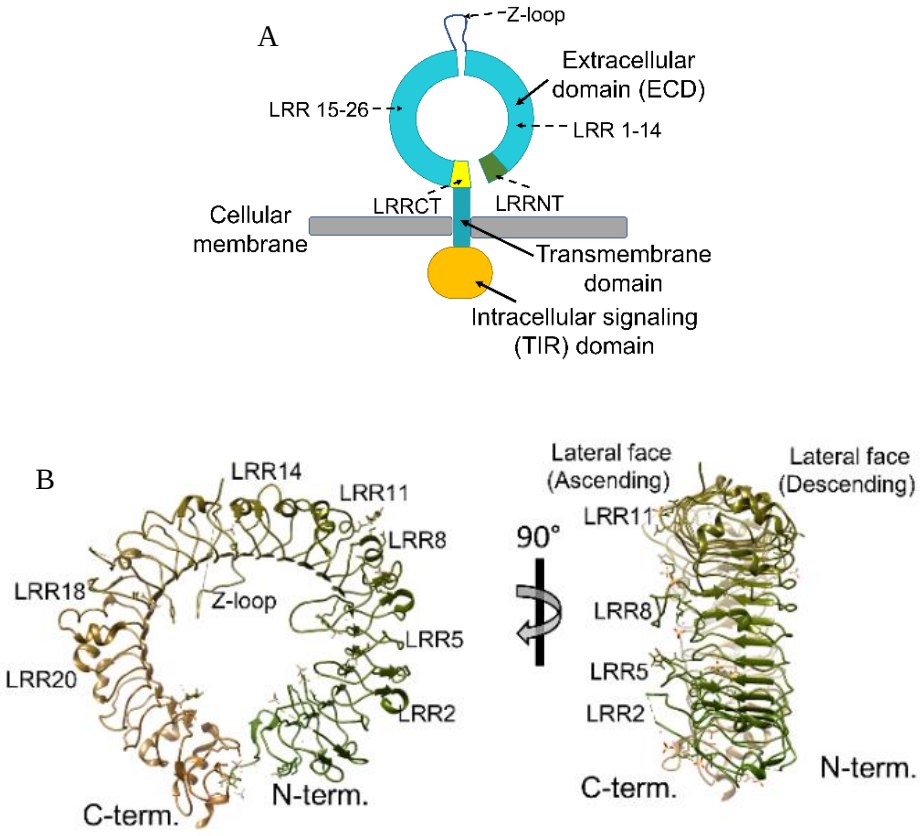

Figure 1.4 Structures of TLR9. (A) Schematic illustration of TLR9 structure. (B) Monomer structure of unliganded mouse TLR9 extracellular ligand-binding domain (PDB ID: 3WBF).[17]

The crystal structures of the LRR domain of TLR9 in the unliganded, and agonistic-DNA-bound forms were determined by Ohto et al..[17] The unliganded TLR9 is a monomer in the crystal form[17] (**Fig. 1.4B**), whereas the agonistic-DNA1668_12mer-bound forms of TLR9 are dimeric (**Fig. 1.5**). In the agonistic-DNA-bound form, the C-termini of the two TLR9 protomers are located in the center, so they form an m-shaped 2:2 complex (**Fig. 1.5**). Hereafter, the first and the second TLR9 within the dimer and their residues are indicated without and with asterisks (TLR9 and TLR9*), respectively. The DNA1668_12mer binds to two equivalent positions in the dimer, and each DNA strand is recognized by both TLR9 and TLR9* in a bent form (**Fig. 1.5**). The DNA molecule twists around the N-terminal fragment of TLR9 from the ascending lateral face to the concave face. DNA1668_12mer interacts simultaneously with a region spanning from

LRRNT to LRR10 in the N-terminal fragment of TLR9 (interface 1) and the loop regions from LRR20–22 in the C-terminal fragment of TLR9* (interface 2). The accessible surface area of TLR9 and TLR9* buried by DNA1668_12mer is approximately 1,136 Å^2 and 294 Å^2, respectively, indicating that the N-terminal binding site of TLR9 for DNA1668_12mer contribute relatively more greatly to binding.[17]

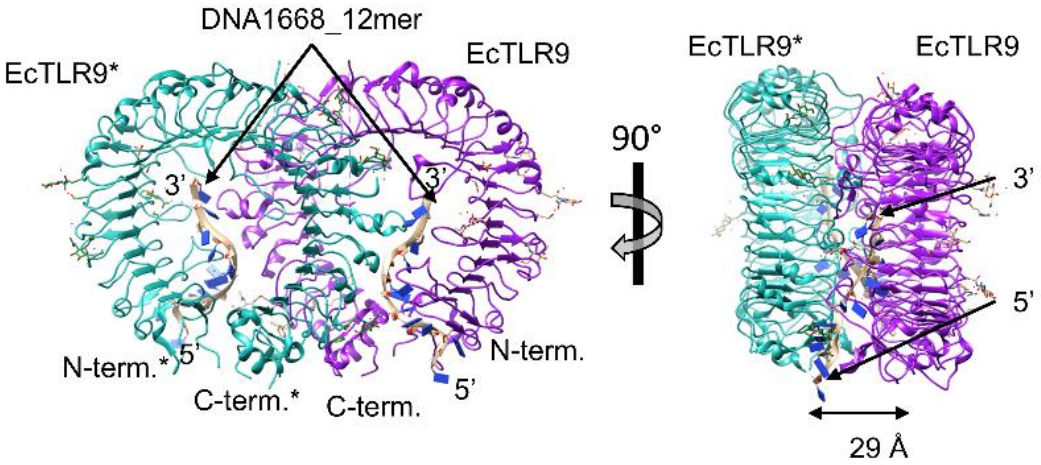

Figure 1.5 Dimer structure of the DNA1668_12mer-bound form of mTLR9. EcTLR9 and its dimerization partner EcTLR9* are shown in purple and cyan, respectively. The second TLR9 within the dimer and its residues are indicated with asterisks. The DNA1668_12mer molecules are shown in stick representation. (PDB ID: 3wpc).[17]

1.2.3. Immunostimulatory activity of CpG ODNs

In human, TLR9 is mainly expressed in B cells and plasmacytoid dendritic cells (pDCs). CpG DNA directly activates these cells, initiating both innate and adaptive immune responses (**Fig. 1.6**).[18]

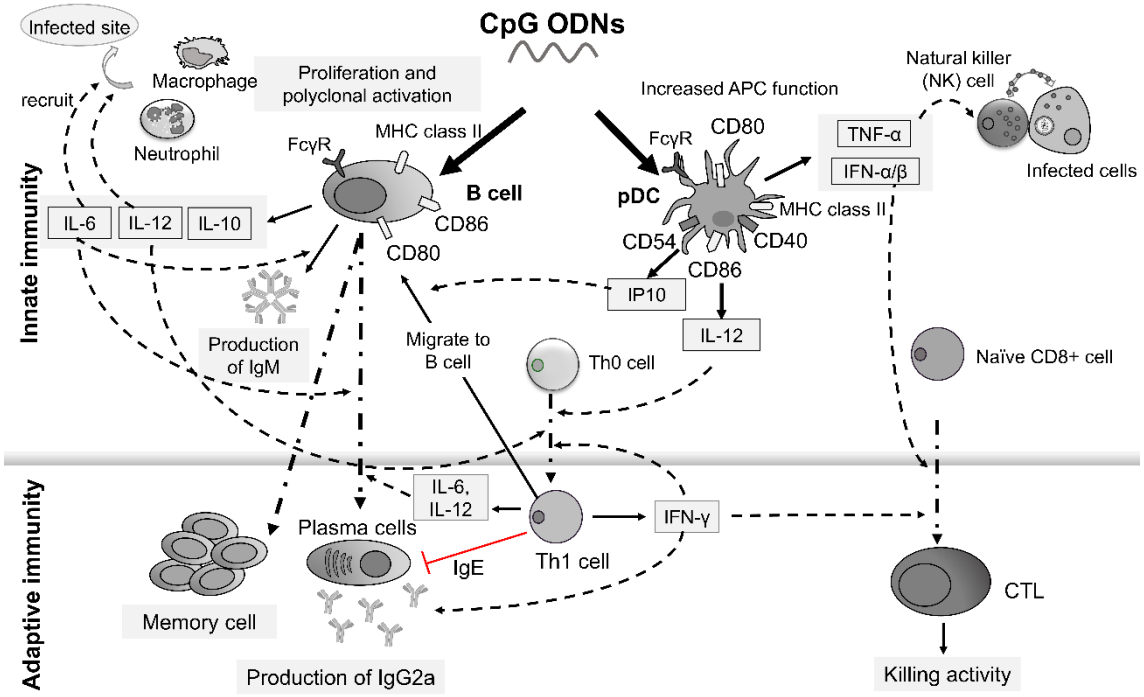

Figure 1.6 Immunostimulatory effect of cytosine-phosphate-guanosine (CpG) oligodeoxynucleotides (ODNs). Solid thick line: direct stimulation; Solid thin line: production; Dashed line: increase or upregulate; Thin dash-dotted line: proliferation or maturation; Thick dash-dotted line: differentiation; Red line: inhibition. Abbreviations: APC, antigen-presenting cell; CD, cluster of differentiation; CTL, cytotoxic lymphocytes; MHC, major histocompatibility complex; IL-6/10/12, Interleukin-6/10/12; IP-10, IFN-γ-inducible protein of 10 kDa IFN; Th1, T helper 1 cell; IgG, immunoglobulin G; TNF, tumor necrosis factor-alpha; FcγR, Fc receptor for IgG.[18]

TLR9 activation in B cells leads to secretion of IL-6, IL-10, and IL-12. CpG ODNs also promote B cells proliferation and differentiation into plasma cells and memory B cells. Inflammatory cytokines such as IL-6, and IL-12 secreted from B cells play important roles in innate immune response, as they increase recruitment of macrophages and neutrophils to the infected site to eliminate pathogens. CpG ODNs also upregulate expression of Fc receptor (FcR) and costimulatory molecules including MHC class II, CD40, CD80 and CD86 on B cells.[19] IL-6 and IL-12 secreted from B cells are also contribute to adaptive immune response. IL-6 increases

the multiplication and activation of B cells, which results in an enhanced IgM and IgG2a antibody production. IFN-γ secreted from Th1 cells inhibits a B cells switching to IgE producing type and prevent the production of IgE. Secreted IL-10 from CpG-activated CD5+ B cells inhibits IL-12 production from DCs, which thereby inhibits their Th1 priming function (**Fig. 1.6**).

CpG-stimulated pDCs are characterized by their upregulation of CD40, CD54, CD80, CD86 and MHC class II molecules.[19] TLR9 activation increases production of cytokines relating to type I IFN (IFN-α, IFN-β), and tumor necrosis factor-alpha (TNF-α)[18], which increase the function of natural killer cells. IFN-α secreted from pDCs promotes CD8+ cytotoxic T lymphocyte response. In addition, pDCs activated by CpG secrete IL-12 and promote the differentiation of T helper (Th) 0 into Th1. IFN-γ produced from Th1 cells mediates CD8+ T-cell cytotoxic function[20], induces the differentiation of helper T cells into type 1 helper T cells, and enhances immunoglobulin isotype switching to IgG2a.[21] Furthermore, CpG-stimulated pDCs produce IFN-γ-inducible protein of 10 kDa (IP10), which induce Th1 to migrate to B cells. Then, B cells that interact with Th1 differentiate into plasma cells, which have the ability to produce antibodies, playing a crucial role in adaptive immunity (**Fig. 1.6**).[18]

With the ability in activation of innate and adaptive immune responses, CpG ODNs are a promising vaccine adjuvant to prevent or treat infectious diseases, cancers, and allergies.

1.2.4. Strategies for enhancing the immunostimulatory effects of CpG ODNs

The therapeutic application of CpG ODNs is limited because they are rapidly cleared from the site of administration to the systemic circulation. The major factors leading this rapid clearance are the short in vivo half-life of ODN caused by rapid degradation by nucleases, and its rapid absorption into the systemic circulation. In these conditions, the local ODN level is generally lower than threshold levels to stimulate immune cells.[22] Moreover, TLR9 is localized in small compartments called endosome inside of cells, so internalization of CpG ODNs is important for TLR9 activating. The negative charge of ODN backbone is repelled by negative

charge of cell membrane, so it is difficult to obtain a high intracellular uptake level of CpG ODNs.[23] Therefore, there are several mechanisms to increase the amount of CpG ODNs delivered to the immune cells, which are summarized in **Table 1.1.** In some studies, these mechanisms may act synergistically to further increase the CpG-mediated effects.

Table 1.1 Possible strategies for enhancing the immunostimulatory activity of CpG ODNs[22]

• Increasing the half-life of CpG ODNs
• Localization of CpG ODNs in tissue
• Local cell recruitment and sustained stimulation of cells
• Increasing APC uptake of CpG ODNs
• Delivery of antigen and CpG ODNs to the same APC

1.2.4.1. Increasing the half-life of CpG ODN

The half-life of phosphodiester ODN is only approximately 5 min, so the transient immunostimulatory effects of ODNs in vivo have been a significant disadvantage. Increasing the half-life of ODNs would be a logical approach to gain its sustainable activity. Substitution of the oxygen of the phosphate group with sulfur creates a phosphorothioate ODN, which has higher resistance to endogenous nucleases, with a half-life of 30–60 min in plasma and about 48 h in tissue.[22] However, phosphorothioate CpG ODNs have been reported to prolong the time of coagulation due to the inhibition of the tenase complex, cause acute toxicity due to complement activation, and distribute of cell signaling due to nonspecific binding to proteins such as transcription factors. In addition, phosphorothioate modification to ODNs causes thrombocytopenia, anemia, and neutropenia. This raises concern about safety of phosphorothioate ODNs.

1.2.4.2. Localization of ODN in tissues

Another strategy is to increase retaining time of CpG ODN in tissue by using a delivery vehicle to create a ‘‘depot’’ where the ODN is maintained locally at the site of administration, safe from DNase degradation but slowly released over a period of time. This is the underlined mechanism for increase activities of CpG ODNs by encapsulating them in liposomes. Finding a suitable delivery system, which can balance between slow release and simultaneously reaching threshold concentrations of CpG ODN, is a challenge of this approach.

1.2.4.3. Local cellular recruitment and activation

Recruitment immune cells such as dendritic cells to a local area where they can encounter with CpG ODN would be an alternative approach to enhance activity of CpG ODNs. Some materials such as emulsigen mixed with CpG ODN can create a depot associated with an ability in recruitment cells locally. Formulation of CpG in emulsigen enhances cellular recruitment and probably cellular activation at the site of injection, thereby enhances efficacy of CpG ODNs. The addition of a chemoattractant molecule like a chemokine may involve to this cellular recruitment.

1.2.4.4. Increasing cellular uptake and binding

In addition, increasing cellular uptake and binding to cell surface protein is one of logical strategies increase the activity. The uptake and immunomodulatory activity of phosphodiester CpG ODNs can be strongly enhanced by poly guanosine runs added at the 3' end of the ODN probably due to their binding with scavenger receptors on plasma membranes.[24] Furthermore, nanomaterial based delivery system also enable CpG ODN to target to antigen-presenting cell such as dendritic cells. CpG ODN can be encapsulated within nanomaterials or bind to the surface of nanomaterials. Biodegradable poly(lactic-co-glycolic acid) (PLGA), a US Food and Drug Administration approved polymer, is one of the extensively studied materials for CpG ODN formulation in clinical application.[23]

1.2.4.5. Delivery of antigen and CpG ODN to the same APC

When antigen and CpG are delivered as a mixture, there is high possibility that only one, not both agents might be internalized into the same APC, leading to either an CpG-activated APC but not present the antigen to T-cells or an APC present the antigen but without CpG-activated. Therefore, this leads to low activation of T-cell response. Delivery of antigen and CpG ODN to the same APC has been achieved by including the antigen and CpG ODNs into or onto a particle or by directly associating the antigen and CpG ODNs to each other. Co-delivery of an antigen with CpG has been shown an enhanced immune response in vitro and in vivo, with the antigen presentation to T-cells, Th0 activation and differentiation into Th1 and cytotoxic T lymphocytes CTL, and the cytotoxicity of effector T-cells higher than when delivery as a mixture.[25]

1.2.5. Class of CpG ODNs

Because phosphodiester backbone of CpG ODNs is susceptible to DNase degradation, phosphorothioate-modification, where the oxygen in the phosphate group is replaced by sulfur, has been used to increase the DNase resistance of CpG ODNs. At least, four classes of chemically modified synthetic CpG ODNs have been described, based on their distinct structural and biological properties (**Table 1.2**).[18]

Class A CpG ODN (CpG-A), also referred to as type D, has a mixed of phosphodiester and phosphorothioate backbone. This class contains a phosphodiester central CpG-containing palindromic motif and phosphorothioate-modified poly-G sequence at the 3’ and 5’ ends. This class triggers pDCs maturation and induces high IFN-α production but have no effect on B cells.[19]

Class B CpG ODN (CpG-B), also referred to as type K, contains entirely phosphorothioate backbone and has multiple CpG motifs. This class strongly triggers B cells to proliferate and produce IgM and IL-6. However, it have low ability in stimulating pDCs to secrete IFN-α.[18,19] The difference in activities of class A and class B CpG ODNs is resulted from the difference in retention times of CpG-ODN/TLR9 complexes in the endosomes of pDCs. While class B CpG

ODN is rapidly transported through early endosomes into late endosomes, class A CpG ODN is retained for longer in the early endosome, where it triggers MyD88-IRF-7 signaling cascade that initiates IFN-α production.[19]

Class C contains a full phosphorothioate backbone with one or two CpG motif(s) imbedded in a central palindrome. This class is also characterized by TCG dimer at 5' end. Immunostimulatory activity of class C is intermediate between class A and class B CpG ODN. This class triggers the proliferation of B cells as well as induces strong IFN-α production in pDCs.[18]

Class P CpG ODN has a complete phosphorothioate backbone with two palindromic sequences, which facilitate higher ordered structure formation.[26] It displays a capacity for activating both B cells and pDCs and induces stronger IFN-α production than does class C ODN.[18]

Table 1.2 Characteristics of the four major classes of cytosine-phosphate-guanosine (CpG) oligodeoxynucleotides (ODNs)[a]

Class	Backbone	Example	Immunostimulatory properties
A (Type D)	PO & PS	ODN2216 : 5'-ggGGGACGACGTCGGGGGG-3' 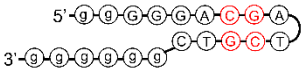	Mainly stimulate: pDCs Innate immune response: IFN-α, TNF-α, IL-12 secretion Adaptive immune response: IL-12, IP10
B (Type K)	PS	ODN2006: 5'-tcgtcgttttgtcgttttgtcgtt-3' 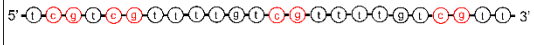	Mainly stimulate: B cells Innate immune response: IL-6, IL-10, IL-12 secretion Adaptive immune response: IL-6, IL-12
C	PS	ODN M362: 5'-tcgtcgtcgttcgaacgacgttgat-3' 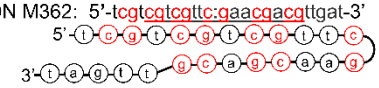	Intermediate between class A and class B
P	PS	ODN 21798: 5'-tcgtcgacgatcggcgcgcgccg-3' 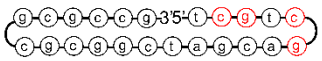	Activate both B cells and pDCs and induces stronger IFN-α production than does class C ODN

[a] Capital letters, phosphodiester bases; lower case letters, phosphorothioate bases; underline, palindromic sequence. Abbreviations: PO, phosphodiester; PS, phosphorothioate; IFNα, interferon-alpha; IL, interleukin; IP10, interferon-gamma-inducible protein of 10 kDa; pDC, plasmacytoid dendritic cell; TNFα, tumor necrosis factor-alpha.

1.3. Evaluation of CpG ODNs as vaccine adjuvants

Vaccines have a critical role in increasing public health and saving millions of lives by preventing infectious diseases. Vaccines compose of live-attenuated form of pathogens, or only purified or recombinant pathogen proteins. Vaccine adjuvant is a component of vaccine which serves to improve poorly immunogenic vaccines. Adjuvant triggers the innate immune response, which initiates an adaptive immune response against the antigens in the vaccine. The role of adjuvants is especially important in pandemic, as adding adjuvants minimizes the amount of antigen required to induce protective immunity.[27] Aluminum salts (alum) are the most widely used adjuvant, but alum have shortcomings including local reactions such as swelling and pain at the injection site due to inflammation. In addition, alum generally produce a Th2-type but not Th1-type cellular response, which is required for immunity against infections with viruses and intracellular bacteria.[27] The next generation of vaccine adjuvants is based on pathogen-associated molecular patterns, which are unique molecules of bacteria, viruses, protozoa, and fungi triggering the innate immune response through stimulation of PRRs. Particularly, CpG ODNs, which activate Toll-like receptor (TLR) 9, a member of PRRs, have attracted significant interest in recent years.

1.3.1. Pre-clinical evaluation

Abundant preclinical studies examining the immunogenicity of CpG-adjuvanted vaccines have been published. Results show that CpG ODN enhance the humoral immune response induced by vaccines against pathogens including anthrax, leishmania, influenza virus, measles virus, lymphocytic choriomeningitis virus, orthopox viruses, hepatitis B surface Ag and tetanus toxoid.[28] CpG ODN also boots cellular (Th1 cells and CTL) immunity, for example in murine model of leishmania infection. Incorporation of CpG ODN into a vaccine consisting of a low dose of metacyclic promastigotes magnified the production of CD4+ IFN-γ-secreting cells and increased the number of IFN-γ-producing CD4+ and CD8+ T cells by two- to threefold.[28] In

addition, CpG ODNs accelerate the induction of vaccine-induced responses. For instance, development of protective response in mice given vaccination with CpG-adjuvant Anthrax Vaccine Adsorbed (AVA [Emergent Biosolutions, MI, USA] the licensed human anthrax vaccine) was faster than that in mice vaccinated with AVA alone. AVA associated with CpG ODN increased the serum IgG anti-anthrax protective Ag (AP) response, giving serum anti-PA titers that were tenfold higher and significantly more effective by day 10 ($p < 0.05$).[28] This accelerating induction of protective response is critical in cases of a quick pathogen-specific immunity is required after exposure to the pathogen.

1.3.2. Clinical evaluation

Human clinical trials have evaluated the utility of CpG ODN in combination with vaccines designed to prevent, hepatitis B (HBV), anthrax, and malaria (**Table 1.3**).

Table 1.3 Use of CpG ODN for vaccines targeting infectious disease[29,30]

Agent	CpG	Disease	Trial phage	Outcome
HBsAg-1018 (HEPLISAV-B™)	CpG 1018	Hepatitis B	Got license from FDA	Faster seroprotection Anti-HBs Ab titers 45-fold higher vs HBs alone 100% seroconversion after 6 weeks vs 63% in controls seroprotection faster and higher vs Engerix-B
Biothrax® + CpG	CpG 1555 CpG 1466	Anthrax	Phage II	8-fold ↑ Ab response. Peak Ab production induced 3-week Faster vs BioThrax alone
Malaria Ag + CpG MSP1/alhydrogel AMA1 + CpG	CpG 7909	Malaria	Phage II	Anti-MSP1 Ab titer ↑ 49-fold after second and 8-fold after third vaccination vs MSP1/alhydrogel alone Anti-AMA1 Ab titer ↑ 6-fold vs AMA1 alone

Abbreviation: Ab: Antibody; Ag: Antigen; MSP1: merozoite surface protein 1; AMA1: apical membrane antigen 1; FDA: The US Food and Drug Administration.

Hepatitis B (HBV) is a hepadnavirus that mainly attacks hepatocytes. The alum-adjuvanted HBV vaccine need to be injected three times over a period of 6 months to achieve protective Ab titers. However, 5–10% of immune-competent individuals still fail to achieve long-lasting seroprotection in spite of receiving a complete series of this vaccine. Furthermore, a large portion of immunosuppressed patients is unsuccessful to achieve protective Ab titers using alum-adjuvanted HBV vaccine. In an effort to accelerate the induction and duration of protective immunity, the utility of CpG 1018 (5'-tgactgtgaacgttcgagatga-3'), which is a class B class CpG ODN, in combination with vaccines HEPLISAV targeting the hepatitis B virus, was examined. The combination of CpG ODN in HEPLISAV showed an improved induction of humoral and cell-mediated immune responses against HBV. In Phase III clinical trials, HEPLISAV elicited higher seroprotective Ab titers with fewer immunizations than did currently licensed alum-adjuvanted vaccines.[29,30] The US Food and Drug Administration (FDA) gave license for CpG 1018-adjuvanted hepatitis B vaccine HEPLISAV-B® in 2017.

Anthrax is resulted from the toxin-producing gram-positive bacterium Bacillus Anthracis. Protection against anthrax is achieved thank to Abs targeting the 'protective antigen' (PA) component of the toxin. Anthrax Vaccine Adsorbed (AVA) is the licensed human vaccine for protection from Anthrax. Phase II clinical trials of a anthrax vaccine containing phosphorothioate CpG ODNs, including CpG ODN 1555 (5'-gctagacgttagcgt-3') and 1466 (5'-tcaacgttga-3'), is conducting. The result shows that CpG ODN-combining AVA improved immunogenicity and accelerated the generation of PA-specific Abs, with eight-fold higher Ab response and peak Ab production induced 3-week faster compared with AVA alone.[29,31]

Phase I and Phase IIa trials of CpG ODN-containing Malaria vaccines are undergoing. These vaccines are designed to provoke immune responses against the merozoite surface protein 1 (MSP1) and apical membrane antigen 1 (AMA1) of the parasite. Results show that volunteers mounted significantly stronger Ab responses to these malaria Ag when they are associated with

CpG 7909 (also known as ODN2006; 5'-tcgtcgttttgtcgttttgtcgtt-3'). Supplementing an AMA1 vaccine with CpG ODN improved the mean anti-AMA1 Ab titer by sixfold compared with AMA1 alone. At 236 days after vaccination, those given immunization with CpG ODN-adjuvanted AMA1 maintained serum Ab titers 4.6-fold higher than those vaccinated with only AMA1, indicating ability in creating a persistent Ab response of CpG ODN. In addition, the combination of CpG provided a 49-fold increase in anti-MSP1 anti-body responses after the second immunization and an 8-fold increase after the third immunization when compared with MSP1/Alhydrogel alone.[29]

1.4. CpG ODNs forming high order structures

As mentioned above, although phosphorothioate CpG ODNs have the longer half-life in vivo (30–60 minutes) than the half-life of natural phosphodiester DNA thank to their higher DNase stability, they have been reported to cause adverse effects. A recent preclinical study shows that mice administered a CpG-B ODN (ODN1826) suffer from major liver damage and spleen damage.[32] Furthermore, in the Phase III clinical trial, combination of a class-B CpG ODN (PF-3512676, also known as ODN2006, or CpG 7909) with standard chemotherapy was reported to cause a high possibility of developing harmful events. The results of these preclinical and clinical studies suggest that natural phosphodiester CpG ODNs are preferable in clinical application. Therefore, the new approaches including self-assembled CpG ODNs, CpG ODNs conjugated/complexed with proteins or peptides, and CpG ODNs complexed with nanomaterials to protect CpG ODNs from degradation by DNases and/or improve their intracellular uptake efficiency has attracted significant interest in recent years. Especially, self-assembled CpG ODNs, which form high-order-structured CpG ODN complexes in nano size utilizing the complementation between DNA bases, provides major advantage in terms of safety, as they can be constructed with phosphodiester CpG ODNs only, without using proteins/peptides and nanomaterials.[23] Several higher-order-structured CpG ODNs with fully PO backbone exhibiting immunostimulatory properties have been reported, consisting of Y-shaped, X-shaped, Dendrimer-

like, dumbbell-like, polypod-like, tetrahedral-like CpG ODNs. Summary of structures, and biophysical, and immunostimulatory properties of higher-order-structured CpG ODNs is presented in **Table 1.4**.

1.4.1. Y-shaped, and dendrimer-like ODNs

Y-shaped oligodeoxynucleotides (Y-ODNs) (**Fig. 1.7A**) consist of three ODNs with the halves of each ODN being in part complementary to a half of the other two ODNs. Cellular uptake efficiency of Y-DNA was about 1.8-fold greater than those of double stranded-ODN, but the resistance to DNase is not improved by Y-shape-like structure. Y-ODN including three CpG motifs (Y-ODN(CpG3)) induced higher amounts of amounts of tumour necrosis factor-a and interleukin-6 from RAW264.7 macrophage-like cells than those did single-stranded ODN (ssODN) or double-stranded ODN (dsODN).[33] In addition, conditioned medium of RAW264.7 cells treated with Y-ODN(CpG3) significantly inhibited the proliferation of tumor cells compared with the media of those treated with other ss-ODNs, and ds-ODNs.[33]

Dendrimer-like DNA (DL-DNA) (**Fig. 1.7B**) was prepared by ligating Y-DNA monomers. The amounts of TNF-α and IL-6 produced from RAW264.7 macrophage-like cells treated with DL-DNAs were greater than those secreted from the cells treated with mixture of Y-DNA with the same sequences as the corresponding DL-DNA. One of the possibilities leading to this high activity is that there is fewer active sites for nuclease attack on the bulky structure of branched DNA.[34]

Table 1.4 Characteristics of CpG ODNs forming high-ordered structure with fully phosphodiester backbone

Structure	Feature	Ref.
Y-shaped	• **Nuclease resistance** Do not increase compared to PO ds ODNs • **Cellular Uptake** 2.5-fold higher than PO ss ODNs • **Immunomodulatory activity** – Induces production of IL-6 – Stimulate pDCs to produce IL-12, TNF-α and express costimulatory molecules CD80 and CD86	35–37
Dendrimer-like	• **Cellular Uptake** Increase compared to PO Y-DNA • **Immunomodulatory activity** Stimulate macrophage cells produce IL-6, TNF-α	38
X-shaped	• **Cellular Uptake** 4-fold higher vs PO ssDNA • **Immunomodulatory activity** – Promoted the expression of CD80 and CD86 on BMDCs – Induce the secretion of IL-12p40 and TNF-α on BMDCs – BMDCs stimulated by X_L-DNA induced differentiation of naïve CD4+ T cell to Th1 cell – Induce production of serum IFN-γ and IL-12 in mice	39,40
Polypod-like	• **Cellular Uptake** About 5-fold higher than ssODN • **Immunomodulatory activity** – Promoted the production of TNF-α and IL-6 in RAW264.7 cell – Promoted the production of IFN-α in hPBMCs	41,42
Dumbbell-like	• **Immunomodulatory activity** • Induce production of IL-6, IL-12, IL-2, IFN-α (preferentially), IFN-γ in hPBMCs	9,43
Tetrahedral	• **Nuclease resistance** Increase compared to PO ds ODNs • **Cellular Uptake** 4-fold increase compared to PO ss ODNs • **Immunomodulatory activity** Stimulate macrophage cells produce IL-6, IL-12, TNF-α	44,45

Abbreviation: BMDCs, bone marrow-derived dendritic cells; ds, double-stranded; ss, single-stranded; PO, phosphodiester; pDC, plasmacytoid dendritic cell; hPBMCs, human peripheral blood monocyte cells; IFN-γ, interferon-gamma; IL, interleukin; TNF-α, tumor necrosis factor-alpha.

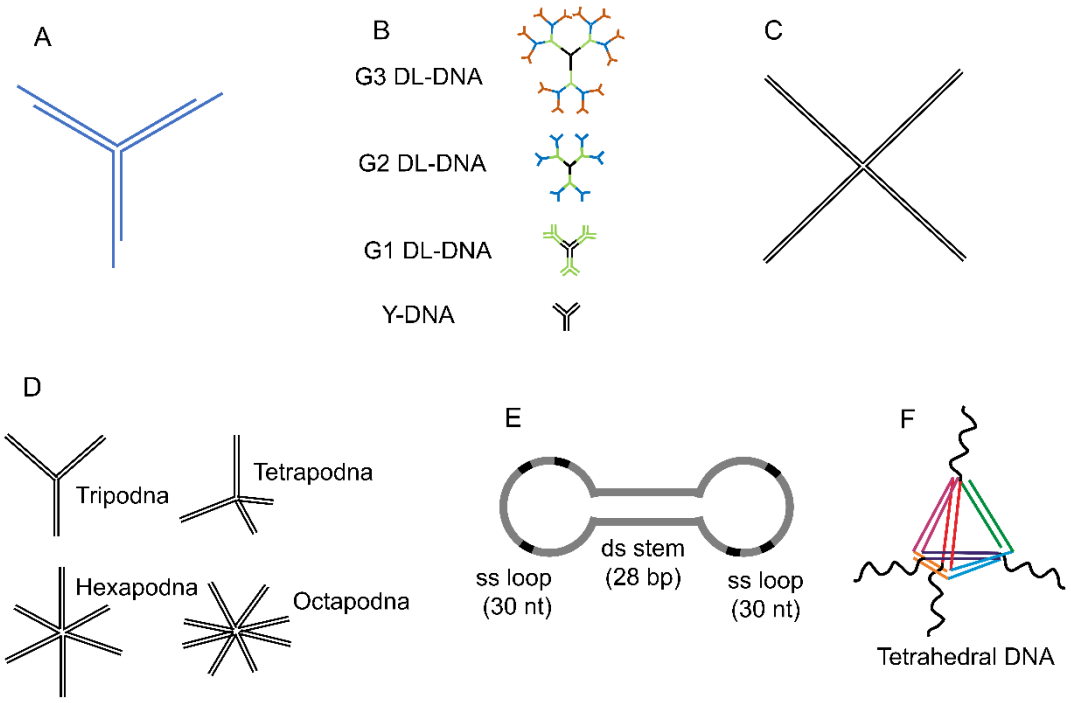

Figure 1.7 High-ordered structures of self-assemble cytosine-phosphate-guanosine (CpG) oligodeoxynucleotides (ODNs) consisting of entirely phosphodiester backbone. (A) Y-shaped[33]; (B) Dendrimer-like[34]; (C) X-shaped[46]; (D) Polypod-like[41]; (E) Dumbbell-like[9]; (F) Tetrahedral-like[45] structure.

1.4.2. X-shaped ODNs

An X-shaped DNA (**Fig. 1.7C**) is constructed from four molecules of natural phosphodiester single-stranded 39-nt CpG ODNs. X-shaped DNA has an ACGT sticky sequence at the 5′ end, which allows crosslinking each a single unit of X-DNA (Xs-DNA) to the other to form a ligated X-DNA complex (X_L-DNA).[46] Cellular uptake of Xs-DNA is 1.5 to 2-fold greater than ss-, ds-DNA.[40] The observation of TNF-α released from RAW264.7 cells at 8 hours after stimulation by X-shaped ODN bearing CpG motifs on entirely of phosphodiester backbone suggests that X-shaped DNA was stable for at least 8 hours.[18,40] X_L-DNA promoted the expression of CD80 and CD86 on mouse bone marrow-derived primary dendritic cells (BMDCs), and

induced the secretion of IL-12p40 and TNF-α. Mice given intravenous injection of X_L-DNA showed an increase in serum IFN-γ and IL-12 levels, demonstrating in vivo efficacy of X_L-DNA to activate Th1 cells and dendritic cells.[46]

1.4.3. Polypod-like ODNs

Results of studies on the self-ligated X-DNA complexes, Y-DNA, and DL-DNA can be suggests that the properties of the branched self-assemble ODNs can impact on the CpG ODN behavior. Therefore, Mohri et al[41] synthesized polypod-like DNA through self-assembly of 3–8 ODN molecules each of which contains CpG motifs (polypodna) (**Fig. 1.7D**) to investigate the relationship between the structural properties and the immunostimulatory activities of branched CpG ODNs. The size of all the polypod-like CpG ODNs that were about 10 nm in diameter. The level of cytokines such as TNF-α and IL-6 secreted in mouse macrophage-like RAW264.7 cells stimulated by polypodna increase with increase of number of pod (the number of ODNs in the polypod-like structure). When pod number of polypodna increases, the cellular uptake increases but resistance to DNase decreased. Therefore, the improved proinflammatory cytokine induction due to the increased pod number is probably caused by increase in cellular uptake efficiency.[41] Furthermore, the polypodna triggers human PBMCs significantly higher amounts of interferon α than did single-stranded DNA.[42]

1.4.4. Dumbbell-like ODNs

A dumbbell-like structure with single-stranded loops and a double-stranded stem can be formed from two molecules of the 5' phosphorylated single-stranded hairpin ODN undergoing ligation with T4-DNA ligase. The structure with no open ends enables dumbbell-like CpG ODNs (**Fig. 1.7E**) to resist to degradation by exonucleases.[47] One of the most well-defined dumbbell-like CpG ODNs is MGN1703, which comprises a 28-base pair (bp) double-stranded stem, linked with two loops of 30 nucleotides (nt), including three CpG motifs at either end.[9] MGN1703 stimulated human peripheral blood mononuclear cells (PBMCs) to produce IFN-α, IL-6, IFN-γ,

IL-12 p40, IL-2, and TNF-α. Moreover, MGN1703 triggered B-lineage RPMI-8226 cells to express human leukocyte antigen D related and intercellular adhesion molecule-1. The CpG motif position, loop size, and stem length in the dumbbell-like structure define the immunostimulatory potential of MGN1703.[43]

1.4.5. Tetrahedral-like ODNs

Li et al[45] reported about tetrahedron-like DNA assembled from four 55-base ODNs, with CpG motif sequence connected to these each ODN by a 7-mer poly-thymine spacer (**Fig. 1.7 F**). The tetrahedral DNA was efficiently taken up into mouse macrophage-like RAW264 cells and remain largely intact in the cells for 8 h. The CpG-containing tetrahedral DNA induced various pro-inflammatory cytokines, consisting of TNF-α, IL-6, and IL-12 through TLR9 activation in RAW264 cells.

1.5. G-quadruplex DNA

1.5.1. G-quadruplex structures

The most widely recognized DNA structure is the right-handed double helix structure, but DNA is able to adopt alternative conformation within specific sequences. One such non-canonical DNA secondary structure is the four-stranded G-quadruplex (G4) (**Fig. 1.8A**), which forms spontaneously in specific Guanine-rich sequences such as in telomeric region of eukaryotic chromosome and in the promoter regions of several important growth-related genes.[48]

In G4 structure, four guanines form a square plane (G-quartet) stabilized by Hoogsteen hydrogen bonds between the N1, N2 and O6, N7 of guanine bases (**Fig. 1.8A**). The stacked tandem G-quartets in the G4 stem are connected by single-stranded loops (**Fig. 1.8A**).[49] The presence of monovalent cations at the center of G-quartets can enhance the G-quartet's structural stability, as the cations neutralize the electrostatic repulsion of guanine O6 oxygens.[50]

Molecularity of G4 is defined as the number of DNA molecules associated with the formation of a G4. Accordingly, G4s can be classified as monomeric (**Fig. 1.8B i-iii**) or multimeric G4 (**Fig. 1.8B iv-v**), which consists of one or more than one molecule, respectively.

G4 structures adopt various topologies, including parallel, anti-parallel, and hybrid, depending on their sequence and the surrounding conditions such as the nature and concentration of cations.[49] In the parallel G4 topology (**Fig. 1.8B i, v**), all four strands have the same 5'→3' orientation, while in the anti-parallel G4 topology (**Fig. 1.8B ii, iv**), two strands adopt the direction opposite to that of the other two strands. Meanwhile, hybrid G4 (**Fig. 1.8B iii**) contains one strand with a different 5'→3' orientation compared with the other three strands.[51]

Despite that G4 structures can be extremely stable[52], the G4 topology and thermodynamic stability structure is determined by several factors, including the nature of the binding cations[53], the length G-tract[54], the composition and length of loops[55], loop location in the sequence [56]. The ability to stabilize G4 differed between cations with the stabilizing preference in the order K^+ >Na^+ >Li^+.[48] The ionic radius is important for complex stability. Accordingly, the hydration energy of monovalent cations inversely correlates with their ionic radii, thus the larger cation is less hydrophilic and preferentially distributes in interior of the G-quartet.[50] In addition, potassium cations have the right size for the cavity between two tetrads, thereby can coordinate with the eight O6, while sodium ions are placed in the middle of tetrad planes and thus can only coordinate with the four O6.[57] G4 structures with three or more G-quartets are more stable than those consists of only two stacks of G-quartets.[54] In K^+, total loop length is inversely proportionate to the melting temperature (T_m) with a 2 °C drop for each added base in to the loop.[55]

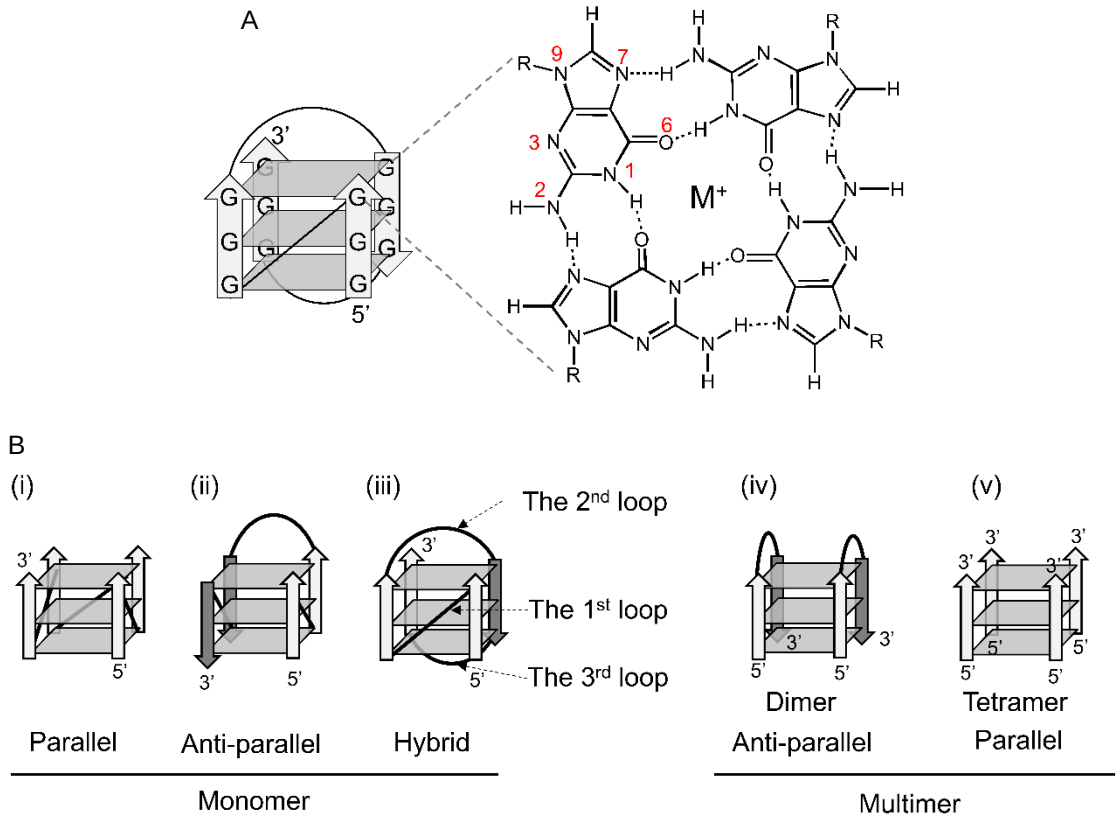

Figure 1.8 (A) Chemical structure of a G-quadruplex and G-quartet. The quartet is schematically illustrated as a square. M^+ represents a monovalent cation. (B) Schematic illustration of G4 molecularities and topologies: (i) parallel monomer, (ii) anti-parallel monomer, (iii) hybrid monomer, (iv) anti-parallel dimer, (v) parallel tetramer.[51]

1.5.2. Biological role of G4

1.5.2.1. G-quadruplexes at telomeres

Telomeres are regions at the end of eukaryotic chromosome and composed of a double-stranded region and a single-stranded 3' over-hang with repetitive nucleotide sequence $(TTAGGG)_n$.[48] Telomeres prevent chromosomes from end-to-end fusion and protect DNA from damage and the loss of genetic information. During division of normal cells, telomeres are typically shortened with 50- to 200- base loss of the telomere for each cell replication. When the telomeric region reaches a critical length, the cell undergoes apoptosis.[58] However, in the cancer

cells, the activation of a reverse transcriptase, telomerase, leads to extension of the telomeric sequence at the chromosome ends, so telomeres of cancer cells do not shorten after replication. This thus stabilizes telomere length and integrity, so maintains the malignant phenotype of cancer cells.[58] G-quadruplexes forming in the human telomere has strong inhibition of the activity of telomerase (**Fig. 1.9**).[59]

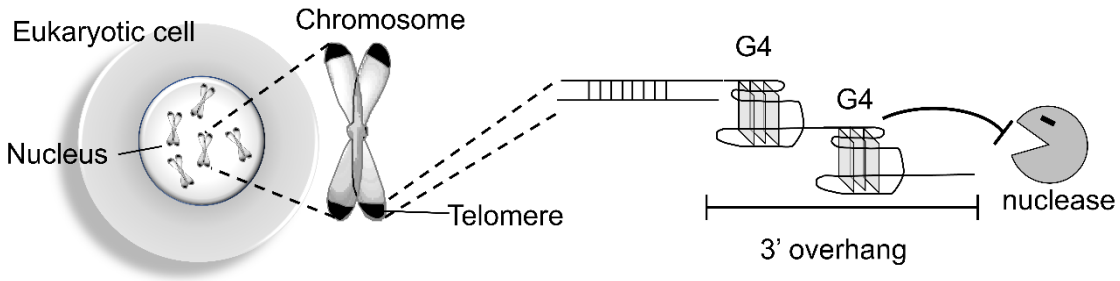

Figure 1.9 G-quadruplexes at telomeres. The G-rich 3'overhang of telomeres can form strings intramolecular G-quadruplex structures, which provide end protection against nucleases or regulate telomerase activity.[60]

1.5.2.2. G-quadruplexes in oncogene promoters

Recently, accumulating evidences have suggested that G-quadruplexes also exist in the proximal location of promoters, which are mostly TATA-less, in numerous human genes associating to growth and proliferation, such as insulin, c-MYC, VEGF, HIF-1α, c-KIT, RET, PDGF-A, c- MYB, hTERT, and PDGFR-β.[61] G-quadruplex formation in gene promoter is most widely studied in c-MYC, an important transcription factor associated with cell proliferation.[52] A great number of human tumorigenesis, including colon, breast, prostate, cervical, and small-cell lung carcinomas, osteosarcomas, glioblastomas, B-cell and T-cell lymphomas and myeloid leukemias are found to be associated with c-MYC overexpression.[58] G4 formation in Nuclease hypersensitive element III_1 (NHE III_1), which is downstream of the MYC promoter, represses the transcription. Small molecules that bind to and stabilize the G-quadruplex structure can reduce c-MYC expression and show anti-tumorigenic function.[58]

1.5.2.3. G-quadruplex based aptamers

DNA aptamers are short single stranded oligonucleotides with lengths typically ranging from 15 to 70 mers, which are identified from a bank of oligonucleotides with random sequences by the systematic evolution of ligands by exponential enrichment (SELEX) technique.[62] The association of base-pairing, π-π stacking, sugar puckering, besides electrostatic, hydrogen bonding and non-canonical intra-molecular interactions, provides each DNA aptamer a unique 3D structures. This allows DNA aptamer strongly and specifically interact with the target of interest including proteins, small molecules, ions, whole cells and even entire organisms, such as viruses or bacteria, with high affinities through hydrogen bonds, salt bridges, van der Waals, hydrophobic and/or electrostatic interactions.[63]

Aptamers forming G4 are characterized by thermodynamic and chemical stability, resistance against numerous serum nucleases, enhanced cellular uptake, extremely high polymorphism several advantages compared with unstructured aptamers.[64] In addition, negatively charged density per unit length of G4 aptamer is 2-fold higher than the duplex DNA, so electrostatic interactions with the positively charged target molecules can be increased.[63] Recently, aptamers forming G4 have been studied and applied in a wide range of fields, especially in diagnostics such as sensing devices, and therapeutics such as anticancer agents (AS1411, T40214, 3R02), and anticoagulant agents (Thrombin-binding aptamer (TBA), HD22, RA-36)) of human diseases.[62]

1.5.3. Methodologies to study G-quadruplex structures

There are many techniques that can be used to determine conformations of G4 ODNs at different levels of resolution. Although high-resolution information is preferable for examining and discussing at the molecular level, in some circumstances such as determining of fold or topology, controlling quality, verifying present of a particular structure, and purity of the structure, using techniques giving low-resolution information can be sufficient.

Native gel electrophoresis is an accessible and straightforward technique to examine the presence of a G-quadruplex. Duplex DNA has the mobility essentially corresponding to the number of base pairs, at least for moderate length oligonucleotides, and the size can be estimated by comparison with a ladder of known lengths.[65] Unlike Duplex DNA, intramolecular G-quadruplexes have a compact structure, so they migrate faster through a cation-containing gel than their linear counterparts. Meanwhile intermolecular G-quadruplexes migrate slower than their linear counterparts due to increase of molecular weight.[50]

Circular dichroism (CD) spectroscopy is a convenient diagnostic technique to revealed early G4 formation and distinguish varying G-quadruplex conformations. CD spectra characterizing different G-quadruplex topologies have been determined empirically. Parallel-stranded G-quadruplexes are characterized by a positive peak at 260 nm and a negative peak at 240 nm, while anti-parallel structures show a positive peak at 295 nm and a trough at 260 nm. Characteristic spectra of the hybrid-type G4 show positive peaks at 290 nm and 260 nm, as well as negative peaks at 235 and 255 nm. In addition, G-quadruplexes also have UV absorbance at 295 nm different from their linear counterparts. Recording CD and UV spectra over a range of temperatures enables building melting curve of G-quadruplex, where thermodynamic parameters such as Tm, ΔH, and $\Delta G°$, which reflect G-quadruplex stability, can be derived.[50]

Single-molecule fluorescence resonance energy transfer (FRET) is a powerful method to detect G-quadruplex conformation and dynamics. In FRET, the oligonucleotide is labeled with a donor and an acceptor fluorophore. When the ODN folds into G4, the energy is transferred from donor fluorophore to the acceptor. The energy transfer efficiency is influenced by the distance apart and relative orientation of the donor and the acceptor. FRET can be performed on a dilute solution or a surface-immobilized sample with the resulting energy emission can be detected using a confocal fluorescence microscope, thus allow observation of the dynamics of folding of a single molecule.[50]

Abundant information about G-quadruplex behavior and conformation can be provided by the above methods, but nuclear magnetic resonance (NMR) and x-ray crystallography are recommended for determining precise molecular structures. NMR provide information about the strand orientations and loop configurations of G-quadruplexes. Crystallography produces the structure of the form that actually crystallizes under the given conditions at highest resolution structures, some with sub-Å resolution.[50]

1.5.4. G-quadruplex ligands

G-quadruplex ligands are small-molecule can bind to G-quadruplexes with high affinity. The binding constant (K_D) between ligands and G-quadruplexes is generally smaller than 10^{-6} mol. L^{-1}. Since the first G4 ligands were reported to promote the formation of quadruplex structures of telomeric DNA, and consequently inhibit the telomerase activity and destabilize telomere end-capping in cancer cells, numerous G4-binding ligands have been reported. Some widely used ligands are shown in **Figure 1.10A**.[50] Structure of G4 ligands commonly includes an aromatic heterocyclic system to interact with G-quartets through π-π stacking and cationic groups to electrostatic interact with loop or groove of G4.[49] G4 ligand generally are sterically bulky to avoid intercalation with double-stranded DNA. Interaction between the G4 ligand MM41 and a human telomeric G4 in an X-ray crystal structure is demonstrated in **Figure 1.10B**.

Depending on the functions of stabilized G-quadruplexes, molecules interacting with quadruplexes can have different effect on cells. For example, stabilizing DNA G-quadruplexes in the promoters suppresses expression of oncogenes; stabilizing G-quadruplexes at the end of chromosomes inhibits telomerase activity and eliminate the unlimited proliferation of tumor cells.[49]

Telomestatin (**Fig. 1.10A**) is a natural macrocyclic compound, which is isolated from *Streptomyces annulatus*. It can change telomere conformation and length, and dissociate the telomere-binding proteins, thereby inhibits tumor cell proliferation. Consequently, telomestatin

induced apoptosis in different types of tumor cells, but does not effect on healthy cells. Some telomestatin-derived G4 ligands such including HXDV and 6OTD strongly inhibited tumor cells with no effect on either duplex or triplex DNA.[49]

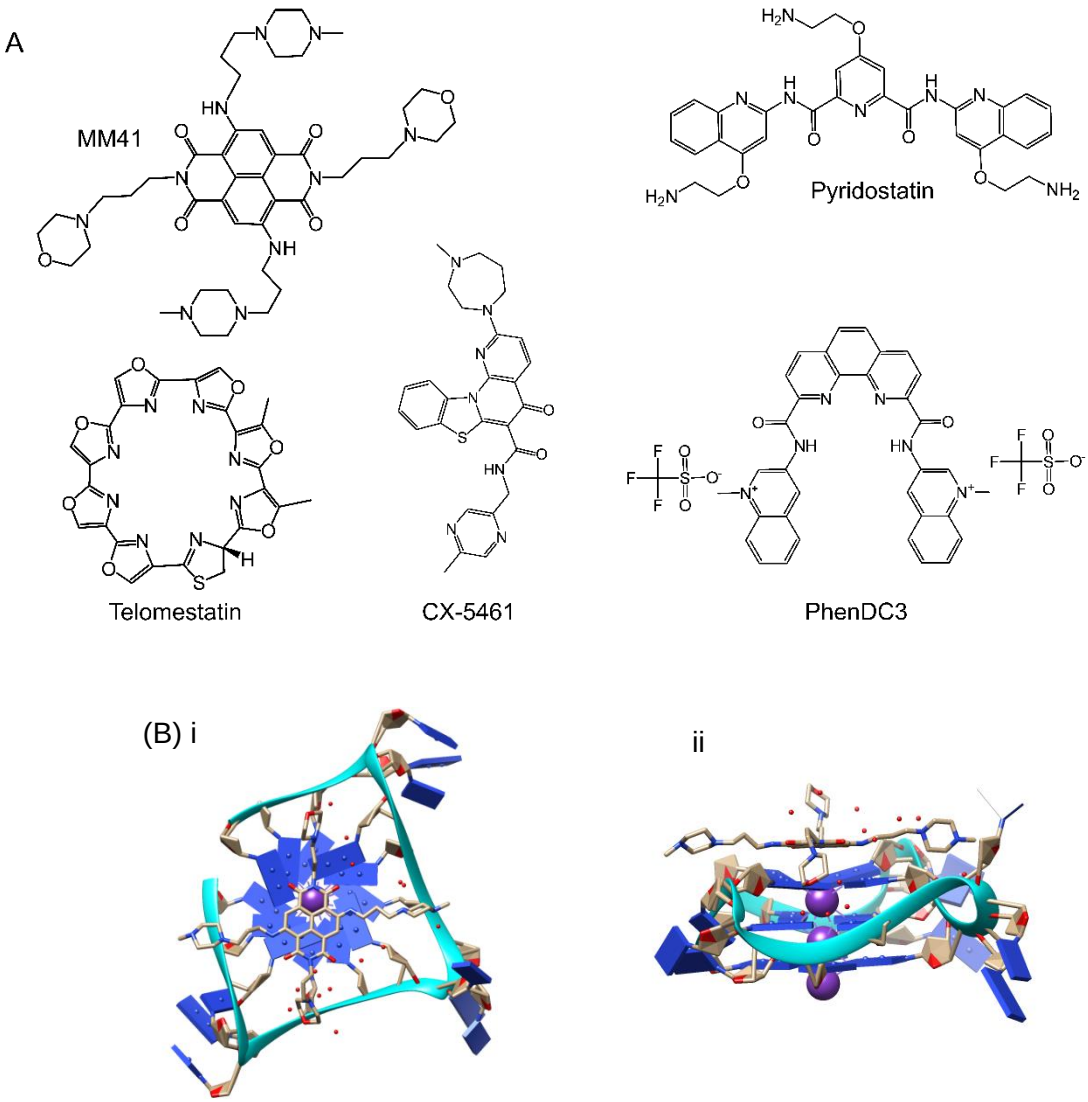

Figure 1.10 G-Quadruplex (G4) Ligands. (A) Structures of some widely used G4 ligands. (B) Crystal structure of complex of a naphthalene diimide, MM41 and an intramolecular human telomeric DNA G4, color-coded by atoms; water molecules are shown as red spheres, backbone of DNA are colored cyan, (Protein Data Bank ID: 3UYH).[48]

1.6. Objective of this study

Synthetic oligodeoxynucleotides (ODNs) containing unmethylated cytosine-phosphate-guanine (CpG) motifs activate innate immune system by stimulating Toll-like receptor 9 (TLR9), thereby, have potential as vaccine adjuvants. However, their application is limited by low nuclease resistance, so in clinical trials, CpG ODNs are phosphorothioate-modified to increase DNase stability. Despite that phosphorothioate-modification increases nuclease stability, it leads to some side effects.[66] An alternative strategy to improve the nuclease resistance of CpG ODNs is utilizing the higher order structure ODNs.[38,45,67] Self-assemble CpG ODNs in high order structure without exploiting backbone chemical modification and nanomaterials have a major advantage regarding safety. However, some high order structured CpG ODNs require an assurance of precise self-association, which causes problem about the high cost and complexity of the operations.[23] Therefore, there is a high demand for self-assemble CpG ODNs with a simple folding process and a potent immunostimulatory activity. Recently, our group reported that G4 enabled higher nuclease stability, cellular uptake, and inflammatory cytokine induction in human B cells line and peripheral blood mononuclear cells (PBMCs) compared to linear phosphodiester CpG ODN.[68] Although the usability of G4 CpG ODNs has been demonstrated, more details of their immunostimulatory properties have been unclear. Understanding these preclinical characteristics of G4 CpG ODNs allow further improvement of a more effective vaccine adjuvant based on this molecule.

The aim of this study is to further investigate preclinical characteristics of CpG ODNs forming G4 structure. To achieve this aim, this study includes following objectives.

1. Design monomeric G4 CpG ODNs
2. Determine structure of designed G4 CpG ODNs
3. Clarify biophysical properties of designed monomeric G4 CpG ODNs
4. Evaluate TLR9-agonistic properties of designed monomeric G4 CpG ODNs

5. Evaluate effect of sequence variation on immunostimulatory properties of monomeric G4 CpG ODNs
6. Assess effects of G4-ligands on of immunostimulatory properties of monomeric G4 CpG ODNs
7. Examine effects of cationic lipid-based transfection reagent DOTAP on immune response to monomeric G4 CpG ODNs.

1.7. Dissertation organization

This dissertation is organized as follows:

In chapter one, we give a general background for this study with information about Innate and adaptive immunity, CpG ODNs, evaluation of CpG ODNs as vaccine adjuvants, CpG ODNs forming high order structures, as well as G-quadruplex structures.

In chapter two, we present the design of sequences forming G4 and bearing immunostimulatory CpG motifs G4 CpG ODNs. Structure and characteristics including thermodynamic stability, and nuclease resistance of the designed ODNs are examined. The TLR9 activation ability and cytokine induction of the obtained G4 CpG ODNs are also included in this chapter.

In chapter three, we investigate more details about intrinsic factors governing immunostimulatory efficiency of G4 CpG ODNs. In this regard, we examine effects of intrinsic factors such as position of loop containing CpG motif, position of CpG motif within a loop, spaces between a CpG motif and G-tracts, and number of CpG ODNs on intensity of inducing cytokine production.

In chapter four, we assess effects of G4-stabilizing ligands on topology, stability in serum, cellular uptake, and cytokine induction of G4 CpG ODNs.

Chapter five present the immune response of several type of cell lines, consisting of mouse macrophage cells, human B cells, and dendritic cells to monomeric G4 CpG ODNs. In addition, the cytokine production of human immune primary cells in response to G4 CpG ODNs are also presented in this chapter.

Chapter six presents result summary and future work.

Chapter 2 Design and characterization of monomeric G4 CpG ODNs

2.1. Introduction

Toll-like receptor 9 (TLR9) is a member of the family of transmembrane-signaling pattern-recognition receptors of the innate immune system, and it contributes to defense against infection by inducing inflammation and initiating the adaptive immune response.[5] TLR9 recognizes cytosine-phosphate-guanine (CpG) dinucleotides, which are present at very low frequencies or methylated in vertebrate DNA but are abundant in bacterial and viral DNA.[2] This recognition triggers the production of inflammatory cytokines, such as interleukin (IL)-6, IL-12, and tumor necrosis factor-α (TNF-α) or type I IFNs.[2] These inflammatory cytokines play a crucial role in innate immune response and guide the adaptive immune responses. Therefore, in the absence of invading pathogens, deliberate stimulation of TLR9 by synthetic CpG ODNs can be a useful strategy in the development of vaccine adjuvants[3] or in the treatment of some diseases such as cancer and allergies.[4] Various CpG ODN agonists for TLR9 have been developed to induce the immune response for several clinical applications. In this strategy, the phosphodiester backbone of natural CpG ODNs are chemically modified into a phosphorothioate backbone to increase the CpG ODN half-life in the body because the phosphodiester backbone is susceptible to DNase degradation.[2] Unfortunately, although phosphorothioate CpG ODNs are more resistant to DNases than the phosphodiester ones are, they have been reported to cause adverse effects[66], which hinder their application in the field of immunotherapy.

To avoid these side effects, strategies to improve the nuclease resistance of CpG ODNs without applying chemical modifications are currently being studied. The construction of ODNs with higher order structures is a potential approach to improve the nuclease resistance of ODNs, as dumbbell-like,[67] tetrahedral,[45] and dendrimer-like ODNs[38] with fully phosphodiester backbones have exhibited serum stability and immunostimulatory activity. However, the complication of operations for manufacture and the manufacturing costs of some high order

structured CpG ODNs[23] lead to a demand for a self-assemble CpG ODNs with a simple folding process and a potent immunostimulatory activity.

In this chapter, we developed phosphodiester CpG ODNs forming G4, a four-stranded structure can form straightforwardly by heating and then cooling gradually in the buffer containing monovalent cations. We determined the structure, clarified the biophysical properties, evaluated TLR9-agonistic properties, and investigated their capacity to stimulate cytokine production in mouse macrophage-like RAW264 cells, human PBMCs, and in mice given intraperitoneal injections. The monomeric G4-based CpG ODNs with enhanced immunostimulatory effect of CpG ODNs were achieved.

2.2. Materials and Methods

2.2.1. ODNs

All ODNs with phosphodiester backbones (sequences are shown in the **Table 2.1**) were HPLC-grade and purchased from Eurofins Genomics (Tokyo, Japan).

2.2.2. G-quadruplex structure formation of ODNs

The purchased ODNs were dissolved in sterile Mili-Q water to prepare stock solutions. The stock solutions were stored at -30 °C until use. To form the G4 structure, ODNs were diluted from the stock solution using Dulbecco's phosphate-buffered saline (D-PBS, DS Pharma Biomedical, Osaka, Japan) containing 2.68 mM KCl, 137 mM NaCl, 1.47 mM KH_2PO_4, and 8.10 mM Na_2HPO_4. For example, to prepare 20 μL of 10 μM G4 CpG ODN solution from a stock ODN solution at 100 μM, 2 μL of 10× D-PBS, 2 μL of 100 μM ODNs, and 16 μL of sterile Mili-Q water were added into a PCR tube. The ODN solutions were heated to 95 °C for 5 min, then cooled gradually to 30 °C for 30 min, followed by cooling to 4 °C using a thermal cycler (PCR Thermal Cycler Dice Standard TP650, Takara, Kyoto, Japan). The folded ODN solutions were stored at 4 °C until use.

Table 2.1 Sequences of oligodeoxynucleotides used in this chapter

Name	Sequence from 5' to 3'[a]	Length (mer)
GD1	GGGTTGGG**GTCGTT**GGGTTGGG	22
GD2	GGGTTGGG**GTCGTTTT**GTCGTTGGGTTGGG	30
GD3	GGGTTGGG**GTCGTTTT**GTCGTTTT**GTCGTT**GGGTTGGG	38
GD2-Met	GGGTTGGGGTC$_{Met}$GTTTTGTC$_{Met}$GTTGGGTTGGG	30
GD3-Met	GGGTTGGGGTC$_{Met}$GTTTTGTC$_{Met}$GTTTTGTC$_{Met}$GTTGGGTTGGG	38
GD3-GC3	GGGTTGGG**GTCGTTTT**GTCGTTTTGTGCTTGGGTTGGG	38
GD3-GC123	GGGTTGGGGTGCTTTTGTGCTTTTGTGCTTGGGTTGGG	38
2006_PD	TC**GTCGTTTT**GTCGTTTT**GTCGTT**	24

[a] Capital letters, phosphodiester bases; bold letters, human-specific immunostimulatory unmethylated CpG motif; C_{Met}, 5-Methyl deoxy cytidine; underline, G-tract.

2.2.3. Ultraviolet (UV) melting curves and thermal difference spectra (TDS)

The G4 CpG ODN solutions were prepared in D-PBS at a concentration of 10 μM. Before measuring the UV absorbance, the solutions were further diluted to 2 μM with D-PBS. The ODN solutions (600 μL) were added into a quartz cuvette (model T-30 MES10, 1-cm path length), followed by the addition of 100 μL mineral oil to the top of the solutions to prevent evaporation. The UV absorbance spectra were recorded using a Jasco V-670 spectrophotometer (Tokyo, Japan) over a wavelength range of 220–320 nm (scan speed, 400 nm/min; data pitch, 1 nm; band width, 2.0 nm UV/Vis). The UV melting curves were based on the absorbance at 295 nm from 20 °C to 90 °C (temperature gradient: 1 °C/min; data pitch: 1 °C). The denaturation and renaturation profiles of ODNs were obtained during the process of heating, cooling, and reheating. The TDS were obtained by subtracting the absorbance spectra at 20 °C from the spectra at 90 °C.

To determine the melting temperature (T_m) of G4 CpG ODNs, the melting curves at 295 nm were analyzed by the baseline method.[69] A two-state equilibrium analysis was used to derive

the thermodynamic parameters from the melting curve at 295 nm following the method described by Mergny et al.[69] The Gibbs free energies were calculated at 37 °C using the Gibbs equation $\Delta G°_{vH}(T) = \Delta H°_{vH} - T\Delta S°_{vH}$, where T is the absolute temperature and $\Delta G°_{vH}$, $\Delta H°_{vH}$, and $\Delta S°_{vH}$ are the van't Hoff Gibbs free energy, enthalpy, and entropy changes upon folding, respectively.[70]

2.2.4. Circular dichroism (CD) Spectroscopy

To measure the CD spectra, the G4 CpG ODN solutions (20 μM in D-PBS) were further diluted to 2 μM with D-PBS. Then, 100 μL of the 2 μM ODN solution was added into a quartz cuvette (model T-18-ES-10, 1-cm path length, Jasco). The CD spectra were determined using a Jasco J-725 CD spectropolarimeter over a wavelength range of 220–320 nm (scan rate, 50 nm/min; response time, 2.0 s; band width, 1.0 nm; resolution, 0.2 nm; and sensitivity, 100 mdeg) at 25 °C. The presented spectrum of each ODN is the average of 20 scans.

The peak fitting and deconvolution to the CD spectrum were performed using the damped least-squares method by fitting program version 2.06.01 (Jasco). The program cannot analyze a CD spectrum if it contains a negative signal. Therefore, the spectrum is set so that the signal in the entire analysis range becomes positive. Accordingly, 4.34 and 3.83 were added to the spectra of GD2 and GD3, respectively. Analysis was performed in the calculation range of 240–320 nm and 245–320 nm for GD2 and GD3, respectively. The baseline was set to 0 mdeg. Peak setting initial values were (center position, half-width) = (260, 14.6), (295, 14.4), and (280, 22.4) for GD2 and (260, 13), (295, 15.5), and (280, 20.8) for GD3.

For the CD melting and cooling curves, 600 μL of the 2 μM reconstructed ODN solution was added to a quartz cuvette (model T-30 MES10, 1-cm path length), followed by the addition of 100 μL mineral oil to the top of the ODN solution to prevent evaporation. CD measurements were performed at 260 nm and 295 nm over a temperature range of 20 to 90 °C, with a heating or cooling rate of 1 °C/min. CD signals were recorded during the process of heating, cooling, and reheating.

2.2.5. Polyacrylamide Gel Electrophoresis (PAGE)

Gel electrophoresis was performed using 12% polyacrylamide gels (PAGE; 1-mm thick; TEFCO, Tokyo, Japan) in 0.5× Tris-borate-EDTA (TBE) buffer (0.089 M, pH 8.3–8.5; Takara Bio, Kusatsu, Japan) supplemented with 0 or 4 mM KCl, at a constant voltage of 180 V at 4 °C. The 10-base pair (bp) DNA ladder (Invitrogen, Carlsbad, CA, USA) was used as a marker. The bands in the gel were stained by SYBR Gold Nucleic Acid Gel Stain (Thermo Fisher Scientific, Waltham, MA, USA).

Linear ODNs ssODN22mer (5'-GTCGTTTTGTCGTTTTGTCGTT-3'; 22 nucleotides), ssODN30mer (5'-GTCGTTTTGTCGTTTTGTCGTTTTGTCGTT-3'; 30 nucleotides), and ssODN38mer (5'-GTCGTTTTGTCGTTTTGTCGTTTTGTCGTTTTGTCGTT-3'; 38 nucleotides) were used as references. The linear ODNs were diluted in Tris-HCl 10 mM (pH 7.4) to a concentration of 20 μM. Before their application to the PAGE gel, they were heated at 95 °C for 5 min and immediately put on ice to preserve their linear structure.

2.2.6. Serum stability assay

The nuclease resistance of the ODNs was determined by examining their serum stability. Each reconstructed G4 CpG ODN (4 μL of the 10-μM solution) was added to 36 μL of 20% or 55.6% (v/v) FBS and incubated at 37 °C for 0, 1, 2, 4, and 24 h. After the indicated time, the reaction was stopped by adding 4 μL 250 mM ethylenediaminetetraacetic acid (EDTA) and heating to 80 °C for 2 min. The treated ODNs were stored at 4 °C for PAGE analysis. Quantification of the remaining ODNs was performed by determining the fluorescence intensities of the corresponding bands in PAGE using Image Studio Lite software (LI-COR Biotechnology, Lincoln, NE, USA).

2.2.7. Cell cultures

The mouse macrophage-like RAW264 cell line (RCB0535), purchased from RIKEN BioResource Center (Tsukuba, Japan), was cultured in Minimum Essential Medium (MEM) (Gibco, Carlsbad, CA, USA) containing 10% (v/v) fetal bovine serum (FBS) (Sigma-Aldrich, St Louis, MO, USA) and 1% (v/v) MEM non-essential amino acid solution (100×, Wako Pure Chemical Industries, Osaka, Japan). Dulbecco's Modified Eagle Medium (DMEM; Sigma-Aldrich) supplemented with 4.5 g/L glucose, 2 mM L-glutamine, 10% (v/v) heat-inactivated FBS, and 0.5% (v/v) penicillin/streptomycin (100×, P/S; Thermo Fisher Scientific) was used for culturing the 293XL-hTLR9A and 293XL/null cells (the control cell line) (InvivoGen, San Diego, CA, USA). The 293T cell line (RCB2202), purchased from RIKEN BioResource Center, was cultured in DMEM (Sigma-Aldrich) supplemented with 4.5 g/L glucose, 2 mM L-glutamine, and 10% (v/v) heat-inactivated FBS. The cells were incubated at 37 °C in a humidified incubator with 5% CO_2.

2.2.8. Intracellular uptake

RAW264 cells were seeded in a 48-well plate at 2×10^5 cells per well and then incubated for 24 h at 37 °C in a humidified incubator with 5% CO_2. GD3 and 2006_PD were labelled at the 5' end by Cy5 ($GD3^{5'Cy5}$ and $2006\_PD^{5'Cy5}$). After 24 h, the culture medium was replaced by 200 μL of Opti-MEM (Thermo Fisher Scientific) containing 5 μM $GD3^{5'Cy5}$ or $2006\_PD^{5'Cy5}$. After 2 h-incubation at 37 °C or 4 °C, the cells were washed with 500 μL phosphate-buffered saline (PBS; Wako Pure Chemical Corporation) twice and harvested. Then, flow cytometric analyses were conducted using a flow cytometer (SP6800; Sony, Tokyo, Japan). Mean fluorescence intensity (MFI) was measured, and $\Delta MFI_{37°C-4°C}$ ($MFI_{37°C} - MFI_{4°C}$) was calculated.

2.2.9. Confocal image analysis

Cellular uptake and co-localization of CpG ODNs were examined by confocal laser scanning microscope. 293T cells were seeded in a CELLview™ cell culture dish with a glass bottom (Greiner Bio-One, Kremsmunster, Austria) at 4×10^4 cells per well. After 36 h, the 293T cells were transfected with pcDNA3-TLR9-YFP (gifted by Doug Golenbock [Addgene plasmid # 13642; http://n2t.net/addgene:13642; RRID:Addgene_13642]), the plasmids encoding human TLR9 fused with yellow fluorescence protein (YFP) ($hTLR9^{YFP}$), using transfection reagent Lipofectamine 3000 (Invitrogen).[71] GD3 was labelled at the 5' end by Cy5 ($GD3^{5'Cy5}$). After 36 h, the culture medium was replaced by 400 μL of fresh medium containing 4 μM $GD3^{5'Cy5}$ and then incubated for 14 h at 37 °C in a humidified incubator with 5% CO_2. After the cells were washed of medium, 400 μL fresh medium was added to the cells. The cells were visualized using a confocal laser scanning microscope (TCS SP5 II, Leica). LAS AF software (Leica Microsystems) was used to process the images.

2.2.10. Immunostaining

RAW264 cells in culture medium supplemented with 1% (v/v) P/S were seeded in a CELLview™ cell culture dish with a glass bottom (Greiner Bio-One) at a density of 2.85×10^4 cell/compartment. The plates were coated with collagen solution prior to seeding cells. After 18 h, the cells were stimulated by 4 μM of $GD3^{5'Cy5}$ and then incubated for 4 h at 37 °C in a humidified incubator with 5% CO_2. Then, the cells were washed twice with 500 μL phosphate buffered saline (PBS). Fixation was done with 4% paraformaldehyde (PFA) for 10 min at 25 °C, afterwards which samples were washed again three times with PBS. Permeabilization of the cells was done with 0.2% Tween20/PBS for 5 min at 25 °C, and then the cells were washed three times with PBS. Then the cells were incubated with 3% bovine serum albumin in PBS for 1 h at RT. Samples were stained with primary antibodies (10 μg/mL Lysosome Marker (anti-LAMP1 antibody), 1 μg/mL antibody-Early Endosome Marker (anti-EEA1 antibody), or 3.33 μg/mL

TLR9 Antibody (26C593.2)) in PBS at 25 °C for 1 h. After removal of primary antibody, washing with PBS three times for 5 min was done. Samples were stained with Alexa488 labelled secondary antibodies diluted 1:200 in PBS for 1 h at 25 °C. After removal of secondary antibodies, the cells were washed with PBS three times, for 5 min. Antifade solution with 4',6-diamidino-2-phenylindole (DAPI) (100 μL) was added into each well. Samples were stored at 4°C without exposure to light. Images were acquired using a 63x/1.40 objective on Leica TCS SP5. Antibodies used in immunostaining method are presented in **Table 2.2**.

Table 2.2 Primary and secondary antibody used in immunostaining

Antibody	**Type**	**Host species**	**Target/ Specificity**	**Clonality**	**Company**	**Product number**
Anti-LAMP1 antibody - Lysosome Marker	Primary	Rabbit	LAMP1	Polyclonal	Abcam	ab24170
Anti-EEA1 antibody Early Endosome Marker	Primary	Rabbit	EEA1	Polyclonal	Abcam	ab2900
TLR9 Antibody (26C593.2)	Primary	Mouse	TLR9	Monoclonal	Novus Biologicals	NBP2-24729
Alexa488 labelled antibody	Secondary	Goat	Rabbit/IgG	Polyclonal	Jackson ImmunoResearch	111-545-003
Alexa488 labelled antibody	Secondary	Donkey	Mouse/IgG	Polyclonal	Invitrogen	A21202

2.2.11. TLR9 reporter assay

TLR9 activation was assayed by observing NF-κB activity. First, 293XL-hTLR9 cells and 293XL/null cells were seeded at 2.5×10^5 cells per well. Next, pNiFty-Luc (InvivoGen) containing the firefly luciferase gene under the NF-κB-inducible element and an expression

control plasmid, pGL4.74 (Promega, WI, US) expressing a Renilla reniformis luciferase gene under the HSK-TK promoter, were transfected into the cells using the LyoVec (InvivoGen) transfection reagent. The cells were incubated for 20 h, and then 10 μM G4 CpG ODNs was added to a final concentration of 0.5 μM. A passive lysis buffer was used to lyse cells after 24 h of stimulation, and then the luciferase signals from the lysates were measured using a luminometer TD-20/20 (Promega) based on the manufacturer's instructions. The data were presented as the NF-κB activity of G4 ODN-stimulated cells relative to that of the control cells (no ODN stimulation).

2.2.12. Immunoprecipitation binding assay

The binding of the G4 CpG ODNs to mouse TLR9 was determined using Recombinant Mouse TLR9 Fc Chimera (mTLR9Fc, R&D Systems, Minneapolis, MN, USA) and the Dynabeads Protein G Immunoprecipitation Kit (Thermo Fisher Scientific) according to the manufacturer's instructions. mTLR9Fc was diluted in phosphate-buffered saline (PBS[-]; 137 mM NaCl, 2.92 mM NaH_2PO_4, and 9.01 mM Na_2HPO_4; Wako Pure Chemical Corporation) to a final concentration of 1 μg/mL. Magnetic beads (50 μL Dynabeads) were resuspended in 200 μL binding and washing buffer with 5 μg mTLR9Fc or with PBS(-) as the non-mTLR9Fc control. Then, suspensions were incubated for 20 min with rotation at a speed of 10 rpm at 25 °C. Next, the Dynabead-mTLR9Fc complex was washed once with the binding and washing buffer. Then, the reconstructed G4 CpG ODNs (250 pmol) in 125 μL of 10 mM 2-(N-morpholino)ethanesulfonic acid buffer (pH 6.5, containing 150 mM K^+ and 20 mM Na^+) were added to the tubes with Dynabeads; D-PBS was used as a non-CpG-ODN control. The samples were incubated for 20 min with rotation at a speed of 10 rpm at 25 °C, followed by washing three times with the washing buffer. For ODN and mTLR9Fc elution, the Dynabead-mTLR9Fc-ODN complex was resuspended in 10 μL elution buffer and incubated at 25 °C for 4 min.

The mTLR9Fc was detected by sodium dodecyl sulfate (SDS)-PAGE using 15% polyacrylamide gels (ATTO, Tokyo, Japan), 1× Tris-glycine-SDS running buffer (EMD Millipore Corp., Bedford, MA, USA), and Coomassie brilliant blue stain (Nacalai Tesque, Kyoto, Japan). The presence of bound CpG ODNs in eluted samples was examined by PAGE in 10-20% polyacrylamide gels (ATTO) with 1× Tris-glycine running buffer and visualized by SYBR Gold.

2.2.13. Stimulation of RAW264 cells

RAW264 cells in culture medium supplemented with 1 (v/v) P/S (100×) were seeded into a 96-well plate at a density of 1×10^5 cells/well (5.3×10^5 cells/mL, 190 μL). After incubation for 18 h, 10 μL of 80 μM ODN was added to the culture medium to a final concentration of 4 μM. Then, the cells were incubated for 24 h before evaluation of the relative transcript levels and the secretion levels of cytokines.

The relative transcript levels of cytokines in RAW264 cells were determined by reverse transcription/real-time quantitative-polymerase chain reaction (RT/RQ-PCR). Total RNA was extracted from the cells using ISOGEN (Nippon Gene, Tokyo, Japan) following the manufacturer's instructions. The extracted RNA was treated with DNase I (RNase-free) (Takara Bio, Shiga, Japan) prior to reverse transcription into cDNA (Takara Bio). IL-6, IL-12, and IFN-β transcript levels were measured by quantitative real-time PCR using a LightCycler 480 System (Roche, Basel, Switzerland) with LightCycler®480 SYBR Green I Master (Roche) and the primers (FASMAC, Kanagawa, Japan) listed in **Table 2.3**.

Table 2.3 Primer sequences for analysis of murine cytokines

Gene	Sequence from 5' to 3'
GAPDH	FW[a]: GTGGACCTCATGGCCTACAT
	RV[b]: TGTGAGGGAGATGCTCAGTG
IL-6	FW: TCCTTCCTACCCCAATTTCC
	RV: CGCACTAGGTTTGCCGAGTA
IL-12	FW: GAAAGGCTGGGTATCGG
	RV: GGCTGTCCTCAAACTCAC
IFN-β	FW: GGTCCGAGCAGAGATCTTCA
	RV: TCACTACCAGTCCCAGAGTCC

[a] forward primer; [b] reverse primer.

Amplification was performed using 50 ng cDNA in a total volume of 15 μL for 45 cycles of 10 s each at 95 °C, 10 s at 60 °C, and 10 s at 72 °C. After PCR, the crossing point value, the cycle at which the fluorescence starts to become significantly higher than the background fluorescence, was determined. The mRNA levels were normalized against that of glyceraldehyde 3-phosphate dehydrogenase (*GAPDH*), a housekeeping gene. In addition, the specificity of the amplified products was verified by analyzing the melt curves.

To analyze the transcription product levels, the supernatants form the RAW264 cells stimulated by G4 CpG ODNs were collected by centrifuging (10,000 ×*g*) for 10 min at 4 °C. IL-6 and IFN-β secretion levels in the supernatants were determined by Mouse IL-6 Enzyme-linked immunosorbent assay (ELISA) Ready-SET-Go kit (eBioscience, San Diego, CA, USA), and VeriKineTM mouse IFN-β ELISA kit (PBL InterferonSource, Piscataway, NJ, USA), respectively, according to the manufacturer's instructions.

2.2.14. Stimulation of human peripheral blood mononuclear cells (PBMCs)

Human PBMCs (Sample ID: 20110727; ethnicity: Hispanic; age: 29; gender: Female; ABO/Rh: O/Pos), purchased from Cellular Technology Limited (Shaker Heights, OH, USA), were thawed according to the manufacturer's instructions and resuspended in Roswell Park Memorial Institute 1640 medium (Thermo Fisher Scientific) containing GlutaMAX, 4-(2-hydroxyethyl)-1-piperazineethanesulfonic acid), 1% (v/v) P/S (100×), and 10% (v/v) heat-inactivated FBS. The cells (190 μL) were seeded into a 96-well plate at a density of 1×10^6 cells/well and stimulated with ODNs. After incubation for 4, 24, or 48 h, the cells were centrifuged (10,000 ×*g*) for 10 min at 4 °C to collect the supernatants. IL-6 and IFN-γ Ready-Set-Go kits and Human IFN-α Module Set ELISA (Thermo Fisher Science) were used according to the manufacturer's instructions to evaluate cytokine expression levels in the supernatants. 2006_PD was used as control ODNs that form a random coil structure.

2.2.15. *In vivo* immunostimulatory properties of G4 CpG ODNs

In vivo studies were approved by the Animal Care and Use Committee at the National Institute for Materials Science and were in compliance with the Guidelines for Proper Conduct of Animal Experiments established by the Science Council of Japan. Seven-week-old female C57BL/6 mice (Charles River Laboratories Japan, Yokohama, Japan) were intraperitoneally injected with 10 nmol of GD3 or 2006_PD. Blood samples were collected before injection and 2, 4, and 24 h after injection from the facial veins of the mice using Goldenrod Animal Lancets (Braintree Scientific, MA, USA). The blood was centrifuged (12,000 ×*g*) for 10 min at 4 °C to collect the plasma. The collected plasma was stored at -30 °C until use. The plasma IL-6, IL-12p70, and IFN-γ concentration was determined by ELISA using the mouse IL-6, IL-12p70, and IFN-γ Ready-Set-Go kit (Thermo Fisher Science) according to the manufacturer's instructions.

2.2.16. Statistical analysis

Statistical comparisons of the data were conducted by one-way analysis of variance (ANOVA) followed by Tukey's multiple comparisons test for comparison with other groups or by Dunnett's multiple comparisons test for comparison with a control group. Two-way ANOVA followed by the Sidak's multiple comparisons test was used for comparison of the groups in the TLR9 reporter assay, human PBMC, and *in vivo* assay. All statistical analyses were performed using GraphPad Prism version 8.2.0 for Windows (GraphPad Software, La Jolla, CA, USA). A p-value < 0.05 was considered statistically significant.

2.3. Results and discussion

2.3.1. Formation of the G-quadruplex (G4) structure in the designed CpG ODNs

We designed monomeric G4 CpG ODNs based on the model sequence of TBA-3G (5'-GGGTTGGGTGTGGGTTGGG-3') (**Fig. 2.1A**), which is a variant of the thrombin-binding aptamer TBA (5'-GGTTGGTGTGGTTGG-3'), a well-known monomeric G4 ODN.[54] TBA-3G is a monomeric G4 ODN, but it consists of three quartets instead of two quartets as in TBA, which provides TBA-3G a higher thermodynamic stability than TBA.[54] Our designed CpG ODNs, named GD1, GD2, and GD3, contain one, two, and three "GTCGTT" CpG motifs, respectively (**Table 2.1**). These G4 CpG ODNs also contain four tracts of three guanines (hereafter referred to as G-tracts). To form G-quadruplex structures, the designed CpG ODNs were diluted in D-PBS, a buffer containing potassium and sodium ions, which stabilized the G-quadruplex structure. Then, the temperature was raised to 95 °C to enable ODN random linear structure formations. Afterwards, the temperature was slowly decreased. During this gradual cooling step, the ODN chains containing G-tracts fold spontaneously in the presence of potassium and sodium ions to form the G4 structure.

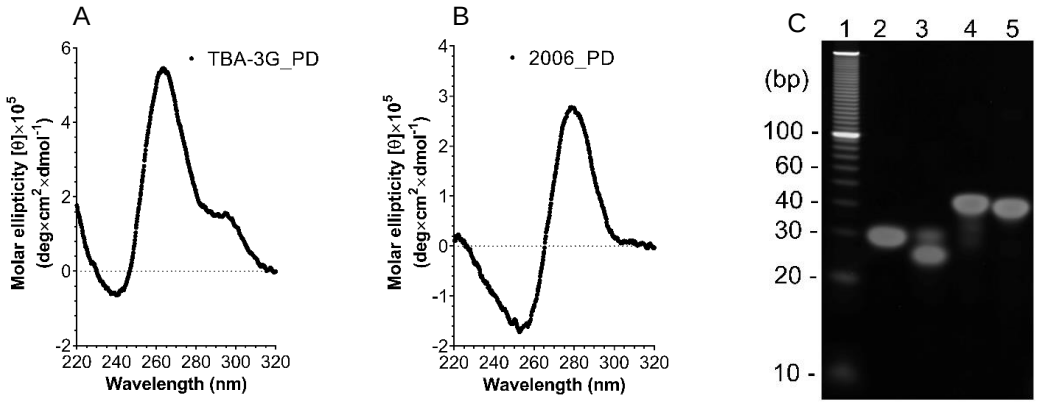

Figure 2.1 Circular dichroism (CD) spectra of (A) thrombin-binding aptamer with three G-quartets and (B) 2006_PD. (C) Polyacrylamide gel electrophoresis analysis without K^+; lane 1, 10-bp DNA ladder; lane 2, ssODN30mer; lane 3, GD2; lane 4, GD3; lane 5, ssODN38mer.

The TDS were used to examine the formation of the G4 structures in the designed CpG ODNs. The TDS of GD1, GD2, and GD3 show two positive peaks at 244 and 274 nm and a negative peak at 295 nm (**Fig. 2.2A**), which are similar to the typical TDS of a G-quadruplex structure[72]; the negative peak at 295 nm in the TDS specifically indicates the denaturation of the G4 structures. Taken together, these results suggest that GD1, GD2, and GD3 form the G4 structure.

The CD spectra of the designed CpG ODNs are shown in **Figure 2.2B**. The CD spectra of GD1 and GD2 exhibit one negative peak at around 240 nm, and two positive peaks at around 260 nm and 290 nm, which characterize a hybrid G4 topology,[73] suggesting that these ODNs form the hybrid-type G4. The GD3 CD spectrum also had a negative peak at around 240 nm. However, in contrast to the two distinct positive peaks of GD1 and GD2, GD3 displayed one broad positive peak from 260 to 290 nm.

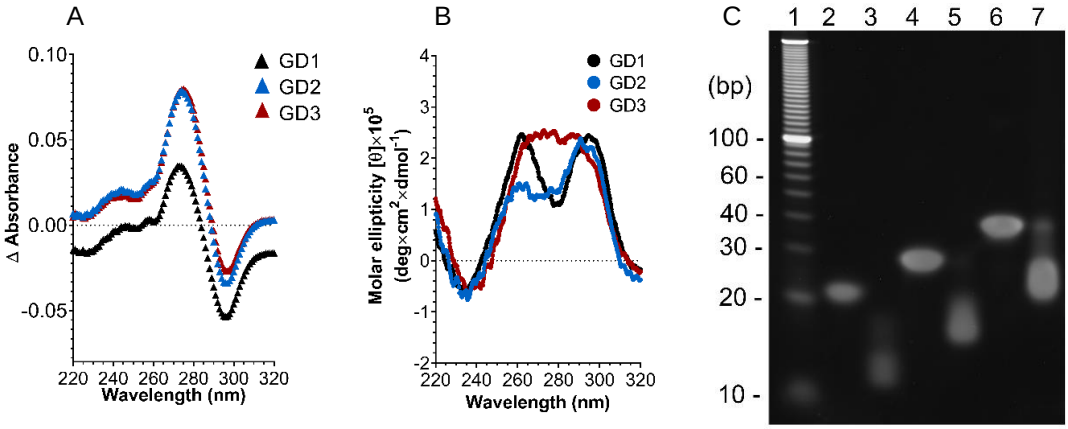

Figure 2.2 Structural analysis of the designed CpG oligodeoxynucleotides (ODNs). (A) Thermal difference spectra obtained by subtraction of the spectra obtained at 20 °C from those obtained at 90 °C. (B) Circular dichroism spectra at 25 °C in the presence of 4 mM K^+. (C) Polyacrylamide gel electrophoresis analysis in the presence of 4 mM K^+; lane 1, 10-bp DNA ladder; lane 2, ssODN22mer; lane 3, GD1; lane 4, ssODN30mer; lane 5, GD2; lane 6, ssODN38mer; lane 7, GD3.

The peak fitting and deconvolution of GD2 and GD3 CD spectra are presented in **Figure 2.3** and **Table 2.4**. GD2 and GD3 CD spectra consist of three component peaks at around 260, 295, and 280 nm. As shown in **Table 2.4**, the area proportion of the 280-nm peak in the GD3 CD spectrum is larger than that in the GD2 CD spectrum. Villar-Guerra et al. reported that the total CD signal of the G4 ODNs includes the contribution of the signal from the loop regions and from the G4 stem.[73] The long central loop of GD3 may behave as a single strand with a random coil structure. The CD spectrum of a random coil structure is characterized by a positive peak at 280 nm, which can be observed in the CD spectrum of a linear CpG ODN such as 2006_PD (**Fig. 2.1B**). Therefore, GD3 seems to also form a hybrid G4 structure, and the broad positive peak in the GD3 CD spectrum may be caused by the overlaps of the 260-nm and 295-nm peaks with the 280-nm peak due to the structure of the long central loop. GD1 and GD2 have shorter central loops than GD3, so the CD signal of the loop regions of GD1 and GD2 were not strong enough

to overlap with those of the other components of the G4 structure.[73] Taken together, these results suggest that the designed G4 CpG ODNs form the hybrid-type G4 structure.

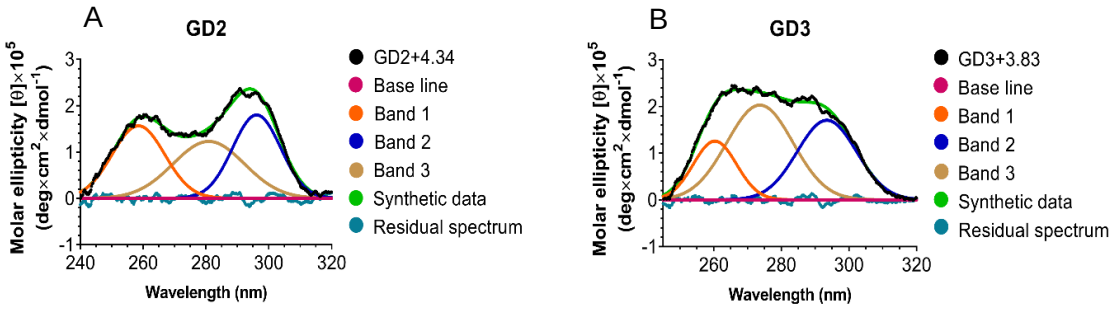

Figure 2.3 Peak fitting and deconvolution of circular dichroism (CD) spectra of (A) GD2, (B) GD3. Note: CD spectra (black curves), fitted curves (green curves), component band 1 (orange curves), component band 2 (blue curves), component band 3 (light brown curves), and residual spectra (cyan curves). The baseline was set at 0 mdeg (pink curves).

Table 2.4 CD spectra deconvolution of GD2 and GD3

ODNs		Spectra deconvolution					
	Component	Center position (nm)	Half width (nm)	Height	Area	Proportion (area) (%)	Function
GD2	Band 1	258.506	19.7051	3.12764	65.6036	32.1	Gaussian
	Band 2	296.132	17.9871	3.596	68.8513	33.7	Gaussian
	Band 3	280.887	26.7624	2.45509	69.9398	34.2	Gaussian
GD3	Band 1	260.602	15.1732	2.58686	41.7812	19.8	Gaussian
	Band 2	293.951	19.6637	3.20731	67.1335	31.9	Gaussian
	Band 3	274.473	23.5045	4.0664	101.741	48.3	Gaussian

We replaced the third CpG dinucleotide or all CpG dinucleotides in the central loop of GD3 by GpC dinucleotide inversion to obtain ODNs named GD3-GC3 or GD3-GC123 (**Table**

2.1), respectively. These ODNs showed similar CD spectra to that of GD3, with a broad peak in the range of 260–290 nm (**Fig. 2.4A**). Additionally, GD3-GC123 showed a band position in PAGE similar to that of GD3 (**Fig. 2.4B**). These results indicate that replacing sequences for the loop region did not change the overall folding of GD3. This is consistent with the hypothesis that the loop region of GD3 behaves as single-strand ODNs with a random coiled structure.

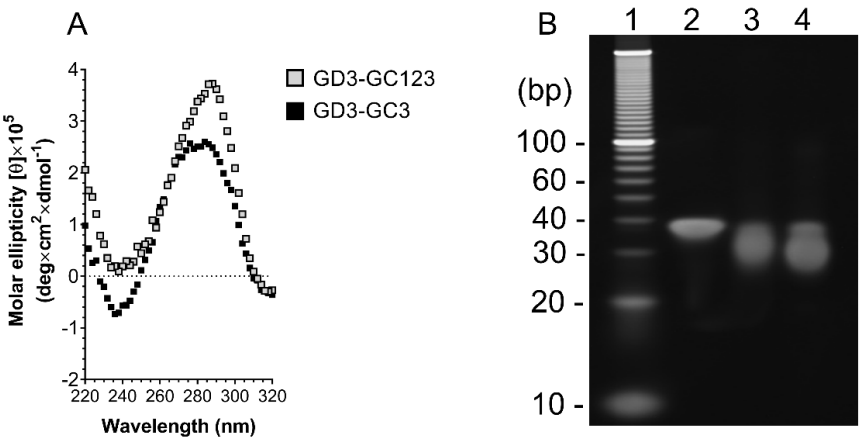

Figure 2.4 Replacing the sequence in the central loop of GD3 did not change the overall G4 folding. (A) Circular dichroism (CD) spectra of GD3-GC3 and GD3-GC123 at 25 °C in the presence of 4 mM K^+. (B) Polyacrylamide gel electrophoresis analysis in the presence of 4 mM K^+; lane 1, 10-bp DNA ladder; lane 2, ssODN38mer; lane 3, GD3; lane 4, GD3-GC123.

PAGE was used to identify the molecularity of G4. We used ODNs named ssODN22mer, ssODN30mer, and ssODN38mer as linear single-stranded reference ODNs having the same number of nucleotides as GD1, GD2, and GD3, respectively. PAGE analysis of CpG ODNs in the presence of K^+ in the running buffer (**Fig. 2.2C**) showed that GD1, GD2, and GD3 had higher mobilities than did ssODN22mer, ssODN30mer, and ssODN38mer, respectively, indicating that the designed CpG ODNs formed more compact structures than their linear counterparts. These results suggest that GD1, GD2, and GD3 form the monomeric G4 structure.[74] In addition, distinct bands of G4 ODNs were observed, suggesting that the molecules may be uniform in structure. In

the absence of K^+, the G4 CpG ODNs had similar mobilities as those of their linear ODN counterparts (**Fig. 2.1C**), suggesting that the G4 structures of the designed CpG ODNs were stabilized by monovalent cations. In summary, based on the results of TDS, CD, and PAGE analysis, we concluded that GD1, GD2, and GD3 form monomeric hybrid-type G4 structures.

The replacing the "TGT" central loop of TBA-3G (5'-$G_3T_2G_3TGTG_3T_2G_3$-3') (**Fig. 2.1A**) by sequences containing CpG motifs enabled the formation of intramolecular G4 CpG ODNs (**Fig. 2.2**). This monomeric G4 formation was observed not only in CpG ODNs with short central loops like GD1 (6-mer), but also in those with longer central loops such as GD2 (14-mer) and GD3 (22-mer). This is consistent with the findings that modifications in the loop regions of thrombin aptamer do not change the molecularity of the obtained G4.[54]

The G-tracts in the G4 ODNs are involved in G-quartet formation, while the nucleotides between these G-tracts usually form loop regions.[75] Therefore, the CpG motifs in our G4 CpG ODNs are most likely located in the loop region. A schematic diagram of the central loop in different possible monomeric hybrid G4 structures is shown in **Figure 2.5**.[76]

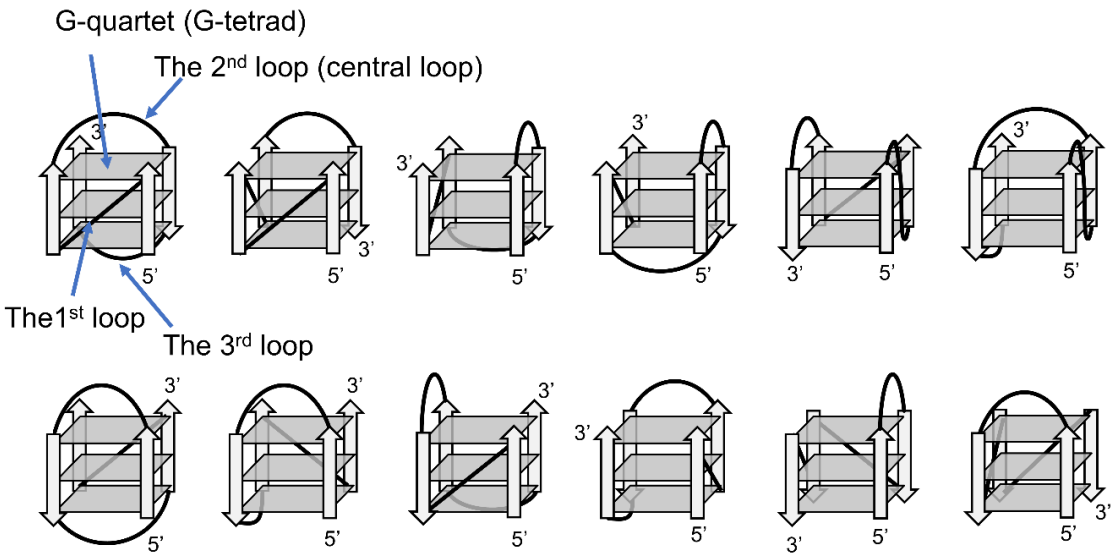

Figure 2.5 Schematic illustration of the possible hybrid G4 topologies.[76]

2.3.2. Thermodynamic stability of the designed CpG ODNs

In clinical applications or in experiments examining the immunostimulatory properties of CpG ODNs, the working temperature of CpG ODNs is 37 °C, so understanding the thermodynamic stability of the G4 structure at physiological temperature is important. The thermodynamics of G4 formation of the designed G4 CpG ODNs can be elucidated by analyzing their UV denaturation-renaturation profiles at 295 nm[69] as shown in **Figure 2.6A**. There was no hysteresis between the heating and cooling curves of the three G4 CpG ODNs. This is in keeping with the folding of the monomeric G4,[77] as indicated by PAGE. The melting temperature and van't Hoff thermodynamic parameters of GD1, GD2, and GD3 derived from their melting curves are presented in **Table 2.5**. GD1 (T_m = 62 °C; $\Delta G°_{vH310K}$ = -4.41 kcal·mol^{-1}) formed the most thermodynamically stable G4 with the highest melting temperature and the lowest Gibbs free energy among the designed G4 CpG ODNs. GD2 (T_m = 49 °C; $\Delta G°_{vH310K}$ = -2.42 kcal·mol^{-1}) is more thermodynamically stable than GD3 (T_m = 41 °C; $\Delta G°_{vH310K}$ = -0.63 kcal.mol^{-1}). The negative Gibbs free energies of all designed G4 CpG ODNs at 37 °C suggest that the folded species of the G4 structure are predominant at physiological temperature.[78]

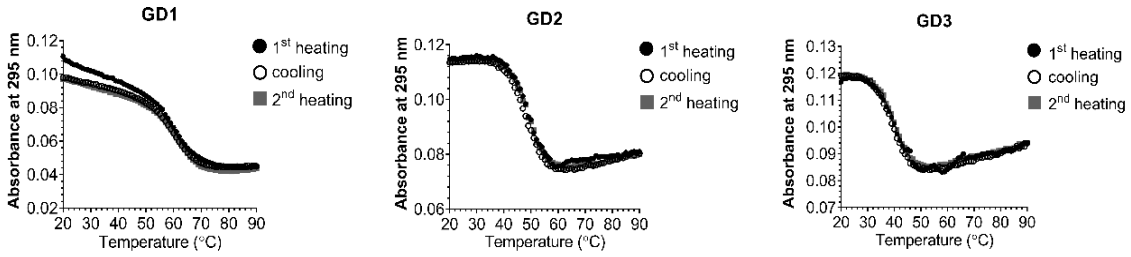

Figure 2.6 Ultraviolet (UV) and circular dichroism melting profiles of monomeric CpG oligodeoxynucleotides (ODNs). UV absorbance at 295 nm was monitored during the heating (closed circle), cooling (open circle), and reheating (square) process of GD1 (left panel), GD2 (center panel), and GD3 (right panel).

Table 2.5 Melting temperatures and van't Hoff thermodynamic parameters of G4 CpG ODNs[a]

ODNs	T_m (°C)[b]	$\Delta H°_{vH}$ (cal/mol^{-1})[c]	$\Delta S°_{vH}$ (cal.mol^{-1}.K^{-1})[d]	$\Delta G°_{vH310K}$ (kcal.mol^{-1})[e]
GD1	62	-59.0×10^3	-176.1	-4.41
GD2	49	-65.2×10^3	-202.5	-2.42
GD3	41	-52.9×10^3	-168.6	-0.63

[a]G4 CpG ODNs were prepared at a concentration of 2 μM in D-PBS with about 4 μM K^+ and 150 μM Na^+.

[b]The melting temperatures of G4 CpG ODNs, which were determined from the UV melting curves at 295 nm by the baseline method.

[c, d, e]$\Delta G°_{vH}$, $\Delta H°_{vH}$, and $\Delta S°_{vH}$ are the van't Hoff Gibbs free energy, enthalpy, and entropy changes upon folding, respectively.

The melting temperatures of GD1, GD2, and GD3 are in the range of 41–62 °C, which is comparable to those of other intramolecular G4 ODNs with two external short loops and one central long loop in the range of 6- to 22-mers.[55] The melting temperatures of the designed G4 CpG ODNs decreased with increasing central loop length, which is consistent with a previous study that demonstrated an inverse correlation between total loop length and melting temperature.[55] Despite this decrease, all the designed G4 CpG ODNs still had melting temperatures higher than 37 °C.

We also examined the CD melting profiles of G4 CpG ODNs. Subtraction of the spectra at high temperature from those at low temperature (**Fig. 2.7A**) shows that the largest differences in ellipticity occurred at 295 nm and 260 nm, so we monitored the CD melting curves at these wavelengths. The dramatic drops in the CD signal at 260 nm and 295 nm upon temperature increase (**Fig. 2.7A**) are suggestive of the denaturation of the hybrid G4 structure. The CD melting

and cooling curves of G4 CpG ODNs at 295 nm (**Fig. 2.7B**) and 260 nm (**Fig. 2.7C**) revealed a transition and were superimposable, suggesting a reversible intramolecular G4 structure.[79]

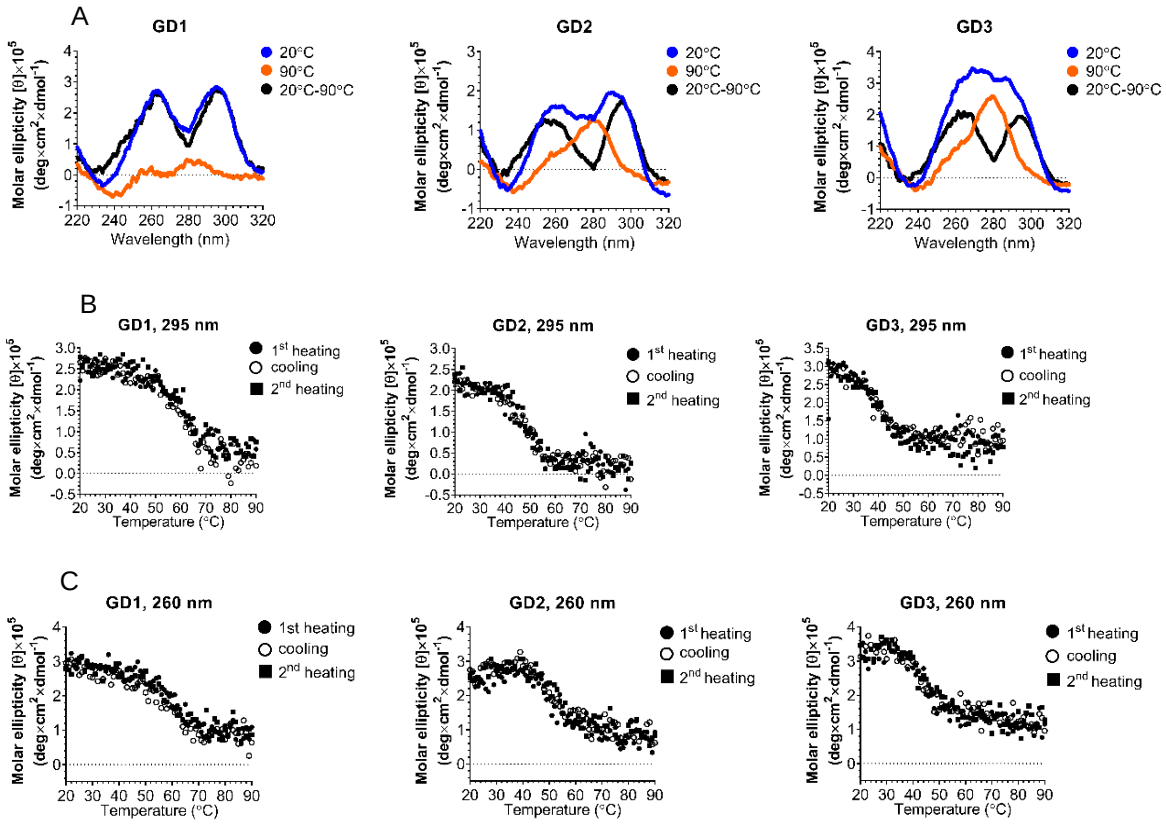

Figure 2.7 (A) Circular dichroism (CD) spectra at 20 °C and 90 °C, and CD-thermal difference spectra of GD1 (left panel), GD2 (center panel), and GD3 (right panel) in 2 μM Dulbecco's phosphate-buffered saline. CD melting profiles of G4 CpG oligodeoxynucleotides at (B) 295 nm and (C) 260 nm. The molar ellipticity at 295 and 260 nm was monitored during the heating (close circle), cooling (open circle), and reheating (close square) process of GD1 (left panel), GD2 (center panel), and GD3 (right panel).

2.3.3. Serum stability of monomeric G4 CpG ODNs

Nuclease resistance of the G4 CpG ODNs was examined and compared with that of a linear phosphodiester ODN, 2006_PD. The designed CpG ODNs were incubated with 50% or 18% FBS, and PAGE was performed to evaluate the amount of the remaining ODNs after incubation for 1, 2, 4, or 24 h (**Fig. 2.8**) in both serum concentrations. **Figure 2.8A** shows that,

after 1 h of incubation, 81%, 50%, and 32% of GD1, GD2, GD3, respectively, remained, while only 2% of 2006_PD remained. After 2 h of incubation, 76%, 35%, and 16% of GD1, GD2 and GD3, respectively, had not been degraded, while no 2006_PD remained. The designed G4 ODNs degraded more slowly than the linear phosphodiester ODN in 50% serum. As shown in **Figure 2.8B**, 62% of GD3 had not degraded when 18% FBS was used, while only 32% of GD3 remained after 1 h at the higher FBS percentage. This result indicates that higher FBS concentration leads to faster ODN degradation. The nuclease resistance tendency of these G4 CpG ODNs was similar at 50% and 18% FBS, showing nuclease resistance in the following order: GD1 > GD2 > GD3 >> 2006_PD.

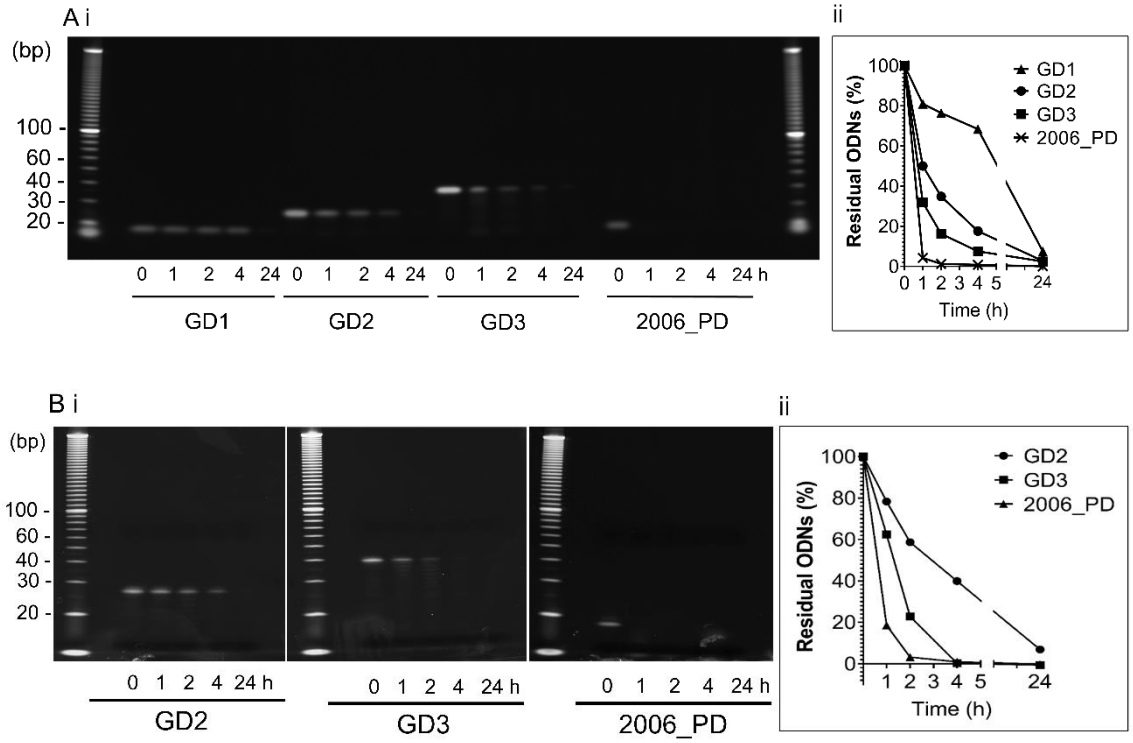

Figure 2.8 Stability of monomeric G4 CpG oligodeoxynucleotides (ODNs) in serum. Polyacrylamide gel electrophoresis (PAGE) analysis of GD1, GD2, GD3, and 2006_PD after incubation for 1, 2, 4, and 24 h with (A) 50% and (B) 18% fetal bovine serum (FBS). (A ii and B ii) Percentage of residual ODNs relative to ODN quantity at the start of incubation.

In section 2.3.2, we have demonstrated the predominance of the folded species of the G4 structure at physiological temperature, which indicates that CpG motifs form highly nuclease-resistant G4 structures and not fragile random coils under physiological conditions. As expected, G4 CpG ODNs had higher stability in serum than 2006_PD, a linear CpG ODN, although the G4 CpG ODNs in this study and 2006_PD contain entirely phosphodiester backbones. The lower nuclease resistance of GD3 than that of GD2 may be due to the longer central loop of GD3 behaving as a single-stranded ODN that is more easily attacked by nucleases.

2.3.4. Preservation of G4 structure in various conditions

The result from stability in serum (**Fig. 2.8**) shows that the G4 structure is important for the high nuclease resistance of CpG ODNs. However, the conformation of G4 structure depends on surrounding environment including monovalent cation concentration.[52] Meanwhile, during the process of G4 CpG ODNs may alternately expose to various environments including extracellular fluid, early endosome, late endosome and lysosome, which generally have differential pH, potassium and sodium cation (K^+ and Na^+) concentration as shown in **Figure 2.9**.[80–82] The high concentrations of Na^+ in extracellular fluid decrease along the endocytic pathway, while luminal concentration of K^+ higher than its extracellular concentration. Additionally, process of endosomal maturation is characterized by an increase in luminal acidification, with the luminal pH of early endosome, late endosome, and lysosome may be 6.5, 5.5, and 4.5, respectively.[82]

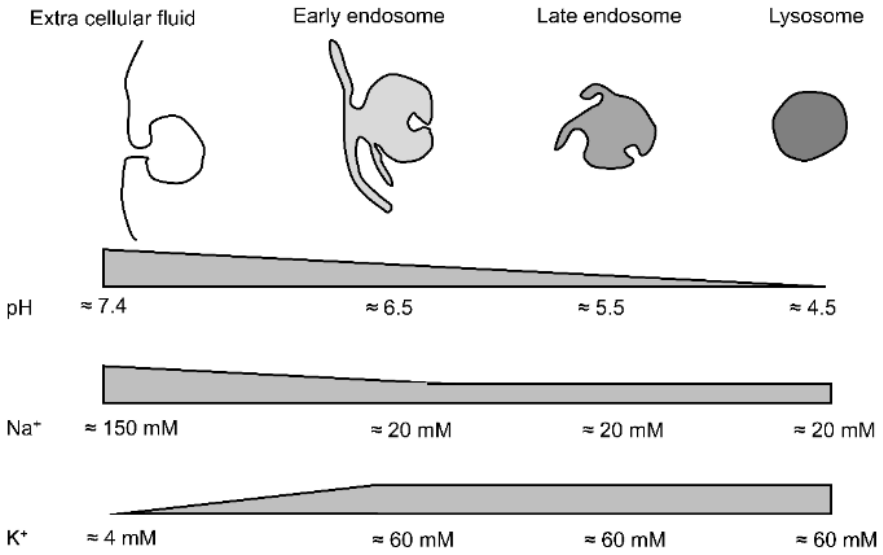

Figure 2.9 Summary of changes in pH and monovalent cationic composition of the endosomal lumen along the endocytic progress.[80–82]

The G4 formation of designed CpG ODNs in D-PBS buffer, which has pH 7.34, and contains 4 mM K^+ and 150 mM Na^+, similar to extracellular fluid,[83] has been confirmed in the previous section (**Fig. 2.2**). In this section, we estimate if the G4 formation maintains in the buffers similar to intracellular context. We prepared GD2 and GD3 in D-PBS buffer, then diluted them in the different buffers, containing 60 mM K^+ and 20 mM Na^+ at pH 6.5, 5.5 and 4.5. CD spectra of GD2 and GD3 in these buffer shows a trough at 240 nm, and two positive peaks at around 265 and 290 nm, which are characterized for hybrid-type G4 (**Fig. 2.10 A-C**). In addition, PAGE analysis using the gel and running buffer supplementing with 150 mM K^+ (**Fig. 2.10 D**) shows that GD2 and GD3 migrate faster than ss30mer, and ss38mer, respectively, indicating that GD2, and GD3 still form monomeric G4 at high K^+ concentration. Taken together, these results suggest that the designed CpG ODNs may maintain the G4 formation during the process of TLR9 activation.

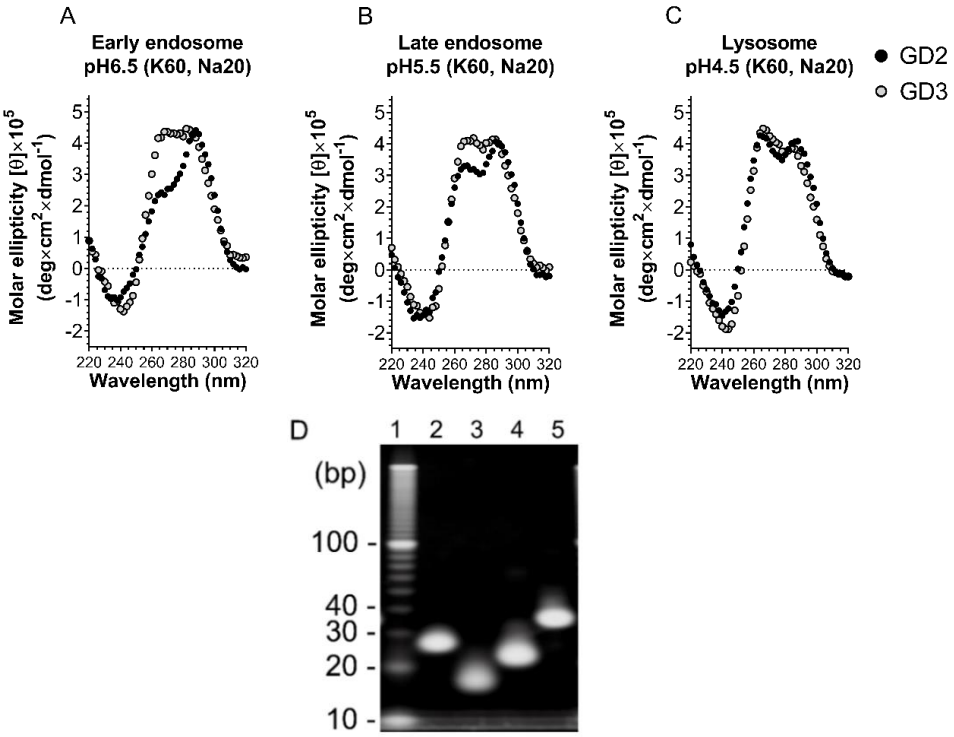

Figure 2.10 G4 structure of designed CpG ODNs is preserved in various environments. CD spectra of GD2 and GD3 in **(A)** 2-(N-morpholino)ethanesulfonic acid (MES) buffer 10 mM pH6.5 buffer containing 60 mM K^+, 20 mM Na^+ (K60, Na20); **(B)** MES buffer 10 mM pH5.5 (K60, Na20); **(C)** Acetate buffer 10 mM pH4.5 (K60, Na20). **(D)** Polyacrylamide gel electrophoresis analysis in the presence of 150 mM K^+; lane 1, 10-bp DNA ladder; lane 2, ssODN30mer; lane 3, GD2; lane 4, GD3; lane 5, ssODN38mer.

2.3.5. Intracellular uptake of monomeric G4 CpG ODNs

Cellular uptake of CpG ODNs is requisite for TLR9 activation, since TLR9 locates in endosomes inside cells. Therefore, we next examined cellular uptake of designed G4 CpG ODNs using cytometry analysis. MFI of the cells incubated at 4°C demonstrates for ODNs that bind to cell surface, while MFI of the cells incubated at 37°C demonstrates for both cell-surface bound ODNs and internalized ODNs. Histograms showing fluorescence of the cells treated with G4 CpG ODN at 4 °C and 37 °C are displayed in **Figure 2.11A i and Figure 2.11A ii**, respectively. **Figure 2.11B** shows that, at 4°C, the MFI values of cells treated with GD2, and GD3 are 4 times and 10

times higher than that of the cells incubated the linear ODN. **Figure 2.11B** also shows that the MFI values of cells treated with all Cy5 labelled ODNs at 37 °C were greater than those at 4 °C, indicating that these ODNs were taken up into the cells. The difference between MFI at 37°C and that at 4°C ($\Delta MFI_{37°C-4°C}$) was calculated as measure of internalized Cy5 labelled ODN. As shown in **Figure 2.11C**, the $\Delta MFI_{37°C-4°C}$ of cells incubated with $GD3^{5'Cy5}$ was 1.5 times higher than the $\Delta MFI_{37°C-4°C}$ of those incubated with $2006\_PD^{5'Cy5}$, suggesting that monomeric G4 increased cellular uptake of CpG ODNs.

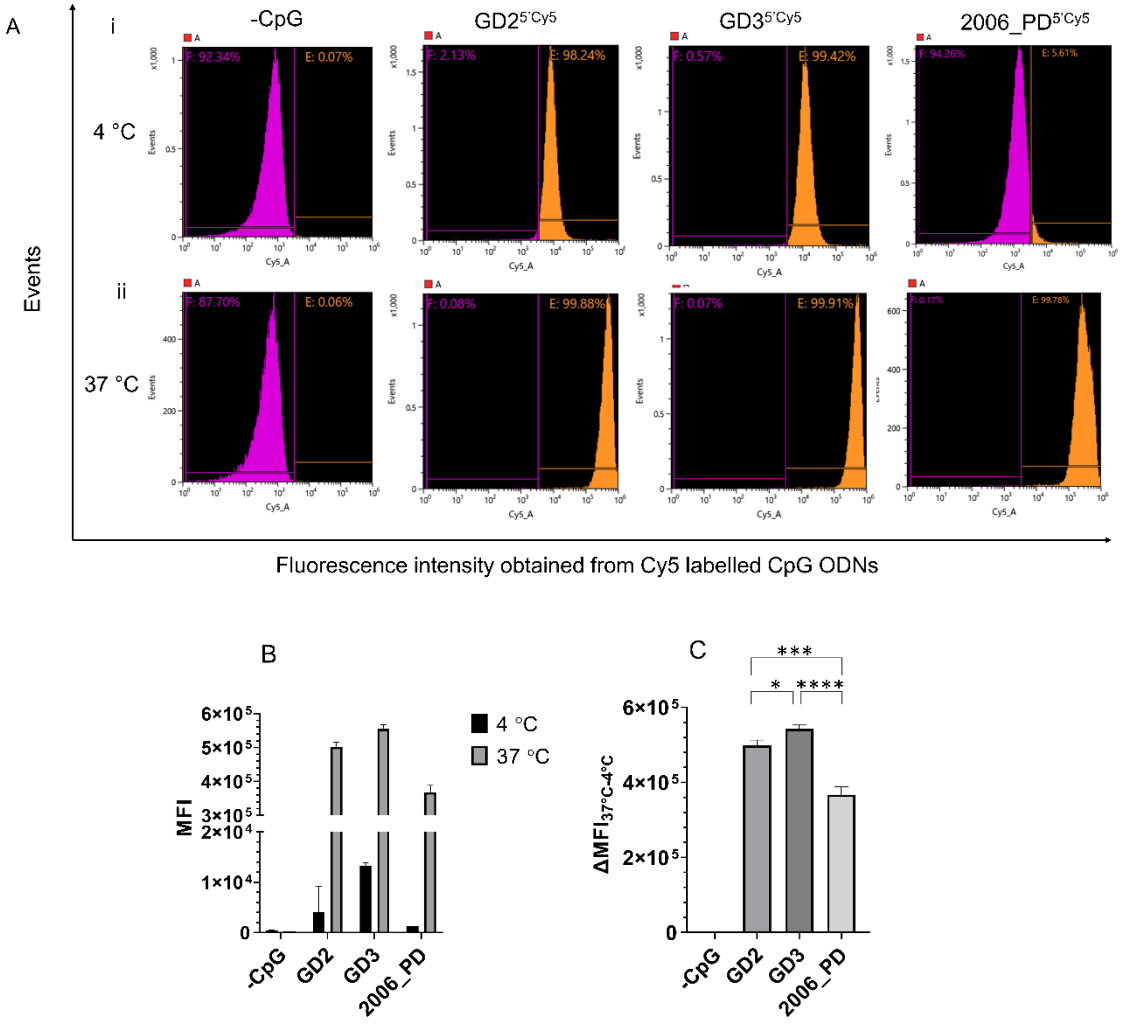

Figure 2.11 Uptake of Cy5 labelled CpG ODNs in RAW264 cells. (A) Histogram analysis of fluorescence intensity at (i) 4 °C and (ii) 37 °C. (B) Mean fluorescence intensity (MFI) of the cells incubated at 37 °C and 4 °C; (C) Internalized Cy5 labelled CpG ODNs were measured by

$\Delta MFI_{37°C-4°C}$. RAW264 cells were incubated with 5 μM GD2, GD3 or 2006_PD labeled at the 5'end by Cy5 for 2 h. Data represent mean ± SD (n = 5). ****p < 0.0001, ***p < 0.001, **p < 0.01, *p < 0.05, ns (not significantly different) p > 0.05 (one-way ANOVA, Tukey's multiple comparisons test).

The observed increase in cellular uptake of ODNs by G4 in our study is consistent with previous study, which reports that aptamers forming G4 show higher cellular uptake compared with non-G4 sequences.[84] Various pathways have been proposed for the internalization of G4 ODNs, consisting of endocytosis, macropinocytosis and other unknown mechanisms. The mechanism by that G-quadruplex structure increase cellular uptake varies depending on the cell type.[84] Because receptor-mediated uptake is significantly restrained at 4 °C, we can only observe the ligand-receptor binding at the cellular surface.[85] The increase in cellular uptake by G4 associated with increase in cell surface binding indicates that the enhanced uptake of the G4 CpG ODNs may via enhanced receptor-mediated endocytosis.

2.3.6. Endosomal localization of G4 CpG ODNs

To examine the endosomal distribution of G4 CpG ODNs, RAW264 cells stimulated with $GD3^{5'Cy5}$ or $2006\_PD^{5'Cy5}$ before being stained with Early Endosome Marker (anti-EEA1 Ab) and Lysosome Marker (anti-LAMP1 Ab)). Then, the cells were incubated with an Alexa488 labelled secondary antibody (2^{nd} $Ab^{Alexa488}$), and confocal images of the cells were acquired to examine the colocalization of G4 CpG ODN^{Cy5} with LAMP1 and EEA1.[86] **Figure 2.12A** shows that there are a few colocalization of $GD3^{5'Cy5}$ with EEA1. **Figure 2.12B** shows that $GD3^{5'Cy5}$ were mainly distributed in lysosomes at 4 h-post stimulation, as it showed a strong colocalization with LAMP1. Honda et al. report that in plasmacytoid dendritic cell, CpG-B-Cy5 merged with lysosomal marker but not endosomal marker 90 min after its delivery, while CpG-A-Cy5 did not merge with the lysosomal marker even 5 h after delivery.[14] This suggests that GD3 has similar endosomal distribution with class B CpG ODNs.

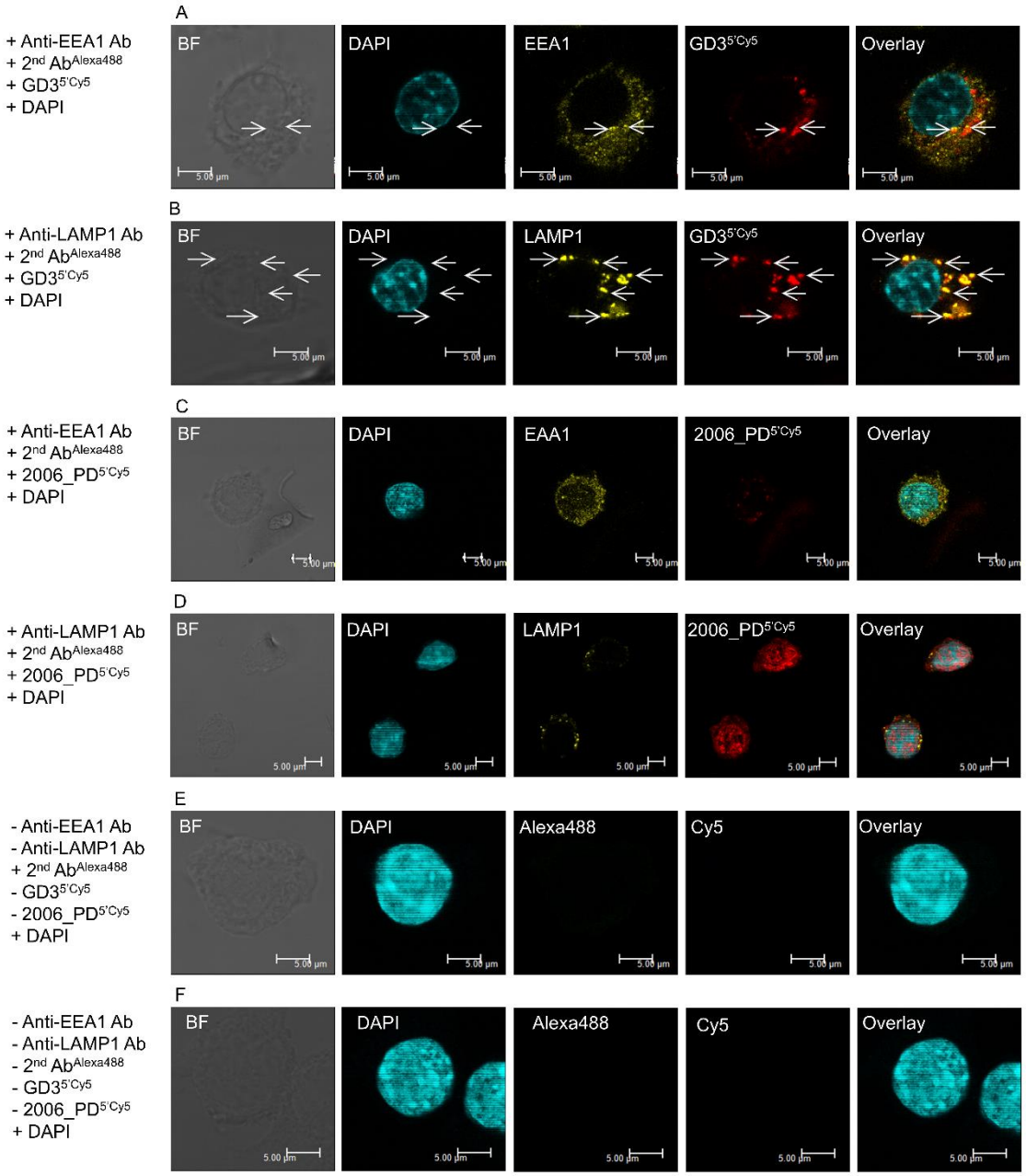

Figure 2.12 Endosomal localization of G4 CpG ODNs in RAW264 cells. (A) There are little colocalization of GD3$^{5'Cy5}$ with early endosome. (B) GD3$^{5'Cy5}$ strongly colocalizes with lysosome. (C, D) 2006_PD$^{5'Cy5}$ distributed in cytoplasm and nucleus. (E) The Alexa488 labelled secondary antibody (2nd Ab^{Alexa488}) is specific to the primary anti-EEA1 or anti-LAMP1 Ab. (F) The observed fluorescent signal is specific to the signal emitted from the 2nd Ab^{Alexa488}. RAW264 cells were incubated with (A, B) 4 μM GD3$^{5'Cy5}$, (C, D) 2006_PD$^{5'Cy5}$, or medium for 4 h. To visualize endosomes or lysosomes the cells were incubated with (A, C) Early Endosome Marker (anti-

EEA1 Ab), or (B, D) Lysosome Marker (anti-LAMP1 Ab) for 1 h, then the cells were incubated with the 2nd $Ab^{Alexa488}$ for 1 h. (E) The cells were incubated without anti-EEA1 and anti-LAMP1 Ab, but with 2nd $Ab^{Alexa488}$. (F) The cells were incubated without anti-EEA1 Ab, anti-LAMP1 Ab, and 2nd $Ab^{Alexa488}$. All confocal images were acquired with the same laser intensity and gaining condition. GD3, and 2006_PD were labeled with Cy5 are shown in red. Immunostaining of the endosome marker anti-EEA1 or lysosome marker anti-LAMP1 is shown in yellow. BF, bright-field images; DAPI, 4′,6-diamidino-2-phenylindole, a nucleus marker.

In **Figure 2.12C, D**, fluorescence from $2006\_PD^{5'Cy5}$ appeared to distribute in all areas including cytosol and nucleus. Due to its low nuclease resistance, $2006\_PD^{5'Cy5}$ is degraded in 4 h, and free Cy5 dye molecules may migrate from the intracellular compartments to the cytosol and nucleus. As shown in **Figure 2.12E**, the signals of Alexa488 do not appear in the cells not incubated with anti-EAA1 and anti-LAMP1 Ab at the same laser intensity and gaining condition that used to acquired **Figure 2.12A-D**, suggesting that the 2nd $Ab^{Alexa488}$ is specific to the primary anti-EEA1 or anti-LAMP1 Ab. In addition, the fluorescent signal is not observed in the cells incubated without anti-EEA1 Ab, anti-LAMP1 Ab, and 2nd $Ab^{Alexa488}$ (**Fig. 2.12F**), indicating that the observed fluorescent signal is specific to the signal emitted from the 2nd $Ab^{Alexa488}$, not from the background.

2.3.7. Localization of G4 CpG ODNs with TLR9

Because CpG ODNs have to encounter TLR9 to activate them, we examine the ability of designed G4 CpG ODNs to co-localized with TLR9 in cell compartments. The spatial distribution of G4 CpG ODNs in mammalian cells were visualized in 293T cells transfected with hTLR9 tethered to YFP ($hTLR9^{YFP}$). GD3 labeled at the 5'-end by Cy5 ($GD3^{5'Cy5}$) were used to show localization of G4 CpG ODNs in mammalian cells. As shown in **Figure 2.13**, $TLR9^{YFP}$ was expressed in intracellular compartments in 293T cells. Fourteen hours after addition of CpG ODNs in 293T cells expressed $hTLR9^{YFP}$, $GD3^{5'Cy5}$ was observed inside the cell. The Cy5 signals did not appear to be evenly distributed but appeared to be locally concentrated. This suggests that

the G4 CpG ODNs were taken up into cells and likely localized in intracellular compartments rather than in cytosol. In addition, GD3 showed colocalization with hTLR9^{YFP}.

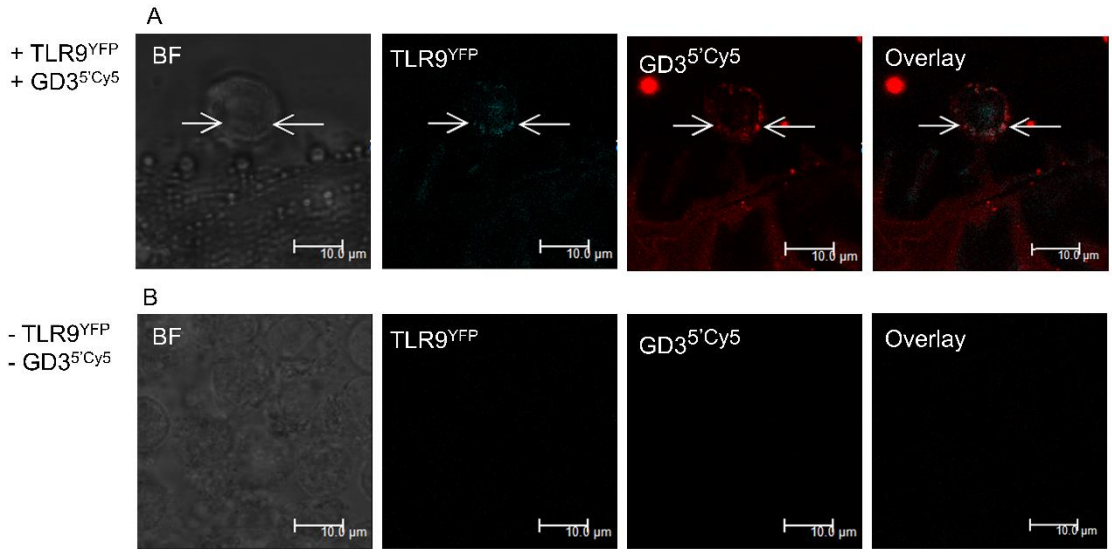

Figure 2.13 Co-localization of GD3$^{5'Cy5}$ with hTLR9^{YFP} in 293T cells. (A) Human TLR9^{YFP} was transfected into 293T cells. After 36 h, the cells were treated with 4 µM GD3$^{5'Cy5}$. The cellular distribution of GD3 and TLR9 was analyzed after 14 h. Arrows indicate areas where GD3$^{5'Cy5}$ co-localized with TLR9^{YFP}. (B) The control 293T cell without transfection of TLR9^{YFP} and stimulation with GD3$^{5'Cy5}$. BF, bright-field images.

In addition, the intracellular localization of GD3$^{5'Cy5}$ and TLR9 marker in mouse macrophage RAW264 cells, which express TLR9 endogenously, was examined. RAW264 cells were stimulated with 4 µM GD3$^{5'Cy5}$ before being stained with an anti-mouse (m) TLR9 antibody. Then, the cells were incubated with an 2nd Ab^{Alexa488} before collecting confocal images. In **Figure 2.14A**, anti-TLR9 appear to localize in cytoplasm and in small intracellular vesicles. GD3$^{5'Cy5}$ appears to colocalize with the anti-mTLR9 antibody only in a few areas indicated by arrows, while most of GD3$^{5'Cy5}$ show a different distribution with anti-TLR9 antibody. The intracellular localization of TLR9 and CpG ODNs is time-dependent, so additional experiments need to be done to examine the colocalization of TLR9 and GD3$^{5'Cy5}$ at various time points such as 30 min,

1 h, 2 h, and 14 h after stimulation. Futthermore, an endosomal compartment marker should be used to examine the subcellular localization of TLR9 in RAW264 at those time points.

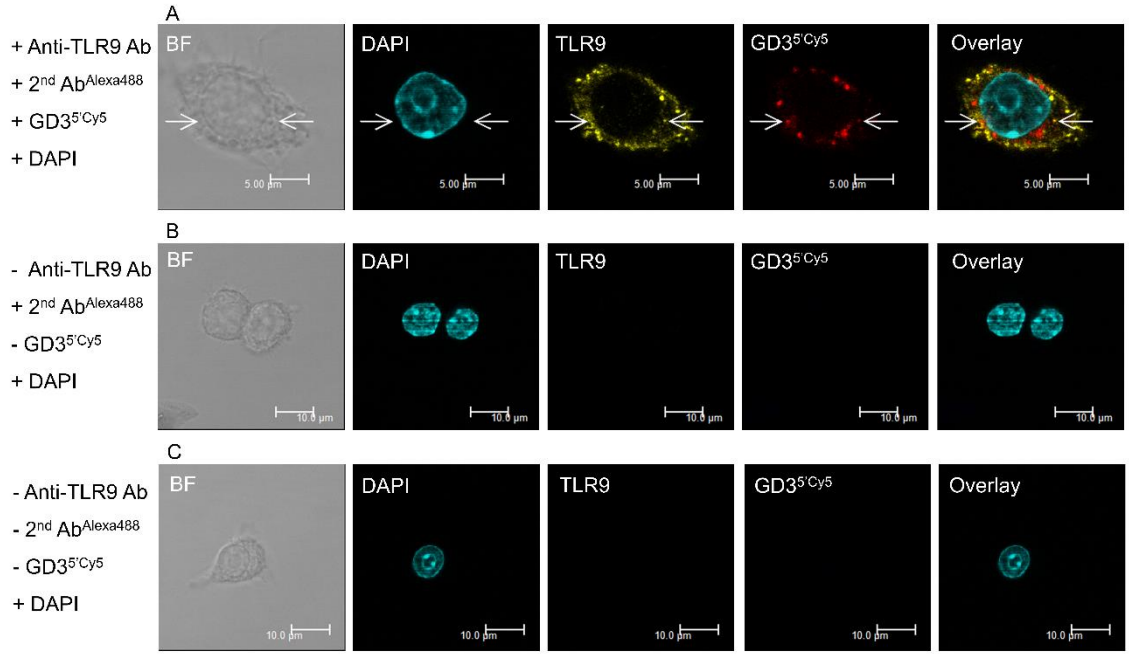

Figure 2.14 Intracellular distribution of GD3 and TLR9 in RAW264 cells. (A) RAW264 cells were stimulated with 4 μM $GD3^{5'Cy5}$ for 4 h before being fixed with 4% paraformaldehyde and stained with anti-mouse TLR9. Cells were incubated with an Alexa488 labelled secondary antibody (2^{nd} $Ab^{Alexa488}$) before collecting confocal images. (B) The control RAW264 cells without incubation with anti-mTLR9 antibody and stimulation with $GD3^{5'Cy5}$. (C) The control RAW264 cells without incubation with anti-mTLR9 antibody, 2^{nd} $Ab^{Alexa488}$, and stimulation with $GD3^{5'Cy5}$. BF, bright-field images; DAPI, 4′,6-diamidino-2-phenylindole, a nucleus marker.

2.3.8. TLR9-agonistic properties of monomeric G4 CpG ODNs

TLR9 activation by G4 CpG ODNs was examined through observation of NF-κB-driven luciferase activity in human TLR9-expressing cells (293XL-hTLR9) (**Fig. 2.15A**). GD2 and GD3 had strong NF-κB-regulated luciferase activities, while GD1 showed little NF-κB activity. Non-TLR9-expressing cells (293XL-null) did not show NF-κB activity after stimulation with G4 CpG ODNs, indicating that NF-κB induction by G4 CpG ODNs is regulated by TLR9 in mammalian

cells. The binding ability of G4 CpG ODNs to ectodomains of mouse TLR9 was assessed by immunoprecipitation (**Fig. 2.15B**). The comparable intensities of the TLR9 bands in SDS-PAGE ensured that the amounts of mTLR9Fc bound to protein-G-conjugated beads were similar in all samples. PAGE analysis of the eluted solutions indicated that GD2 and GD3 bound to mTLR9Fc. These results indicate that GD2 and GD3 are not only able to bind TLR9 but are also able to activate the TLR9-dependent NF-κB signaling pathway.

In addition, the binding between the G4 CpG ODNs and TLR9 (**Fig. 2.15B**) suggests that the CpG motif in the loop region comes into contact with TLR9.

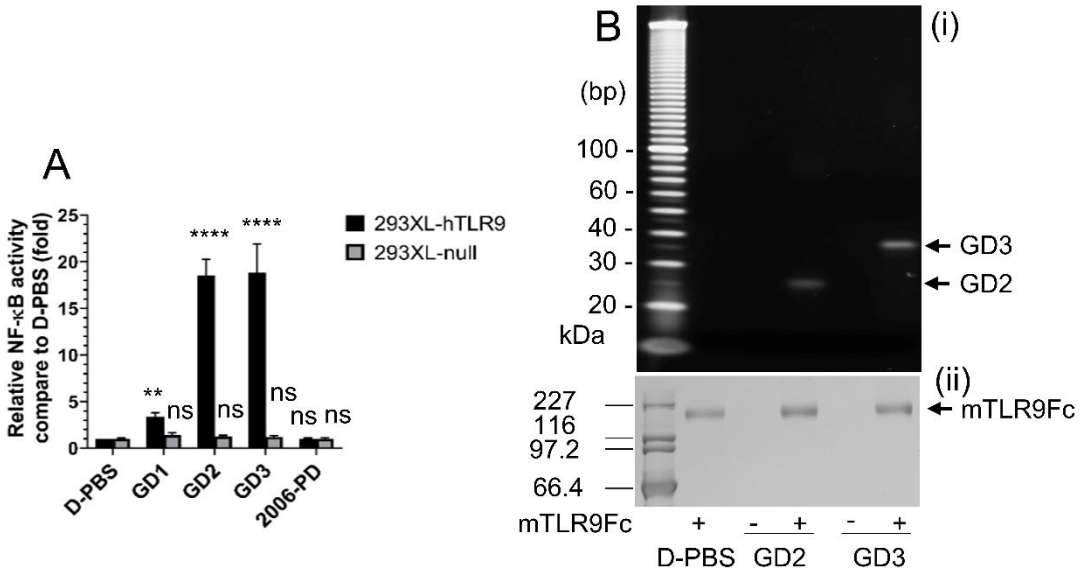

Figure 2.15 TLR9-agonistic properties of monomeric CpG oligodeoxynucleotides (ODNs). (A) NF-κB activation in human TLR9-expressing cells (293XL-hTLR9) was analyzed 24 h after stimulation with G4 CpG ODNs. Data represent mean ± SD (n = 5). ****p < 0.0001, ***p < 0.001, **p < 0.01, *p < 0.05, ns (not significantly different from D-PBS) p > 0.05, two-way ANOVA, Sidak's multiple comparisons test. (B) Immunoprecipitation was performed to examine the binding of G4 CpG ODNs to mouse TLR9 at pH 6.5. (i) The DNA bound to the beads was examined by polyacrylamide gel electrophoresis (PAGE) (ii) mTLR9Fc bound to protein-G-conjugated beads was detected by SDS-PAGE.

TLR9 binding and NF-κB production are two important events in the TLR9-mediated signaling pathway induced by CpG ODNs. Upon binding to agonistic CpG ODNs, the ectodomain of the TLR9 dimers undergoes a conformational change. This leads to allosteric changes in the TIR cytoplasmic domains,[11] enabling the recruitment of the adaptor protein MyD88, which triggers the NF-κB signaling pathway. After translocation into the nucleus, NF-κB activates the transcription of inflammatory cytokine genes.[5] The designed G4 CpG ODNs induced NF-κB activity in TLR9-expressing cells and were able to bind TLR9, suggesting the role of G4 CpG ODNs as TLR9 agonists.

2.3.9. Stimulation of RAW264 cells

The immunomodulatory activities of monomeric G4 CpG ODNs were evaluated by examining relative transcript level of cytokines produced in mouse macrophage-like RAW264 cells. The relative transcript levels cytokines expressed by RAW264 cells exposed to GD1, GD2, and GD3 are shown in **Figure 2.16A**. We observed cytokine induction by GD2 and GD3, which have two and three CpG motifs, respectively, in the central loop of the G4 structure. The levels of *IL-6*, *IL-12*, and *IFN-β* mRNAs induced by GD1 were the same as those in the negative control. We also examined the level of IL-6 and IFN-β proteins secreted into the culture medium and verified the correlation of the transcript level with secretion level of cytokines in RAW264 cells (**Fig. 2.16B**). GD3 induced higher cytokine transcript levels than did GD2 (**Fig. 2.16B**). Both GD2 and GD3 exhibited concentration-dependent immunostimulatory effects (**Fig. 2.17A**). The effect of incubation time on *IL-6*, *IL-12*, and *IFN-β* mRNA induction in mouse macrophage-like RAW264 cells stimulated with G4 CpG ODNs is shown in **Figure 2.17B**. GD1 showed a similar cytokine induction as that of D-PDS during the examined time period. In the cases of GD2 and GD3, *IL-6* mRNA increased with time and was not saturated within 48 h, while *IL-12* and *IFN-β* mRNA were saturated within 24 h and 4 h, respectively.

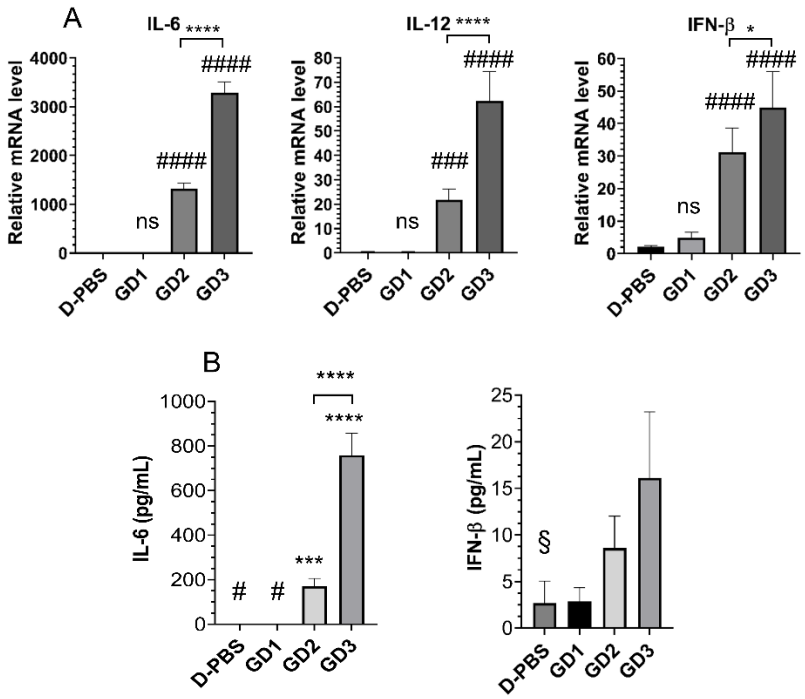

Figure 2.16 Cytokine induction in mouse macrophage-like RAW264 cells stimulated with G4 CpG oligodeoxynucleotides. (A) Relative mRNA levels of *IL-6*, *IL-12*, and *IFN-β* in mouse macrophage-like RAW264 cells after 24 h of stimulation with 4 μM GD1, GD2, or GD3; (B) Level of IL-6 and IFN-β secreted into the culture medium by mouse macrophage-like RAW264 cells after 24 h of stimulation with 4 μM GD1, GD2, or GD3. Culture media were collected and assayed by ELISA for each cytokine. Data represent mean ± SD (n = 5). ****p < 0.0001, ***p < 0.001, **p < 0.01, *p < 0.05, ns (not significantly different) p > 0.05 (*, one-way ANOVA, Tukey's multiple comparisons test for comparison with other groups; #, Dunnett's multiple comparisons test for comparison with the Dulbecco's phosphate-buffered saline [D-PBS] control group).

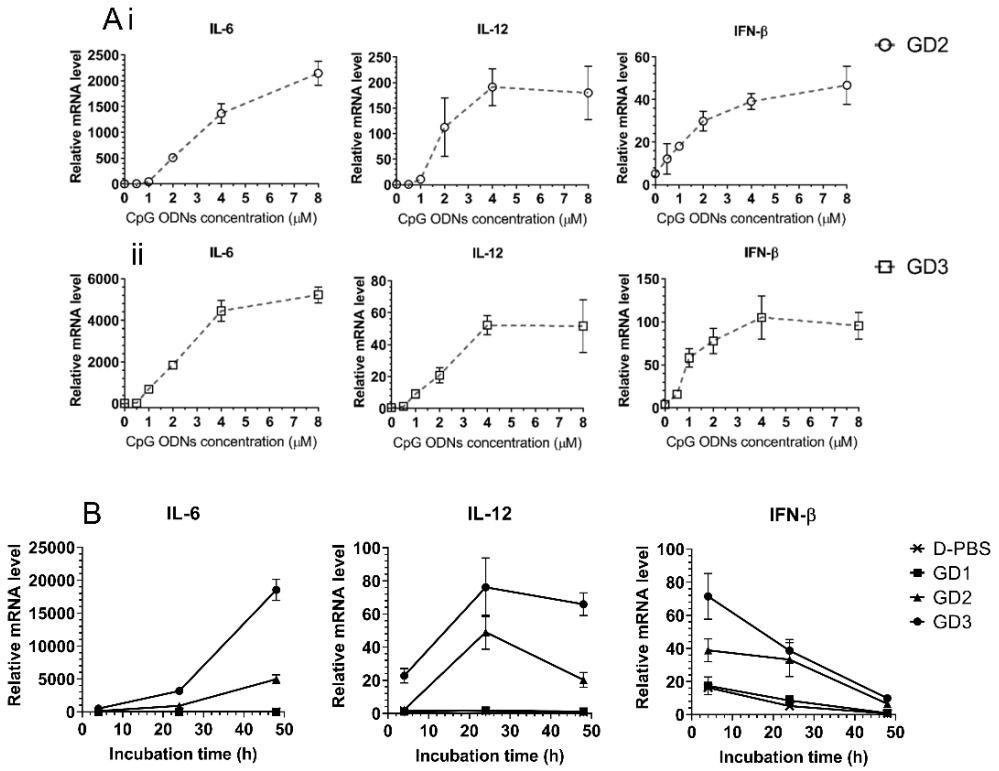

Figure 2.17 (A) Oligodeoxynucleotide (ODN) concentration-dependent induction of cytokines in mouse macrophage-like RAW264 cells stimulated with (i) GD2 and (ii) GD3 at 0, 0.5, 1, 2, 4, and 8 μM. *IL-6*, *IL-12*, and *IFN-β* mRNA in RAW264 cells were examined after 24 h of stimulation. Data represent mean ± SD (n = 5). (B) Effect of incubation time on induction of cytokines in mouse macrophage-like RAW264 cells stimulated with G4 CpG ODNs at 4 μM. *IL-6*, *IL-12*, and *IFN-β* mRNA in RAW264 cells were examined after 4, 24, and 48 h of stimulation. Data represent mean ± SD (n = 4). D-PBS, Dulbecco's phosphate-buffered saline.

TLR9 specifically recognizes unmethylated CpG motifs, which is the main difference between bacterial and mammalian DNA,[6] so methylation of the CpG motif is reported to abrogate the activity of CpG DNA.[87] The impact of methylation on the immunostimulatory properties of G4 CpG ODNs was examined. According to the CD spectra, cytosine methylation of all CpG motifs in GD2 and GD3 did not change the G4 structure of GD2 and GD3 (**Fig. 2.18A**). As displayed in **Figure 2.18B**, methylation leads to the abrogation of cytokine induction by G4 CpG

ODNs in RAW264 cells. These results suggest that the G4 structure alone does not have immunostimulatory properties.

Modification, such as methylation, in the central loop containing the CpG motifs dramatically changes the immunostimulatory activity of the G4 CpG ODNs (**Fig. 2.18B**), so this region has a key role in TLR9 stimulation.

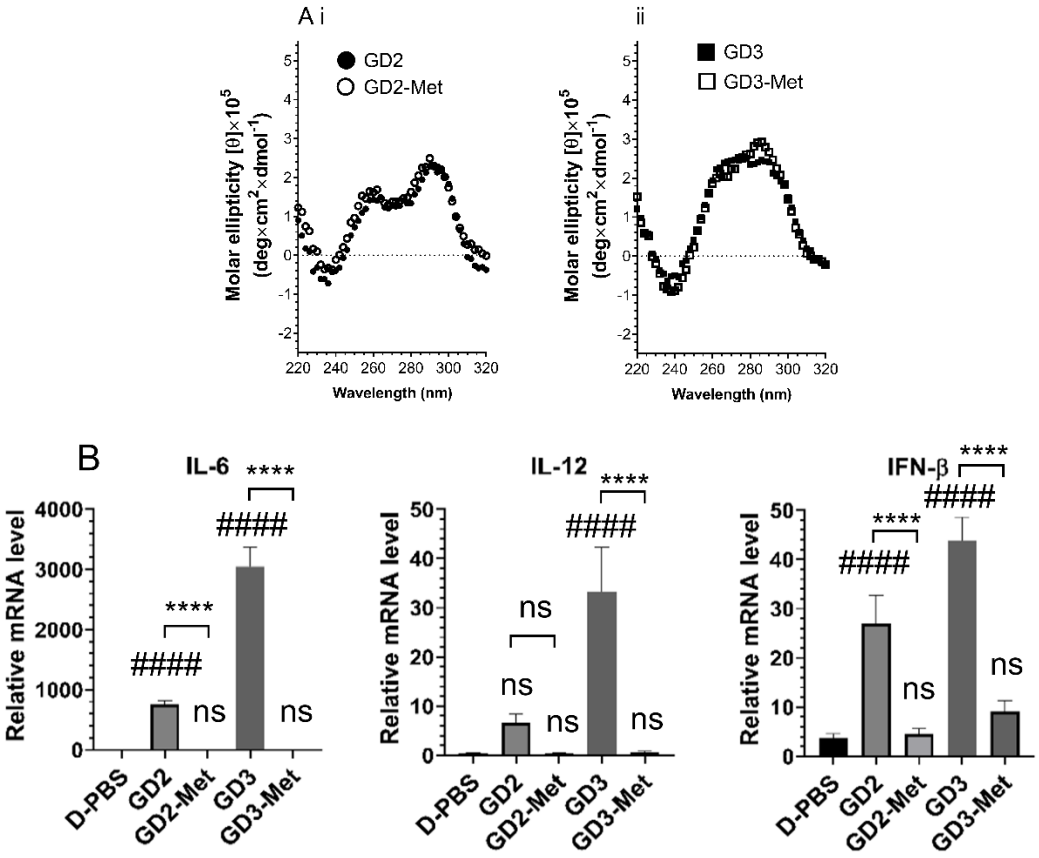

Figure 2.18 (A) Circular dichroism spectra of (i) GD2 and methylated variants, and (ii) GD3 and methylated variants. (B) Methylation of cytosine in all the CpG motifs of GD2 and GD3 led to the abrogation of *IL-6*, *IL-12*, and *IFN-β* mRNA induction in RAW264 cells. Data represent mean ± SD ($n = 5$). ****$p < 0.0001$, ***$p < 0.001$, **$p < 0.01$, *$p < 0.05$, ns (not significantly different) $p > 0.05$ (*, one-way ANOVA, Tukey's multiple comparisons test for comparison with other groups; #, Dunnett's multiple comparisons test for comparison with the Dulbecco's phosphate-buffered saline [D-PBS] control group).

2.3.10. Responses of human PBMCs to G4 CpG ODNs

Compared with mice, humans have more stringent regulation of TLR9 activation since TLR9 expression is restricted to B cells and pDCs. In addition, human TLR9 requires dual recognition of CpG and 5'-xCx motifs for full activation.[88] Therefore, in this study, the immunostimulatory potential of G4 CpG ODNs in humans was also evaluated by measuring cytokine secretion from primary human immune cells. **Figure 2.19A** shows the IL-6 induction by G4 CpG ODNs at different incubation times. For both GD2 and GD3, the IL-6 production reached a peak at 24 h and decreased afterwards. In all cases, GD3 induced significantly higher IL-6 from PBMCs than GD2 did. Furthermore, both GD2 and GD3 also induced IFN-γ at 48 hours; however, the secreted amount of IFN-α was lower than the limit of detection (**Fig. 2.19B**). **Figure 2.19C** shows the IL-6 and IFN-γ induction of G4 CpG ODNs in comparison with the control, 2006_PD. 2006_PD is a conventional CpG ODN consisting of three CpG motifs (GTCGTT) with a random (linear) structure. The sequence located in the loop region of GD3 is similar to that of 2006_PD. GD3 was more efficient in inducing IL-6 and IFN-γ than was 2006_PD. GD3 may have a higher potential in therapeutic application compared with linear phosphodiester CpG ODNs.

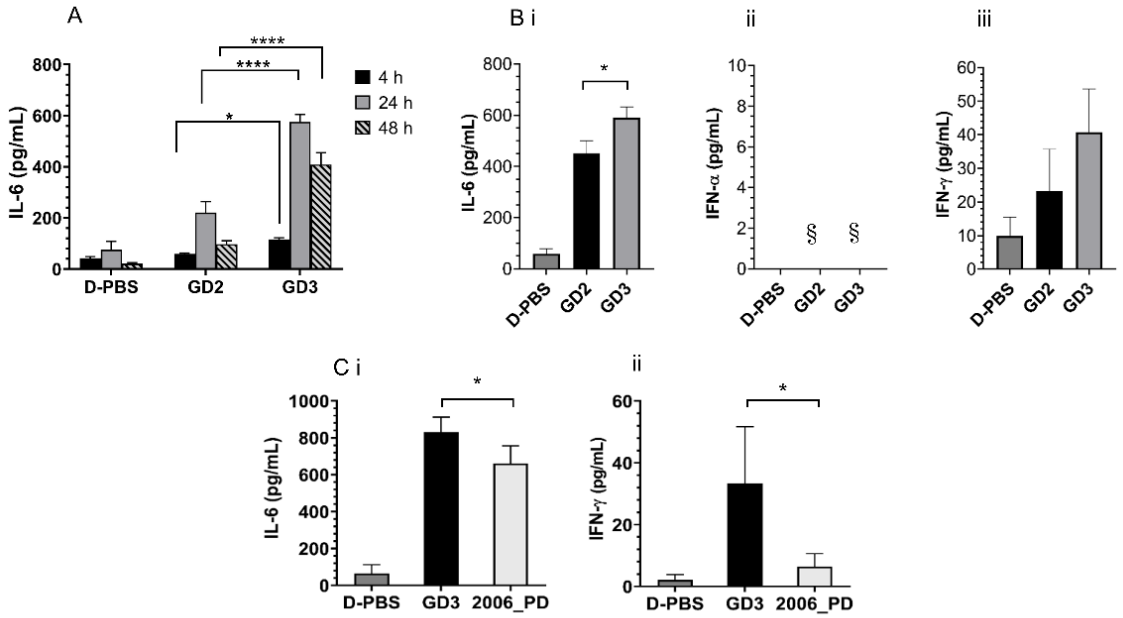

Figure 2.19 G4 CpG oligodeoxynucleotide (ODN)-induced cytokine production in human peripheral mononuclear cells (PBMCs). (A) Effect of incubation time on cytokine induction of G4 CpG ODNs in human PBMCs. Supernatants from human PBMCs incubated with 8 μM G4 CpG ODNs for 4, 24, and 48 h were assayed by ELISA for IL-6. (B) G4 CpG ODNs induced IL-6 and IFN-γ but not IFN-α production in human PBMCs. Supernatants from human PBMCs incubated with 8 μM G4 CpG ODNs for 48 h were assayed by enzyme-linked immunosorbent assays for IL-6, IFN-α, and IFN-γ. (C) Cytokine induction of G4 CpG ODNs in comparison with positive control 2006_PD. Supernatants from human PBMCs incubated with 8 μM GD3 or 2006_PD for 24 h were assayed by ELISA for IL-6 and IFN-γ. Data represent mean ± SD (n = 4). ****p<0.0001, *p < 0.05, ([A] two-way ANOVA, Tukey's multiple comparisons test; [B] and [C] one-way ANOVA, Tukey's multiple comparisons test).§: lower than limit of detection (3.9 pg/mL).

GD2 and GD3 promote IL-6 and IFN-γ production in human PBMCs, indicating their potential in activating human primary immune cells. These cytokines play important roles in the innate and adaptive immune response. IL-6 is a pro-inflammatory cytokine, which can induce the maturation of B cells into antibody-secreting cells. Meanwhile, IFN-γ, a type II IFN, activates macrophages, induces the differentiation of helper T cells into type 1 helper T cells, and enhances

immunoglobulin isotype switching to IgG_2a.[89,90] The ability of GD2 and GD3 to promote IL-6 and IFN-γ production in human PBMCs suggests their potential as vaccine adjuvants.

2.3.11. Immunostimulatory properties of G4 CpG ODNs in mice

As G4 formation is useful for enhancing the immunostimulatory activity of CpG ODN, the immunostimulatory properties of GD3 *in vivo* were evaluated in mice (**Fig. 2.20A**). Before injection, blood was collected from all mice to examine initial cytokine production. The result from ELISA shown that the plasma concentrations of all examined cytokine before injection were lower than the limit of detection of the assays (3.9 pg/mL for IL-6, and 7.8 pg/mL for IL-12p70, and IFN-γ). The plasma IL-12p70, and IFN-γ induced by GD3 and 2006_PD were lower than the detection limits. **Figure 2.20B** shows the IL-6 concentration in plasma induced by intraperitoneal injection of CpG ODNs into mice at 10 nmol/mouse. The IL-6 concentration in plasma increased 2 h after injection. The plasma IL-6 level peaked at 4 h and then decreased, falling below the detection limit at 24 h. GD3 induced a 4-fold increase in plasma IL-6 compared with the linear CpG ODN, 2006_PD, at 4 h post-administration. The increased immunostimulatory activity of CpG ODNs by G4 forming via intraperitoneal injections in mice demonstrates the potential application of G4 CpG ODNs *in vivo*.

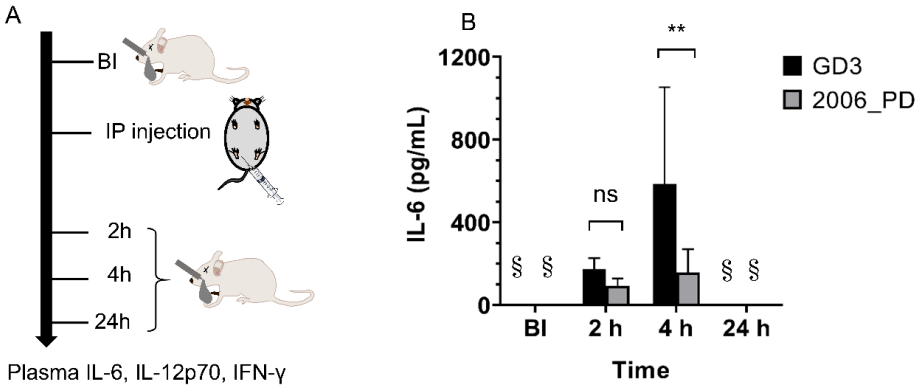

Figure 2.20 Induction in mice of IL-6 by GD3 or 2006_PD over time. (A) A mice intraperitoneal injection protocol; (B) IL-6 expression. Data represent mean ± SD of 5 mice. $^{**}p < 0.01$, ns (not significantly different) $p > 0.05$, two-way ANOVA, Sidak's multiple comparisons test. §, lower detection limit (3.9 pg/mL). BI, before injection; IP, intraperitoneal.

2.4. Conclusion

The new CpG ODNs forming G-quadruplex-based were successful prepared using a simple process. The molecularity of G4 was control well in monomeric form. The obtained monomeric G4 structure is stable at physiological temperature and preserved in various buffers mimicking cellular environments. The intracellular uptake and DNase resistance of the G4 CpG ODNs are higher than those of the linear CpG ODNs. G4 CpG ODNs induced immunostimulatory cytokines interleukin (IL)-6, IL-12, and interferon (IFN)-β in mouse macrophage-like RAW264 cells. Incubating human peripheral blood mononuclear cells with G4 CpG ODNs promoted IL-6 and IFN-γ production, confirming their stimulatory effects on human immune cells. Mice given intraperitoneal injections of G4 CpG ODNs produced higher plasma IL-6 compared with injections of linear ODNs. These results suggest potential as vaccine adjuvants of G4 CpG ODNs.

Chapter 3 Effect of variation of loop residues on immunostimulatory properties of monomeric G4 CpG ODNs

3.1. Introduction

Activation of the immune system based on the recognition of synthetic CpG ODNs by TLR9 is a promising strategy for the development of immunotherapies for cancer, allergies, and infectious diseases. However, the application of this strategy is hindered by low nuclease resistance of the natural backbone of CpG ODNs. Phosphorothioate modification provides higher nuclease stability to CpG ODNs, but it raises safety concerns due to their side effects.[66] Designing CpG ODNs with higher order structures has been revealed as a potential approach to improve the nuclease resistance of CpG ODNs without requiring any chemical modification.[38,45,67] Immunomodulatory properties of CpG ODNs higher-ordered structure are influenced by their molecule structure.[43,91]

In chapter 2, we reported that CpG ODNs forming the G-quadruplex structure displayed higher nuclease resistance and higher immunostimulatory activities than linear CpG ODNs. Although the usability of G4 CpG ODNs as potential and safe TLR9 agonists has been demonstrated, details about their immunostimulatory properties have been unclear. Understanding the influence of intrinsic factors governing TLR9 activation enables further improvement of the immunostimulatory activities of G4 CpG ODNs. We have found in chapter 2 that the loop containing CpG motifs is critical for establishing the immunostimulatory properties of monomeric G4 CpG ODNs. In this chapter, we investigate the influence of variations in the loop residues containing the CpG motifs, including position of loop containing CpG motif, position of CpG motif within a loop, spaces between a CpG motif and G-tracts, as well as number of CpG ODNs, on the immunostimulatory properties of intramolecular G4 CpG ODNs.

3.2. Materials and Methods

3.2.1. ODNs

All ODNs with phosphodiester backbones (sequences are shown in the **Table 3.1**) were HPLC-grade and purchased from Eurofins Genomics (Tokyo, Japan).

Table 3.1 Sequences of oligodeoxynucleotides used in this chapter

Name	Sequence from 5' to 3'[a]	Length (mer)
GD2-1L	GGG**GTCGTT**TT**GTCGTT**GGGTTGGGTTGGG	30
GD2-3L	GGGTTGGGTTGGG**GTCGTT**TT**GTCGTT**GGG	30
GD3-1L	GGG**GTCGTT**TT**GTCGTT**TT**GTCGTT**GGGTTGGGTTGGG	38
GD2T-1L	GGG**GTCGTT**TT**GTCGTT**GGGTGGGTGGG	28
GD2T-2L	GGGTGGG**GTCGTT**TT**GTCGTT**GGGTGGG	28
GD2T-3L	GGGTGGGTGGG**GTCGTT**TT**GTCGTT**GGG	28
GD1	GGGTTGGG**GTCGTT**GGGTTGGG	22
GD2	GGGTTGGG**GTCGTT**TT**GTCGTT**GGGTTGGG	30
GD2-M2	GGGTTGGG**GTCGTT**TTGTC$_{Met}$GTTGGGTTGGG	30
GD3	GGGTTGGG**GTCGTT**TT**GTCGTT**TT**GTCGTT**GGGTTGGG	38
GD3-M1	GGGTTGGGGTC$_{Met}$GTTTT**GTCGTT**TT**GTCGTT**GGGTTGGG	38
GD3-M2	GGGTTGGG**GTCGTT**TTGTC$_{Met}$GTTTT**GTCGTT**GGGTTGGG	38
GD3-M3	GGGTTGGG**GTCGTT**TT**GTCGT**TTTGTC$_{Met}$GTTGGGTTGGG	38
GD3-M13	GGGTTGGGGTC$_{Met}$GTTTT**GTCGTT**TTGTC$_{Met}$GTTGGGTTGGG	38
2006_PD	TC**GTCGTT**TT**GTCGTT**TT**GTCGTT**	24

[a] Capital letters, phosphodiester bases; bold letters, human-specific immunostimulatory unmethylated CpG motif; C$_{Met}$, 5-Methyl deoxy cytidine; underline, G-tract.

3.2.2. Preparation of G-quadruplex ODNs

The purchased ODNs were dissolved in sterile Mili-Q water to prepare stock solutions. The stock solutions were stored at -30 °C until use. To form the G4 structure, ODNs were diluted from the stock solution using Dulbecco's phosphate-buffered saline (D-PBS, DS Pharma Biomedical, Osaka, Japan) containing 2.68 mM KCl, 137 mM NaCl, 1.47 mM KH_2PO_4, and 8.10 mM Na_2HPO_4. For example, to prepare 20 μL of 10 μM G4 CpG ODN solution from a stock ODN solution at 100 μM, 2 μL of 10× D-PBS, 2 μL of 100 μM ODNs, and 16 μL of sterile Mili-Q water were added into a PCR tube. The ODN solutions were heated to 95 °C for 5 min, then cooled gradually to 30 °C for 30 min, followed by cooling to 4 °C using a thermal cycler (PCR Thermal Cycler Dice Standard TP650, Takara, Kyoto, Japan). The folded ODN solutions were stored at 4 °C until use.

3.2.3. Circular dichroism (CD) Spectroscopy

To measure the CD spectra, the G4 CpG ODN solutions (20 μM in D-PBS) were further diluted to 2 μM with D-PBS. Then, 100 μL of the 2 μM ODN solution was added into a quartz cuvette (model T-18-ES-10, 1-cm path length, Jasco). The CD spectra were determined using a Jasco J-725 CD spectropolarimeter over a wavelength range of 220–320 nm (scan rate, 50 nm/min; response time, 2.0 s; band width, 1.0 nm; resolution, 0.2 nm; and sensitivity, 100 mdeg) at 25 °C. The presented spectrum of each ODN is the average of 5 scans.

3.2.4. Polyacrylamide Gel Electrophoresis (PAGE)

Gel electrophoresis was performed using 12% polyacrylamide gels (PAGE; 1-mm thick; TEFCO, Tokyo, Japan) in 0.5× Tris-borate-EDTA (TBE) buffer (0.089 M, pH 8.3–8.5; Takara Bio, Kusatsu, Japan) supplemented with 0 or 4 mM KCl, at a constant voltage of 180 V at 4 °C. The 10-base pair (bp) DNA ladder (Invitrogen, Carlsbad, CA, USA) was used as a marker. The bands in the gel were stained by SYBR Gold Nucleic Acid Gel Stain (Thermo Fisher Scientific, Waltham, MA, USA).

Linear ODNs ssODN22mer (5'-GTCGTTTTGTCGTTTTGTCGTT-3'; 22 nucleotides), ssODN30mer (5'-GTCGTTTTGTCGTTTTGTCGTTTTGTCGTT-3'; 30 nucleotides), and ssODN38mer (5'-GTCGTTTTGTCGTTTTGTCGTTTTGTCGTTTTGTCGTT-3'; 38 nucleotides) were used as references. The linear ODNs were diluted in Tris-HCl 10 mM (pH 7.4) to a concentration of 20 μM. Before their application to the gel, they were heated at 95 °C for 5 min and immediately put on ice to preserve their linear structure.

3.2.5. Cell cultures

The mouse macrophage-like RAW264 cell line (RCB0535), purchased from RIKEN BioResource Center (Tsukuba, Japan), was cultured in Minimum Essential Medium (MEM) (Gibco, Carlsbad, CA, USA) containing 10% (v/v) fetal bovine serum (FBS) (Sigma-Aldrich, St Louis, MO, USA) and 1% (v/v) MEM non-essential amino acid solution (100×, Wako Pure Chemical Industries, Osaka, Japan). The cells were incubated at 37 °C in a humidified incubator with 5% CO_2. RAW-Blue cells, derived from RAW 264.7 macrophages and stably expressing a secreted embryonic alkaline phosphatase (SEAP) gene inducible by NF-κB and AP-1 transcription factor (InvivoGen), were cultured in complete medium Dulbecco's Modified Eagle Medium (DMEM) supplemented with 4.5 g/l glucose, 2 mM L-glutamine, and 10% heat-inactivated FBS (Sigma-Aldrich)

3.2.6. SEAP reporter assay

Each agonist (20 μl) was added at 20 μM per well of a 96-well plate include a negative control, D-PBS. Then, RAW-Blue cells in complete medium DMEM (Sigma-Aldrich) were added at 10^5 cells per well (180 μL, 5.55×10^5 cells/ml). The cells were incubated at 37 °C in a 5% CO_2 incubator for 24 h. Afterward, supernatants were collected, and NF-κB/AP-1 activation linked to SEAP was determined using QUANTI-Blue reagent, according to the manufacturer's instructions (Invitrogen). QUANTI-Blue medium and RAW-Blue cell supernatants were incubated in a flat-bottom 96-well plate (Greiner bio-one Cat No. 655180) at 37°C for 3 h. SEAP

levels were determined using a spectrophotometer at 630 nm. Error bars represent the SD obtained from five biological replicates.

3.2.7. Stimulation of RAW264 cells

RAW264 cells in culture medium supplemented with 1 (v/v) P/S (100×) were seeded into a 96-well plate at a density of 1×10^5 cells/well (5.3×10^5 cells/mL, 190 μL). After incubation for 18 h, 10 μL of 80 μM ODN was added to the culture medium to a final concentration of 4 μM. Then, the cells were incubated for 24 h before evaluation of the relative transcript levels and the secretion levels of cytokines.

3.2.8. Reverse transcription/real-time quantitative-polymerase chain reaction (RT/RQ-PCR)

The relative transcript levels of cytokines in RAW264 cells were determined by reverse transcription/real-time quantitative-polymerase chain reaction (RT/RQ-PCR). Total RNA was extracted from the cells using ISOGEN (Nippon Gene, Tokyo, Japan) following the manufacturer's instructions. The extracted RNA was treated with DNase I (RNase-free) (Takara Bio, Shiga, Japan) prior to reverse transcription into cDNA (Takara Bio). IL-6, IL-12, and IFN-β transcript levels were measured by quantitative real-time PCR using a LightCycler 480 System (Roche, Basel, Switzerland) with LightCycler®480 SYBR Green I Master (Roche) and the primers (FASMAC, Kanagawa, Japan) listed in **Table 2.2**. Amplification was performed using 50 ng cDNA in a total volume of 15 μL for 45 cycles of 10 s each at 95 °C, 10 s at 60 °C, and 10 s at 72 °C. After PCR, the crossing point value, the cycle at which the fluorescence starts to become significantly higher than the background fluorescence, was determined. The mRNA levels were normalized against that of glyceraldehyde 3-phosphate dehydrogenase (*GAPDH*), a housekeeping gene. In addition, the specificity of the amplified products was verified by analyzing the melt curves.

3.2.9. Statistical analysis

Statistical comparisons of the data were conducted by one-way analysis of variance (ANOVA) followed by Tukey's multiple comparisons test for comparison with other groups or by Dunnett's multiple comparisons test for comparison with a control group. All statistical analyses were performed using GraphPad Prism version 8.2.0 for Windows (GraphPad Software, La Jolla, CA, USA). A p-value < 0.05 was considered statistically significant.

3.3. Results and discussion

3.3.1. Effect of position of loop containing CpG motifs

Both conformation and thermodynamic stability of G4 structure are considerably depending on loop permutation, which is defined by order exchange of loop in monomeric G4.[92] In chapter 2, we have designed G4 CpG ODNs containing CpG motifs at the second loop. To examine influences of position of loop containing CpG motifs, here we created GD2-1L, and GD2-3L by swapping place of the long loop containing the CpG motifs (L*) with the first ($L^{\#}$) and the third ($L^{\$}$) short TT loop of GD2, respectively. A variant of GD3, named GD3-1L, also was created by swapping place of the long loop containing the CpG motifs with the first short TT loop in GD3. These variants only differ in the order of the loop containing CpG motif, while they keep length and overall base composition as same as GD2 and GD3. The schematic illustration of loop permutation of GD2 and GD3 is shown in **Scheme 3.1**.

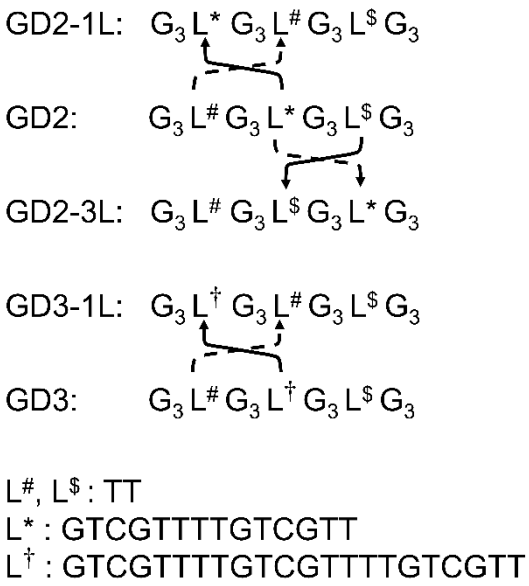

Scheme 3.1 Loop permutation to create GD2-1L, GD2-3L from GD2, and GD3-1L from GD3.

In chapter 2, we have determined that GD2 and GD3 form monomeric hybrid-type G4. The CD spectrum of GD2-1L exhibit one negative peak at around 240 nm, and one positive peak at around 260 nm and a shoulder at around 290 nm (**Fig. 3.1Ai**), which are characteristics of hybrid G4. The CD spectrum of GD3-1L (**Fig. 3.1A ii**) shows a negative peak at 240 nm and a positive peak at 264 nm which characterize for a parallel G4, this indicates that the change in order of the first short loop and the long second loop leads to a change in G4 conformation. PAGE analysis with the presence of K^+ shows that GD2-1L migrated slightly faster than the linear control, but slower than GD2 (**Fig. 3.1B**), indicating that GD2-1L forms a looser structure than GD2. Likewise, PAGE shows that GD3-1L is less compact than GD3 (**Fig. 3.1B**). Furthermore, a part GD3-1L migrated at same rate with the linear control, indicating that GD3-1L is a mixture of G4 and linear molecules. These results suggested that putting CpG motifs into the first loop is not preferable to form a stable G4 structure. Our results are compatible with the findings of Cheng et al., who reported that G4 with a longer central loop tend to form a stable non-parallel topology

and sequences with a short central loop have a high tendency to form a parallel topology of lower stability.[92]

GD2-3L shows one negative peak at around 240 nm, and two positive peaks at around 260 and 290 nm, indicating that GD2-3L forms hybrid G4 (**Fig. 3.1Ai**). GD2-3L moved as same rate as GD2 in PAGE (**Fig. 3.1B**). This indicates that swapping order between the second loop and the short third loop of GD2 may not prevent formation of a stable G4.

RAW-Blue cells stably express a SEAP gene inducible by NF-κB transcription factors. RAW-Blue cells express TLR9, so the presence of G4 CpG ODNs induces signaling pathways leading to the activation of NF-κB, which induces secretion of SEAP into cell culture media. SEAP is easily detectable using QUANTI-Blue medium, which changes from pink to a purple-blue color in the presence of AP. Therefore, the level of SEAP, detected by measuring optical density at 630 nm, correlate with G4 CpG ODN mediated NF-κB activity.

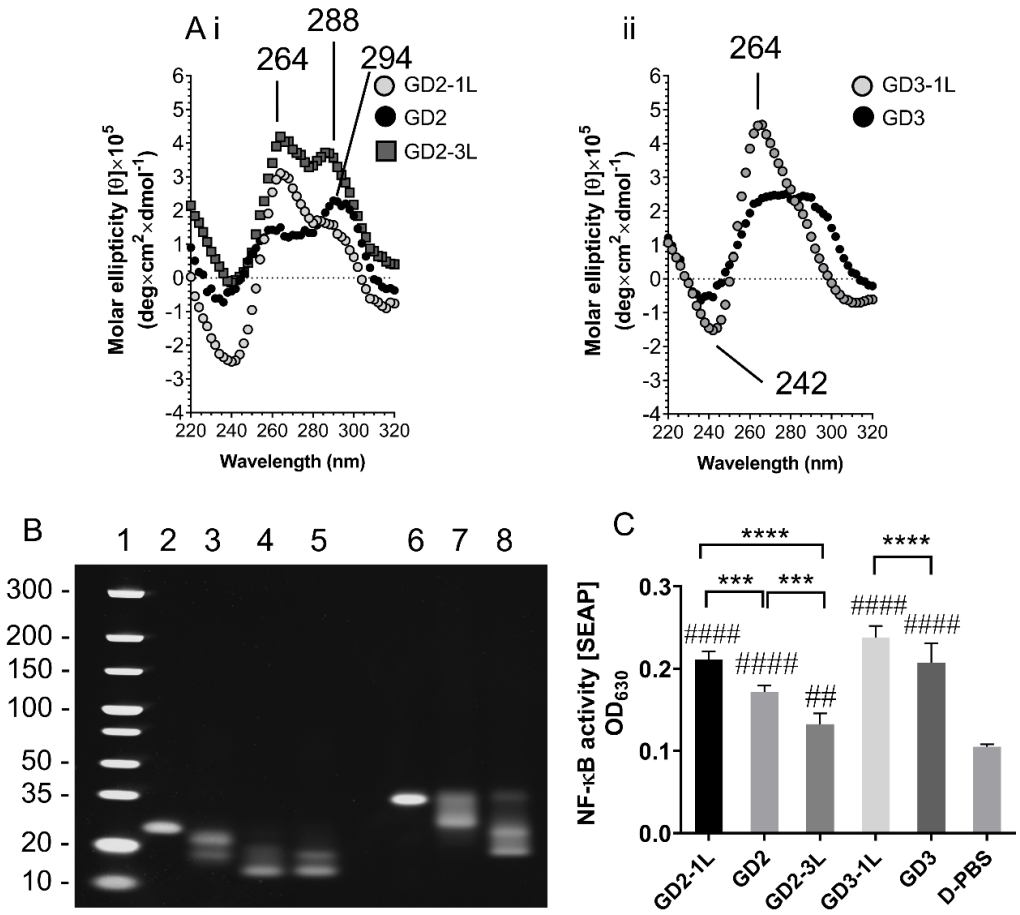

Figure 3.1 (A) Circular dichroism (CD) spectra of (i) GD2-1L, GD2, GD2-3L, and (ii) GD3, and GD3-1L at 25 °C in the presence of 4 mM K^+; **(B)** Polyacrylamide gel electrophoresis analysis in the presence of 4 mM K^+; lane 1, ultra-low range DNA ladder; lane 2, ssODN30mer; lane 3, GD2-1L; lane 4, GD2; lane 5, GD2-3L; lane 6, ssODN38mer; lane 7, GD3-1L; lane 8, GD3. **(C)** Secreted embryonic alkaline phosphate (SEAP) reporter assay of GD2, GD3 and their variants in position of loop containing CpG motifs. RAW-Blue cells were stimulated with GD2-1L, GD2, GD2-3L, GD3, and GD3-1L. The alkaline phosphatase activity under control of the NF-κB promoter was measured 24 h after cell stimulation. Data represent mean ± SD (n = 5). ****p < 0.0001, ***p < 0.001, **p < 0.01 (*, one-way ANOVA, Tukey's multiple comparisons test for comparison with other groups; #, Dunnett's multiple comparisons test for comparison with the Dulbecco's phosphate-buffered saline [D-PBS] control group).

RAW-Blue cells which exposed to examined CpG ODNs can induce SEAP production at levels significantly higher than those exposed to negative control, D-PBS, suggesting that all examined CpG ODNs can activate TLR9 (**Fig. 3.1C**). G4 CpG ODNs including CpG motifs in the first loop are more efficient in TLR9 activation than those including CpG motifs in the second, and the third loop. This may because of their more loosen structure, as shown in PAGE analysis (**Fig. 3.1B**). GD2-3L showed lowest potential in TLR9 stimulation compared with GD2-1L and GD2. Therefore, when we take both G4 stability and TLR9 activation efficiency, which are two critical factors for high potent of G4 CpG ODNs, into consideration, putting CpG motifs into the second loop of a G4 is preferable for immune stimulation.

3.3.2. Effect of position of CpG motif within a loop

To further understand the mechanism underlying TLR9 stimulation by monomeric G4 CpG ODNs, we designed variants of G4 CpG ODNs with different positions and numbers of CpG motifs and then examined their effects on cytokine production in RAW264 cells.

First, we examined the effect of the position of the CpG motif on the immunostimulatory activities of the G4 CpG ODNs. Variants of GD3 containing two CpG motifs at different positions within the central loop were generated by methylation, which abolished the immunostimulatory activity of the CpG motif (**Fig. 2.18B**) without changing the original G4 structure (**Fig. 2.18A**). Accordingly, the first, second, or third CpG motif from the 5'-end of GD3 was methylated one by one to get the ODN variants named GD3-M1, GD3-M2, or GD3-M3, respectively (**Table 3.1**). These variants form the similar G4 structure to GD3, according to the CD spectra (**Fig. 3.2**). The relative cytokine mRNA levels in RAW264 cells after stimulation with these ODNs are shown in **Figure 3.3**. GD3-M2, which contains CpG motifs at the first and third sites, induced dramatically lower cytokine production than did GD3-M1 and GD3-M3, suggesting that the second CpG motif is the most important in the immunostimulatory function of GD3.

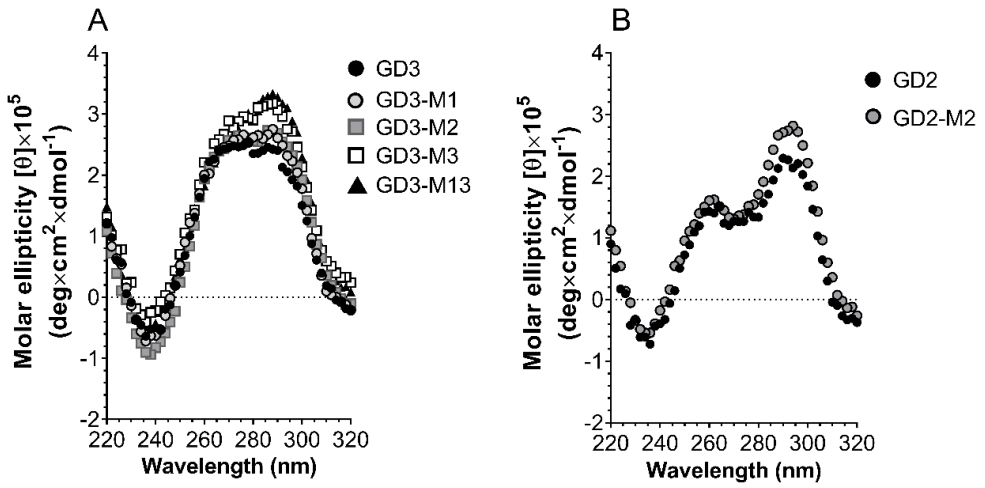

Figure 3.2 Circular dichroism spectra of (A) GD3 and methylated variants, and (B) GD2 and methylated variants in D-PBS at 2 μM.

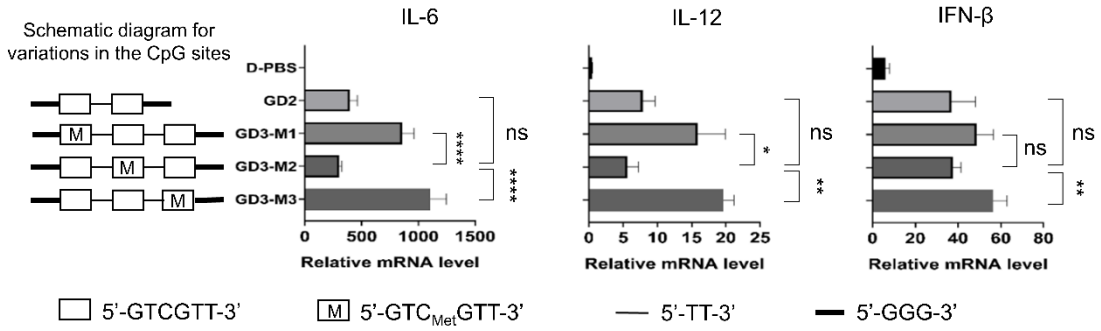

Figure 3.3 The influence of the CpG motif position within a loop on the immunostimulatory properties of G4 CpG oligodeoxynucleotides. Data represent mean ± SD (n = 5). ****p < 0.0001, **p < 0.01, *p < 0.05, ns (not significantly different) p >0.05 (one-way ANOVA, Tukey's multiple comparisons test).

3.3.3. Effect of spaces between a CpG motif and G-tracts

In addition, as shown in **Figure 3.3**, only GD3-M1 and GD3-M3 induced higher cytokine production than GD2, while the cytokine levels induced by GD3-M2 were similar to those induced by GD2. These ODNs have an identical number of CpG motifs, but GD2 has a 14-mer

loop, while the others have 22-mer loops. Not all G4 CpG ODNs with longer loops led to higher cytokine production than that of GD2, indicating that loop length is not the critical factor for the TLR9 stimulatory efficiency of G4 CpG ODNs. A longer loop length is necessary but placing the CpG motif into a proper position in the loop is more important for high TLR9 stimulation efficiency.

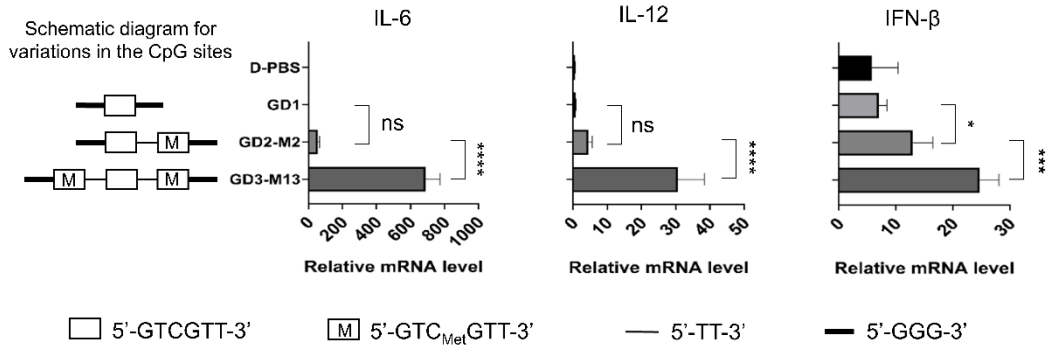

Figure 3.4 The influence of the spaces between CpG motif and G-tracts on the immunostimulatory properties of G4 CpG oligodeoxynucleotides. Data represent mean ± SD (n = 5). ****p < 0.0001, ***p < 0.001, **p < 0.01, *p < 0.05, ns (not significantly different) p >0.05 (one-way ANOVA, Tukey's multiple comparisons test).

A difference between the second site and the other sites is that the second motif is far from the G-tract and does not directly bind guanine in the G-tracts. Considering this difference, we examined whether the spaces between the CpG motifs and the G-tracts affected TLR9 stimulation by G4 CpG ODNs. We created GD2-M2, a variant of GD2, by methylating the second CpG motif of GD2; and GD3-M13, a variant of GD3, by methylating the first and third CpG motifs of GD3. GD2-M2 and GD3-M13 have similar G4 structure to GD2 and GD3, respectively, which is demonstrated by CD spectra (**Fig. 3.2**). **Figure 3.4** shows the cytokine production induced by GD1, GD2-M2, and GD3-M13, which all contain one CpG motif but differ in spaces between the CpG motifs and G-tracts. There is no space between the 6-mer CpG motif "5'-GTCGTT-3'" and the G-tracts in GD1, while there is an 8-mer space separating one side and both sides of the CpG

motif from the G-tracts in GD2-M2 and GD3-M13, respectively. Due to the presence of spaces between the CpG motif and the G-tracts, the length of the central loop increased from 6-mer in GD1 to 14- and 22-mer in GD2-M2 and GD3-M13, respectively. GD2-M2 was slightly more immunostimulatory than GD1, but the induced cytokine levels were still low. GD3-M13 induced much stronger immune responses than did GD1 and GD2-M2. This indicates that the spaces between the CpG motif and G-tracts increase the TLR9 stimulation efficiency of G4 CpG ODNs.

A long loop was found to be necessary for more effective TLR9 stimulation by G4 CpG ODNs, as shown by the higher immunostimulatory activities of GD3-M1 and GD3-M3, each of which has a 22-mer loop, compared with GD2, which has a 14-mer loop (**Fig. 3.3**). Previous studies have reported that the dumbbell-like ODN with CpG motifs with a 30-mer loop has better immunostimulatory properties than one with a 20-mer loop.[32] However, having a long loop alone is not sufficient to confer high efficacy to G4 CpG ODNs, as the position of the CpG motifs within the loop also influences the efficacy. Based on our results, the second position appears to be the most important for the CpG motif (**Fig. 3.3**). Ohto et al. have determined that an agonistic ODN is recognized by both protomers of the TLR9 dimer in a bent conformation.[93] Therefore, a possible reason for this positional effect of the CpG motifs in G4 CpG ODNs is the flexibility of the different positions along the loop. Longer loops may be generally more flexible than shorter loops, but loop positions near G-tracts may be too rigid to adopt the bent conformation. The presence of spaces between a CpG motif and the G-tracts flanking it was found to increase the activity of the CpG motif, which is consistent with the hypothesis that the regions of the loop close to the G-tracts are less flexible than other sites on the loop. Previous studies have revealed that the flexibility of CpG motifs in higher order structures influences TLR9 recognition and subsequent immunostimulatory effects. Sanada et al.[94] suggested that partly loosening the center of a polypod-shaped CpG ODN increases the segregation of strands containing the CpG motif from the rigid double helix structure of the arms. This may in turn increase the chances for interaction with TLR9, which leads to increased TNF-α secretion.[94] In addition, a dumbbell-like ODN with

CpG motifs in a rigid double-stranded stem exhibits a significantly lower immunostimulatory activity than one with CpG motifs in a single-stranded loop.[32]

3.3.4. Effect of number of CpG motifs

Next, we examined the influence of the number of CpG motifs on the immunostimulatory effects of G4 CpG ODNs. We compared the immunostimulatory activities of GD2 and GD2-M2, which have two and one CpG motifs, respectively, and have the same central loop length (14-mer). **Figure 3.5A** shows that GD2 induced higher cytokine production than did GD2-M2. For ODNs with 22-mer central loops, we compared the immunostimulatory properties of GD3-M13, GD3-M3, and GD3, containing one, two, and three CpG motifs, respectively. **Figure 3.5B** shows that GD3-M3 elicited a higher response from RAW264 cells than did GD3-M13. However, there was no difference in the intensity of the RAW264 immunostimulatory responses to GD3-M3 and GD3. These results indicate that increasing the number of CpG motifs from one to two enables higher TLR9 stimulation by G4 CpG ODNs but adding more than two CpG motifs may not result in more effective TLR9 stimulation.

Even with only one CpG motif, G4 CpG ODNs still promote cytokine production, provided that the CpG motif is far from the flanking G-tracts, such as in GD3-M13. Nishikawa et al. reported that a phosphodiester Y-shaped ODN containing only one CpG motif induces IL-6 and TNF-α production in RAW264 cells.[35] The immunostimulatory activity of G4 CpG ODNs increases with increasing number of CpG motifs. This is consistent with the observed augmentation of TLR9 stimulation when the number of CpG motifs was increased in both linear CpG ODNs[95,96] and in ODNs with higher order structures, such as Y-shaped ODNs.[35] An upper limit to the number of CpG motifs beneficial to ODN immunostimulatory activity was observed in our study: Specifically adding more than two CpG motifs did not contribute significantly to the immunostimulatory activity of the ODNs. Klinman et al. have also demonstrated that adding more than four CpG motifs to an ODN decreases its activity.[95]

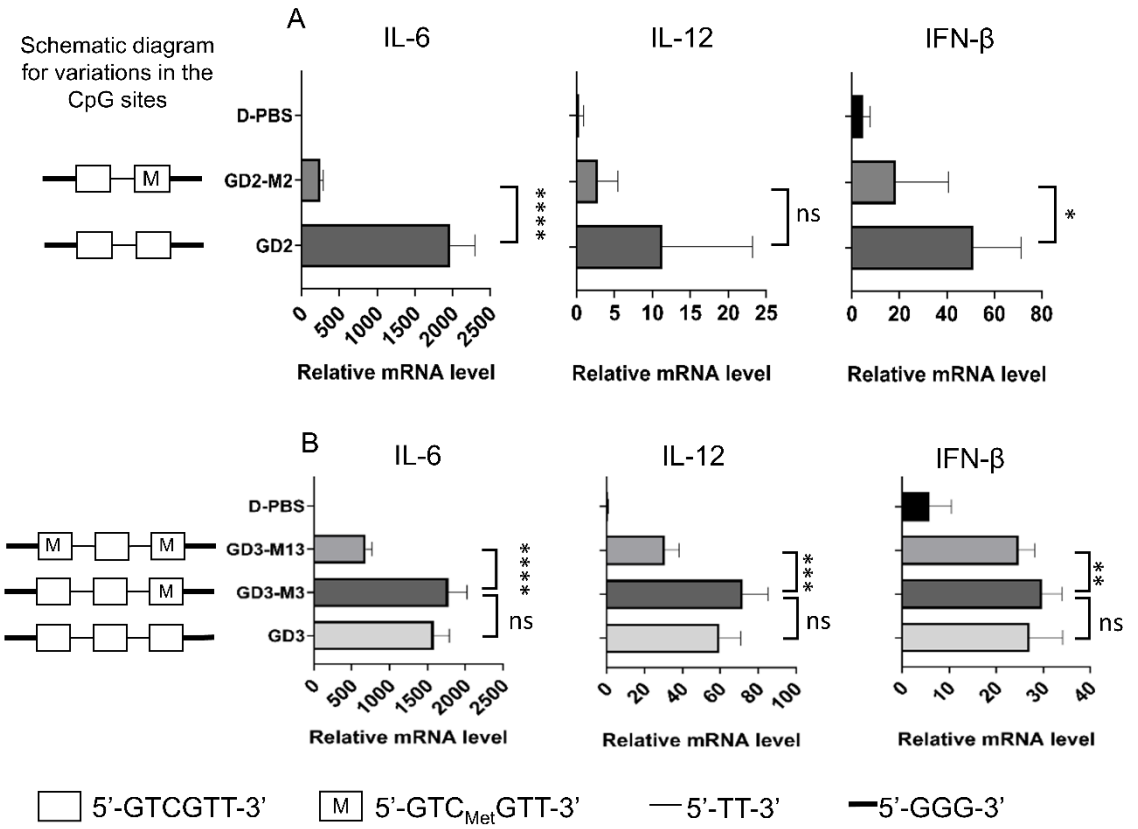

Figure 3.5 The influence the number of CpG motifs on the immunostimulatory properties of G4 CpG oligodeoxynucleotides. (A) In the 14-mer loop, (B) In the 22-mer loop. Data represent mean ± SD (n = 5). ****p < 0.0001, ***p < 0.001, **p < 0.01, *p < 0.05, ns (not significantly different) p >0.05 (one-way ANOVA, Tukey's multiple comparisons test).

Although GD2 was more nuclease-resistant than GD3 (**Fig. 2.8**), it induced lower cytokine production than did GD3 (**Fig. 2.16**), suggesting that nuclease resistance is not the reason for the differences in the immunostimulatory activities of the G4 CpG ODNs. In addition, although GD3 is taken up into RAW264 cells more efficiently compare with GD2, the difference between GD2 and GD3 in uptake efficiency is not as much as the difference in cytokine induction, indicating that the differences in the TLR9 response to the G4 CpG ODNs are not results from cellular uptake. The reason behind variation of cytokine induction of G4 CpG ODNs is probably the differences in the TLR9 recognition of these G4 CpG ODNs due to variations in the central

loop containing the CpG motifs. GD1 contains only one CpG motif with a very short loop (6-mer) and is flanked directly by G-tracts. This results in a rigid CpG motif in GD1, which cannot readjust to a suitable conformation for TLR9 recognition, which probably resulted in the low immunostimulatory effects observed upon GD1 treatment in the present study. A higher cytokine production was induced by GD2 than by GD1, probably because GD2 has a longer loop, which is expected to be more flexible, and also because GD2 has more CpG motifs than GD1. GD3 had the highest immunostimulatory capacity among the G4 CpG ODNs in this study. This is likely due to the second CpG motif, which has high flexibility in GD3 and can easily adopt the bent conformation for TLR9 recognition.

Investigation of the effects of factors relating to the loop region not only provides insight into the possible reasons for the varying immunostimulatory properties of our G4 CpG ODNs, but it also allows us to understand how to improve these properties. Due to the low flexibility of the CpG motif in the G4 structure, the binding affinity of TLR9 for a CpG motif having direct linkage with G-tracts may be lower than that of a CpG motif in a linear CpG ODN. In this regard, adding some space between the CpG motifs and G-tracts provides adequate flexibility for CpG motif and subsequent adequate binding affinity to TLR9, as shown in **Figure 3.4**. There is a trade-off when this strategy is used to increase efficiency of monomeric G4 CpG ODNs, because increases in CpG motif number or spaces between CpG motifs and G-tracts lead to increase in loop length and consequent decrease in thermodynamic stability and nuclease resistance. Therefore, in the future, we will investigate optimizing the sequence within a 22-mer loop where CpG motifs are not adjacent to the G-tract.

3.4. Conclusion

In summary, we evaluate the effects of variations in the loop regions on the immunostimulatory properties of these CpG ODNs. Placing CpG motifs in the second loop of G4, which results in a sequence with a long central loop, and two external short loops, is a rational

design to form a stable and potent monomeric G4 CpG ODNs. Increase in the length of the loop containing the CpG motifs is necessary but not adequate for effective TLR9 stimulation. The number of CpG motifs and the spaces between CpG motifs and G-tracts are critical factors deciding immunostimulatory efficiency of G4 CpG ODNs, likely because of increased flexibility in the loop region. In this chapter, we have identified some properties important to the immunostimulatory effects of G4 CpG ODNs, and these findings provide hints for the design of G4 CpG ODNs for vaccine adjuvant applications.

Chapter 4 G-quadruplex ligands for enhanced stability and immunostimulatory activity of G4 CpG ODNs

4.1. Introduction

We have reported about G-quadruplex-forming oligodeoxynucleotides containing unmethylated cytosine-phosphate-guanine motifs (G4 CpG ODNs) are G-rich single-strand ODNs bearing immunostimulatory CpG motif such as "GTCGTT" in the sequences. The G-tracts in G4 CpG ODNs facilitate G-quadruplex (G4) formation, which enhance nuclease resistance and cellular uptake of CpG ODNs, while CpG motifs play a key role in their immunostimulatory activities. In chapter 2, we have demonstrated the potential of G4 CpG ODNs in activating immune response *in vitro* and *in vivo*.

G4 is a non-canonical four-stranded DNA structure, comprising stacking G-quartets, a square planar arrangement of four guanines via Hoogsteen hydrogen bonds, and several loops connecting these G-quartets. G4 exhibits diversity in topology, which partly caused by variation of strand orientation. Accordingly, parallel G4 have all four strands with a same 5'-3' polarity. Anti-parallel G4 contains two pairs of strands with reversed arrangement of 5'-3' polarity. Hybrid G4 includes one strand in opposite direction with other three strands.[51] Remarkably, topology of G4 ODNs depends on surrounding environment including the nature and concentration of monovalent cations.[52] For instance, Largy et al.[97] found that G-rich DNA named 222 (d[$(G_3T_2)_3G_3$]) and 222T (d[$T(G_3T_2)_3G_3T$]) changed from anti-parallel to parallel G4 when the solutions changed from sodium-rich into potassium-rich.[97] These ODNs also underwent a reformation from 3-quartet parallel to 2-quartet anti-parallel when concentration of K^+ decreased lower than 1 mM.[97]

Recently, small molecules called G4 ligands were developed to stabilize G4 by binding to G4 ODNs with high affinity.[49] Structure of G4 ligands commonly includes an aromatic heterocyclic system to interact with G-quartets through π-π stacking and cationic groups to

electrostatic interact with loop or groove of G4.[49] Ma et al. demonstrated the ability in cation-independent G4 formation of G4 ligands namely L2H2-6OTD[98], L2H2-2M2EA-6OTD and L2G2-2M2EG-6OTD, which have the structure based on a natural G4 ligand, telomestatin.[99] They also showed that L2G2-2M2EG-6OTD induced parallel G4 with high efficiency.[99] Tsukakoshi et al. regulated topology of G4 based aptamers by several G4 ligands including L1H1-7OTD, L2H2-6OTD, Phen-DC3 and TmPyP4.[100] Both G4 based aptamers T-SO530 and bivalent 3R02, which bind to α-synuclein (α-syn) oligomer and vascular endothelial growth factor (VEGF), respectively, showed enhanced binding ability to the target proteins in the presence of the G4 ligands.[100] In addition, Koirala et al. revealed that a higher mechanical stability and thermodynamic stability of human telomeric sequence Tel-4G achieved by binding with G4 ligand pyridostatin (PDS).[101] A stronger forces needed to unfold ligand-stabilizing G4 ODNs may more hinder the activity of DNA telomerase, which cause immortal replication in cancer cells.[48]

Despite the large number of studies on potential of G4 ligands were reported[102], influences of G4 ligands on G4-based CpG ODN functions has not been clarified. With the ability in stabilization of G4 ODNs, we expect that G4 ligands may also stabilize G4 CpG ODNs, which may further increase their immunostimulatory activity. Knowledge about G4 ligands that can enhanced immune response to G4 CpG ODNs will facilitate development of more effective vaccine adjuvants against infectious diseases. Therefore, in this chapter, we evaluate effect of G4 ligands on immunostimulatory properties of GD3, the highest efficient one among monomeric G4 CpG ODNs we have been reported in the previous chapters. We use two types of G4 ligand developed by Nagasawa's group, namely L2H2-6OTD[98] and L2G2-2M2EG-6OTD[99], which hereafter mentioned as L2H2 and L2G2, respectively. Both ligands have macrocyclic hexaoxazole to make π-π stackings with G-quartets. In addition, L2H2 contains two symmetrical amino alkyl side chains, while L2G2 has four symmetrical guanidinylalkyl side chains, which bind to G4 grooves or loops. The topology, thermodynamic stability, nuclease resistance, intracellular uptake, and cytokine induction in mouse macrophage-like RAW264 cells of GD3

alone are compared with those of GD3 in the complexes with L2H2 and L2G2, which hereafter referred to as GD3/L2H2 and GD3/L2G2, respectively.

4.2. Materials and Methods

4.2.1. Chemicals, oligodeoxynucleotides

GD3, which includes entire phosphodiester backbone, was purchased from Eurofins Genomic (Tokyo, Japan) in HPLC grade quality. The sequence of GD3 was present in **Fig 4.1A**. The stock solution of GD3 was prepared at 100 μM in sterile purified water and stored at -30 °C. L2H2-6OTD (**Fig. 4.1B**) and L2G2-2M2EG-6OTD (**Fig. 4.1C**) were synthesized as described in Tera et al. [98] and Ma et al. [99], respectively. Their 1 mM stock solutions in DMSO were store at -30 °C.

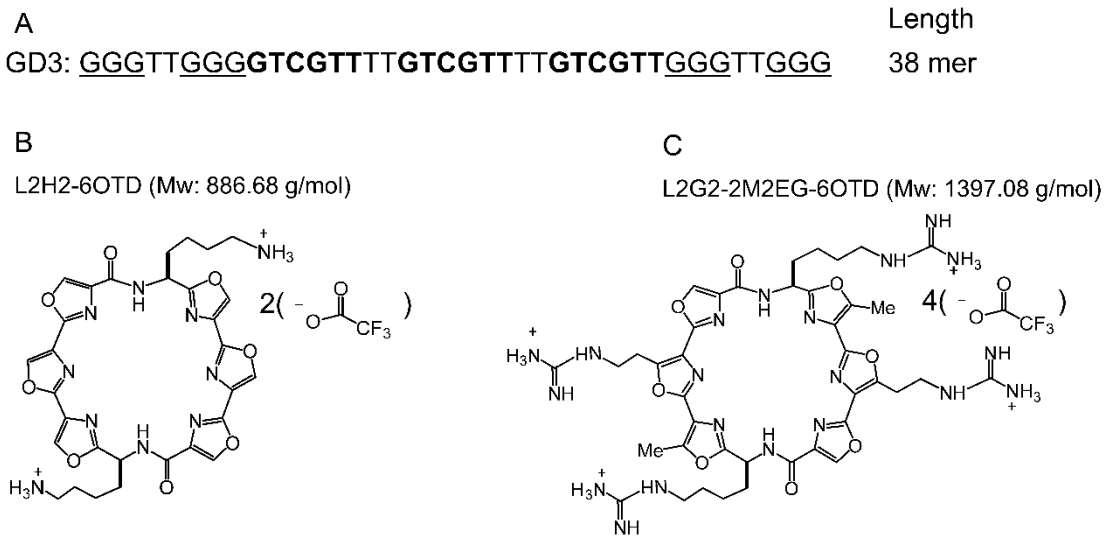

Figure 4.1 Sequence of the ODN and chemical structure of the G4 ligands used in this study. (A) Sequence of GD3. (B) chemical structure of L2H2-6OTD (here referred as L2H2)[98]; (C) chemical structure of L2G2-2M2EG-6OTD (here referred as L2G2)[99].

4.2.2. Preparation of G4 CpG ODNs

GD3 stock solution was diluted with Dulbecco's phosphate-buffered saline (D-PBS, DS Pharma Biomedical, Osaka, Japan), containing 2.68 mM KCl, 137 mM NaCl, 1.47 mM KH_2PO_4 and 8.10 mM Na_2HPO_4. G-quadruplex structures od GD3 was constructed by heating the diluted solution to 95 °C for 5 min, then cooling down gradually to 30 °C for 30 min, followed by cooling down to 4 °C. This reconstructed GD3 solution was stored at 4 °C until use.

4.2.3. Preparation of G4 CpG ODN/G4 ligand complexes

GD3 was reconstructed to form G4 structure in D-PBS as presented in **section 4.2.2.** L2H2 and L2G2 stock solutions of 10 mM were diluted by sterile MiliQ water. For preparation of complex of GD3 and G4 ligands, a solution of reconstructed GD3 was mixed with L2H2 or L2G2, then the mixtures were incubated at 25 °C for 24 h before examinations. The concentration of GD3, and G4 ligand solutions after mixing is specified in each experiment. Regardless the final concentration, the G4 ligand/ODN molar ratio (R) was kept equal to 4 (R = 4).

4.2.4. Ultraviolet (UV) melting curve and thermal difference spectra (TDS)

GD3 was reconstructed in D-PBS. L2H2 and L2G2 stock solution of 10 mM were diluted by sterile MiliQ water to get a concentration of 1 mM. The reconstructed GD3 and G4 ligand were mixed so that the final concentration of GD3 and G4 ligand is 2 μM and 8 μM, respectively (R = 4). The mixtures were incubated at 25 °C for 24 h before the measurement. A quartz cuvette (model T-30 MES10, 1-cm path length) was used to contain the 600 μL ODN solutions and 100 μL mineral oil on the top to prevent evaporation for UV measurement. A Jasco V-670 spectrophotometer (Tokyo, Japan) was used to record UV absorbance spectra from 220 to 320 nm (scan speed, 400 nm/min; data pitch, 1 nm; band width, 2.0 nm UV/Vis) over the temperature range of 20-90 °C (temperature gradient: 1 °C/min; data pitch: 1 °C). The UV melting curves

were presented as the absorbance at 295 nm from 20 °C to 90 °C. The absorbance spectra at 20 °C were subtracted from the spectra at 90 °C to obtain the TDS.

4.2.5. Polyacrylamide Gel Electrophoresis (PAGE)

GD3 was reconstructed in D-PBS. L2H2 and L2G2 stock solutions of 10 mM were diluted by sterile MiliQ water to get a concentration of 1 mM. The reconstructed GD3 and G4 ligands were mixed so that the final concentration of GD3 and G4 ligands is 10 μM and 40 μM, respectively (R = 4). Then, the mixtures were incubated at 25 °C for 24 h. The gel electrophoresis was conducted using 15% polyacrylamide gels with thickness of 1 mm (ATTO, Tokyo, Japan) in 0.5x Tris-Borate-EDTA (TBE) buffer (0.089 M, pH 8.3-8.5, Takara Bio, Kusatsu, Japan) supplemented with 0 or 4 mM KCl, under the constant current of 21 mA, at 4^{o}C. The ultralow range DNA ladder (Invitrogen) was used as a marker. The bands in gel were stained by SYBR Gold Nucleic Acid Gel Stain (Thermo Fisher Scientific, MA, USA). ssODN38mer (5'-GTCGTTTTGTCGTTTTGTCGTTTTGTCGTTTTGTCGTT-3') was used as a reference for a linear CpG ODN having 38 nucleotides. ssODN38mer was diluted in Tris-HCl 10 mM at pH7.4, then it was heated to 95 °C for 5 min and immediately put into ice to form a linear structure.

4.2.6. Circular dichroism (CD) Spectroscopy

GD3 was reconstructed in D-PBS. L2H2 and L2G2 stock solution of 10 mM were diluted by sterile MiliQ water to get a concentration of 1 mM. The reconstructed GD3 and G4 ligands were mixed so that the final concentration of GD3 and G4 ligand is 2 μM and 8 μM, respectively (R = 4). The mixtures were incubated at 25 °C for 24 h before measuring CD spectra. The GD3 without G4 ligands was prepared by diluting 20 μM reconstructed GD3 with D-PBS to 2 μM. 100 μL solution of GD3 without and with G4 ligands was added into a quartz cuvette (model T-18-ES-10, 1 cm path length, JASCO Parts Center). CD spectra were measured on a Jasco J-725 spectropolarimeter between 230 and 320nm. A scan speed of 50 nm/min, a response time of 2 s,

a band width of 1.0 nm, a resolution of 0.2 nm, and a sensitivity of 100 mdeg were used. Five scans were accumulated and averaged for a presented spectrum.

For the CD melting curves, the 2 μM ODN solutions (600 μL) were pipetted into a quartz cuvette (model T-30 MES10, 1-cm path length), then 100 μL mineral oil was added on the surface of the ODN solution to avoid evaporation. CD measurements were performed at 295 nm, 265 nm, and 270 nm for GD3, GD3/L2H2, and GD3/L2G2, respectively, over a temperature range of 20-90 °C, with a heating rate of 1 °C/min.

4.2.7. Stability in serum assay

The stability in serum assay was conducted to examine nuclease resistance of GD3 alone and GD3 in the presence of the G4 ligands. GD3 was reconstructed in D-PBS. L2H2 and L2G2 stock solution of 10 mM were diluted by sterile MiliQ water to get a concentration of 1 mM. The reconstructed GD3 and G4 ligands were mixed so that the final concentration of GD3 and G4 ligand is 10 μM and 40 μM, respectively (R = 4). Then, the mixtures were incubated at 25 °C for 24 h. 4 μL of 10 μM reconstructed G4 CpG ODNs alone or in the mixture with G4 ligands was added into 36 μL of D-PBS containing 20% (v/v) fetal bovine serum (FBS) (Sigma-Aldrich, St Louis, MO, USA) and incubated at 37 °C for 0, 1, 2, 4, and 24 h. After indicated time, 4 μL of 250 mM ethylenediaminetetraacetic acid solution was added into the solution following by heating to 80 °C for 2 min to stop the reactions. The processing ODNs were stored at 4 °C for further PAGE analysis. Percentages of remaining ODNs relative to ODN quantity at the beginning of incubation were calculated based on fluorescence intensity of corresponding bands in PAGE using Image Studio Lite software (LI-COR Biotechnology, Lincoln, NE).

4.2.8. Cell cultures

The mouse macrophage-like RAW264 cell line (RCB0535) purchased from RIKEN BioResource Center (Tsukuba, Japan) were maintained in Minimum Essential Medium (MEM)

(Gibco) supplemented with 10% (v/v) fetal bovine serum (FBS) (Sigma-Aldrich, St Louis, MO, USA), and 1% (v/v) MEM non-essential amino acid (NEAA) solution (×100, Wako Pure Chemical Industries, Osaka, Japan) at 37 °C, in humidified incubator containing 5% CO_2.

4.2.9. Intracellular uptake

GD3 and 2006_PD were labelled at the 5' end by Cy5 ($GD3^{5'Cy5}$ and $2006\_PD^{5'Cy5}$). $GD3^{5'Cy5}$ was reconstructed in D-PBS. L2H2 and L2G2 stock solution of 10 mM were diluted by sterile MiliQ water to get a concentration of 1 mM. The reconstructed $GD3^{5'Cy5}$ and G4 ligands were mixed so that the final concentration of $GD3^{5'Cy5}$ and G4 ligand is 50 μM and 200 μM, respectively (R = 4). Then, the mixtures were incubated at 25 °C for 24 h. RAW264 cells were seeded in a 48-well plate at 2×10^5 cells per well and then incubated for 24 h at 37 °C in a humidified incubator with 5% CO_2. After 24 h, the culture medium was replaced by 200 μL of Opti-MEM (Thermo Fisher Scientific) containing 5 μM $GD3^{5'Cy5}$, $GD3^{5'Cy5}$/L2H2, $GD3^{5'Cy5}$/L2G2 or $2006\_PD^{5'Cy5}$. After 2 h-incubation at 37 °C or 4 °C, the cells were washed with 500 μL phosphate-buffered saline (PBS; Wako Pure Chemical Corporation) twice and harvested. Then, flow cytometric analyses were conducted using a flow cytometer (SP6800; Sony, Tokyo, Japan). Mean fluorescence intensity (MFI) was measured, and $\Delta MFI_{37°C\text{-}4°C}$ ($MFI_{37°C} - MFI_{4°C}$) was calculated.

4.2.10. Immunoprecipitation assay

GD3 was reconstructed in D-PBS. L2H2 and L2G2 stock solution of 10 mM were diluted by sterile MiliQ water to get a concentration of 1 mM. The reconstructed GD3 and G4 ligands were mixed so that the final concentration of GD3 and G4 ligand is 10 μM and 40 μM, respectively (R = 4). Then, the mixtures were incubated at 25 °C for 24 h. Dynabeads Protein G Immunoprecipitation Kit (Invitrogen) and Recombinant Mouse TLR9 Fc Chimera (mTLR9Fc, R&D Systems, Minneapolis, MN, USA) was used to examine the binding between mouse TLR9

to GD3 alone or GD3 in complex with G4 ligands following to the manufacturer's instruction. mTLR9Fc was prepared in phosphate buffer saline (PBS(-), Wako Pure Chemical Corporation, Osaka, Japan) containing 137 mM NaCl, 2.92 mM NaH_2PO_4 and 9.01 mM Na_2HPO_4.

Magnetic beads from 50 μL of dynabeads were collected and resuspended in 200 μL binding and washing buffer containing 5 μg mTLR9Fc. In a non mTLR9Fc control, PBS (-) was used instead of mTLR9Fc. After 20-min-incubation at 25 °C with rotation, the suspensions of Dynabead-mTLR9Fc complex were washed once by the binding and washing buffer. Afterwards, 10 μM GD3 alone or in the mixture with G4 ligands at R = 4 was diluted in MES buffer 10 mM, pH6.5 containing 150 mM K^+, and 20 mM Na^+ to give the concentration of G4 CpG ODNs of 2 μM. G4 CpG ODN solutions at 2 μM (125 μL) was used to resuspend dynabeads. For non CpG ODN control, CpG ODNs were replaced by D-PBS. Next, the suspension of Dynabead-mTLR9Fc complex and G4 CpG ODNs were incubated at 25 °C with rotation for 20 min before washing with the washing buffer three times. To elute bound ODNs and mTLR9Fc on dynabeads, the dynabeads-mTLR9Fc-ODNs complex was resuspended in 12 μL elution buffer and incubated at 25 °C with rotation for 6 min.

Eluted solutions were analyzed by sodium dodecyl sulfate (SDS)-polyacrylamide gel electrophoresis (PAGE) to detect mTLR9Fc binding on the dynabeads, using 15% polyacrylamide gel (ATTO), 1× Tris-Glycine-SDS running buffer (TG-SDS, EMD Millipore Corp., Bedford, MA) with the Coomassie Brilliant Blue (CBB) (Nacalai Tesque, Kyoto, Japan) staining. PAGE analysis of eluted solutions was conducted to detect CpG ODNs binding to mTLR9Fc, in 10-20% polyacrylamide gel (ATTO) with 1× Tris-Glycine running buffer. Ultralow range DNA ladder (Invitrogen) was used as marker. ODNs were visualized by SYBR Gold.

4.2.11. Stimulation of RAW264 cells

GD3 was reconstructed at 85.46 μM in D-PBS. L2H2 and L2G2 stock solution of 10 mM were diluted by sterile MiliQ water to get a concentration of 5 mM. The reconstructed GD3 and

G4 ligands were mixed so that the final concentration of GD3 and G4 ligand is 80 μM and 320 μM, respectively (R = 4). Then, the mixtures were incubated at 25 °C for 24 h. Composition of GD3/G4 ligand solutions is presented in **Table 4.1**. Raw264 cells on a 96-well plate were seeded at a density of 1×10^5 cell/well (5.3×10^5 cell/ml, 190 ml) in the culture medium containing 1 (v/v) P/S (100×), then incubated for 18 h. Afterwards, the cells were stimulated with 4 μM CpG ODNs by adding 10 μL of 80 μM ODNs alone or in the mixture with G4 ligands at R = 4. After 24 h-incubation the relative transcript levels and secretion levels of cytokines were determined.

Table 4.1 Composition of GD3/G4 ligand solutions

Sample	V_{GD3} (μL)[a]	V_{L2H2} (μL)[b]	V_{L2G2} (μL)[b]	$V_{0.5\times DMSO}$ (μL)	$V_{MiliQ\ water}$ (μL)	Total volume (μL)
GD3	56.16	-	-	3.84	-	**60.00**
GD3/L2H2	56.16	3.84	-	-	-	**60.00**
GD3/L2G2	56.16	-	3.84	-	-	**60.00**
D-PBS	-	-	-	3.84	56.16	**60.00**

[a] Volume of GD3 solution at 85.46 μM.

[b] Volume of L2H2 or L2G2 solution at 5 mM.

Relative transcript levels of cytokine in RAW264 cells were examined by RT/RQ-PCR. Total RNA was isolated from cells by ISOGEN (Nippon Gen, Tokyo, Japan) according to the manufacturer's instruction. The isolated RNA had been undergone a genomic DNA digestion step with RNase-Free DNase Set (Takara Bio) and a purification step with Agencourt RNAClean XP (Beckman Coulter, US) before it was converted to cDNA by reverse transcriptase (Takara Bio, Shiga, Japan). IL-6, and IL-12 transcript were measured by quantitative real-time PCR conducted on LightCycler 480 System; SYBR Green MasterMix (Thermo Fisher Science) and the primer listed in **Table 2.1**. Amplification was conducted with 50 ng cDNA in a total volume of 15 μl for 45 cycles, 10 s each at 95 °C, 10 s at 60 °C, and 10 s at 72 °C. Crossing point (Cp), which is PCR cycle where the fluorescence emission increases higher than the background signal, was

determined. The expression level of mRNA was normalized by a house keeping gene, glyceraldehyde 3-phosphate dehydrogenase (GAPDH). Additionally, melting curves were determined to check the specificity of amplified products.

The supernatants form the RAW264 cells stimulated by GD3 or GD3 in the complex with G4 ligands were collected by centrifuging (10,000 ×*g*) for 10 min at 4 °C. IL-6 secretion levels in the supernatants were determined by Mouse IL-6 ELISA Ready-SET-Go kit (eBioscience, San Diego, CA, USA) according to the manufacturer's instructions.

4.2.12. Stimulation of human peripheral blood mononuclear cells (PBMCs)

GD3 was reconstructed at 183.5 μM in D-PBS. L2H2 stock solution of 10 mM were diluted by sterile MiliQ water to get a concentration of 5 mM. The reconstructed GD3 and L2H2 were mixed so that the final concentration of GD3 and G4 ligand is 160 μM and 640 μM, respectively (R = 4). Then, the mixtures were incubated at 25 °C for 24 h. Composition of CpG ODN solutions is presented in **Table 4.2.**

Table 4.2 Composition of GD3/G4 ligand solutions for human peripheral blood mononuclear cell assays

Sample	**V_{GD3} (μL)[a]**	**V_{K3} (μL)[b]**	**V_{K3_PD} (μL)[c]**	**V_{L2H2} (μL)[d]**	**$V_{10\times \text{ D-PBS}}$ (μL)**	**$V_{MiliQ\ water}$ (μL)**	**Total volume (μL)**
GD3	35.77	-	-	-	5.50	14.23	**55.00**
GD3/L2H2	35.77	-	-	7.04	5.50	6.69	**55.00**
K3	-	45.36	-	-	5.50	4.64	**55.00**
K3_PD	-	-	40.55	-	5.50	9.45	**55.00**
D-PBS	-	-	-	-	5.50	49.50	**55.00**

[a] Volume of GD3 stock solution at 246 μM.

[b] Volume of K3 stock solution at 194 μM.

[c] Volume of K3_PD stock solution at 194 μM.

[d] Volume of L2H2 solution at 5 mM.

Human peripheral blood mononuclear cells (PBMCs) (Sample ID: 20110727; ethnicity: Hispanic; age: 29; gender: Female; ABO/Rh: O/Pos), purchased from Cellular Technology Limited (Shaker Heights, OH, USA), were thawed according to the manufacturer's instructions and resuspended in Roswell Park Memorial Institute 1640 medium (Thermo Fisher Scientific) containing GlutaMAX, 4-(2-hydroxyethyl)-1-piperazineethanesulfonic acid), 1% (v/v) P/S (100×), and 10% (v/v) heat-inactivated FBS. The cell suspension (190 μL) was seeded into a 96-well plate at a density of 7×10^5 cells/well and stimulated with ODNs. Afterwards, the cells were stimulated with 8 μM CpG ODNs by adding 10 μL of 160 μM ODNs alone or in the mixture with L2H2 at R = 4. After incubation for 48 h, the cells were centrifuged (10,000 ×*g*) for 10 min at 4 °C to collect the supernatants. IL-6 and IFN-γ Ready-Set-Go kits (Thermo Fisher Science) were used according to the manufacturer's instructions to evaluate cytokine expression levels in the supernatants. K3 with phosphorothioate backbone (5'-atc gac tct cga gcg ttc tc-3') and K3_PD with phosphodiester backbone (5'-ATC GAC TCT CGA GCG TTC TC-3') were used as control ODNs that form a random coil structure.

For examination of Th1-bias immune response induced by CpG ODNs, PBMCs (270 μL) were seeded into a 48-well plate at a density of 2×10^5 cells/well and were stimulated with 10 ng/mL of IL-4 and 8 μM of GD3, or GD3/L2H2. K3, or K3_PD were used as control ODNs that form a random coil structure. After 7-day incubation, supernatants were collected, and IL-13 in the supernatants was examined by ELISA using Human IL-13 Antibody Pair Kit (Invitrogen).

4.2.13. *In vivo* immunostimulatory properties of G4 CpG ODNs

GD3 was reconstructed at 52 μM in D-PBS. L2H2 and L2G2 stock solution of 10 mM were diluted by sterile MiliQ water to get a concentration of 5 mM. The reconstructed GD3 and G4 ligands were mixed so that the final concentration of GD3 and G4 ligand is 50 μM and 200 μM, respectively (R = 4). Then, the mixtures were incubated at 25 °C for 24 h. *In vivo* studies were approved by the Animal Care and Use Committee at the National Institute for Materials

Science and were in compliance with the Guidelines for Proper Conduct of Animal Experiments established by the Science Council of Japan. Seven-week-old female C57BL/6 mice (Charles River Laboratories Japan, Yokohama, Japan) were intraperitoneally injected with 10 nmol of GD3, or GD3/L2H2. K3, which is a common linear phosphorothioate class B CpG ODN, was used as a positive control. Blood samples were collected before injection and 2 h after injection from the facial veins of the mice using Goldenrod Animal Lancets (Braintree Scientific, MA, USA). The blood was centrifuged (12,000 ×*g*) for 10 min at 4 °C to collect the plasma. The collected plasma was stored at -30 °C until use. The plasma IL-6, IL-12p70, and IFN-γ concentration was determined by ELISA using the mouse IL-6, IL-12p70, and IFN-γ Ready-Set-Go kit (Thermo Fisher Science) according to the manufacturer's instructions.

4.2.14. Statistical analysis

Statistical comparisons of the data were conducted by one-way analysis of variance (ANOVA) followed by Tukey's multiple comparisons test for comparison with other groups or by Dunnett's multiple comparisons test for comparison with a control group. All statistical analyses were performed using GraphPad Prism version 8.2.0 for Windows (GraphPad Software, La Jolla, CA, USA). A p-value < 0.05 was considered statistically significant.

4.3. Results and discussion

4.3.1. Structural analysis of GD3 in complex with G4 ligands

A negative peak at 295 nm showed in thermal difference spectra (TDS) of GD3/L2H2 and GD3/L2G2 (**Fig. 4.2A**) corresponds to a denaturation of G4 structure at high temperature.[72] In addition, PAGE analysis with running buffer containing K^+ (**Fig. 4.2B**) showed that the complexes of GD3 with both ligands migrated faster than the linear ODN having the same length (ssODN38mer), indicating that GD3 formed monomeric G4 structure in the complexes with G4 ligands. In the absence of K^+ in running buffer, PAGE analysis (**Fig. 4.2C**) shows that GD3 moved nearly as fast as the 35 bp marker, indicating that GD3 did not keep G4 structure without K^+.

Whereas GD3/L2H2 and GD3/L2G2 showed two bands, with one band has higher migration speed than the linear 35 bp marker, suggesting that G4 ligands stabilized G4 structure even in the absence of K^+.

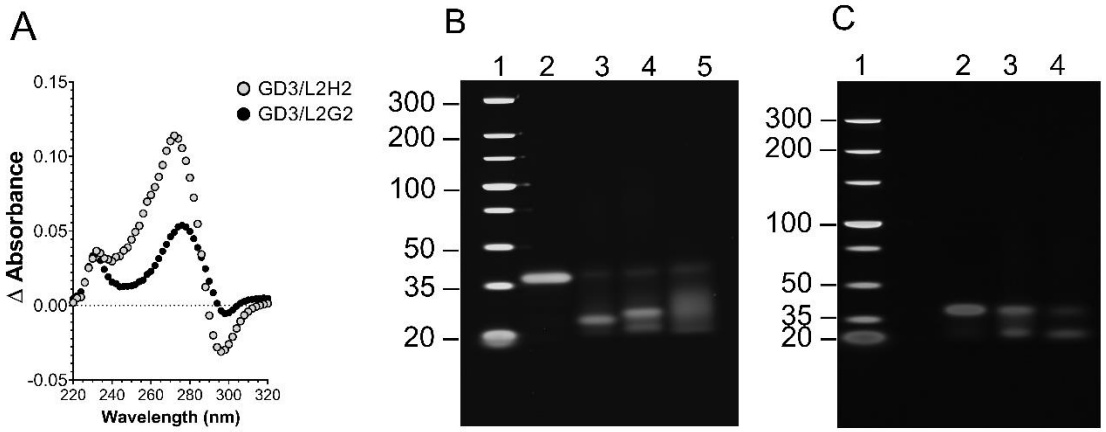

Figure 4.2 Structural analysis of GD3 in the complex with G4 ligands at R = $n_{G4\text{-}ligand}$:n_{GD3} = 4. (A) Thermal difference spectra obtained by subtraction of the spectra obtained at 20 °C from those obtained at 90 °C. (B) Polyacrylamide gel electrophoresis analysis in the presence of 4 mM K^+; lane 1, ultralow-range DNA ladder; lane 2, ssODN38mer; lane 3, GD3; lane 4, GD3/L2H2; lane 5, GD3/L2G2. (C) Polyacrylamide gel electrophoresis analysis in the gel and running buffer not supplemented with KCl; 1, ultra-low range DNA ladder; 2, GD3; 3, GD3/L2H2; 4, GD3/L2G2.

CD spectra was conducted to examine G4 topology of G4 CpG ODN. The GD3 CD spectrum at 25 °C showed a negative peak at 240 nm and a broad positive peak in range of 260-290 nm (**Fig. 2.2B**). The broad positive peak is attributed to an overlap of a positive peak at around 280 nm which corresponds to random structures of the long central loop, on two positive peaks at 260 and 295 nm which correspond to signals of G4 stem in a hybrid type G4 (**Fig. 2.3B**). The contribution of long central loop to the CD spectra can be excluded by subtraction the GD3 CD spectrum at high temperature from the original CD spectra. Resulting spectra after the subtraction thus only characterize G4 stem and reveal the topology of G4 CpG ODNs, not interfered by the random coiled structure of long loop regions (**Fig. 2.7A**).

GD3/L2H2 CD spectrum (**Fig. 4.3A i**) showed a negative peak at 240 nm and a positive at 275 nm. To exclude contribution of the long central loop from the total CD signal, we subtracted the GD3/L2H2 CD spectrum to the GD3 CD spectrum at 90 °C. The resulting CD spectrum (**Fig. 4.3A ii**) showed a negative peak at 240 nm, and two positive peaks at 270 and 290 nm, which may correspond to a hybrid-type G4. This suggests that GD3/L2H2 have similar structure with GD3, and L2H2 only change conformation of GD3 a little. Meanwhile, both CD spectra GD3/L2G2 before (**Fig. 4.3B i**) and after (**Fig. 4.3B ii**) subtracting to GD3 CD spectrum at 90 °C showed a negative peak at 240 nm and a positive peak at 265 nm, which is typical CD pattern of parallel G4. In parallel structure, the long central loop of GD3 was at side of G4 stem, not on top or down of G-quartet, so it may not interfere to the total CD signal. Therefore, there was no difference in CD pattern of GD3/L2G2 before and after subtracting to GD3 CD spectrum at 90 °C. L2G2 dramatically changed topology of GD3 from hybrid into parallel. This result is consistent with the findings of Ma et al., who reported that L2G2 strongly regulated G4 topology of telo24 into parallel type.[99] Taken together, TDS, PAGE analysis, and CD spectra indicate that GD3 formed monomeric G4 structure in the complex with both G4 ligands. Regrading topology, GD3/L2H2 formed hybrid G4, while GD3/L2G2 formed parallel G4.

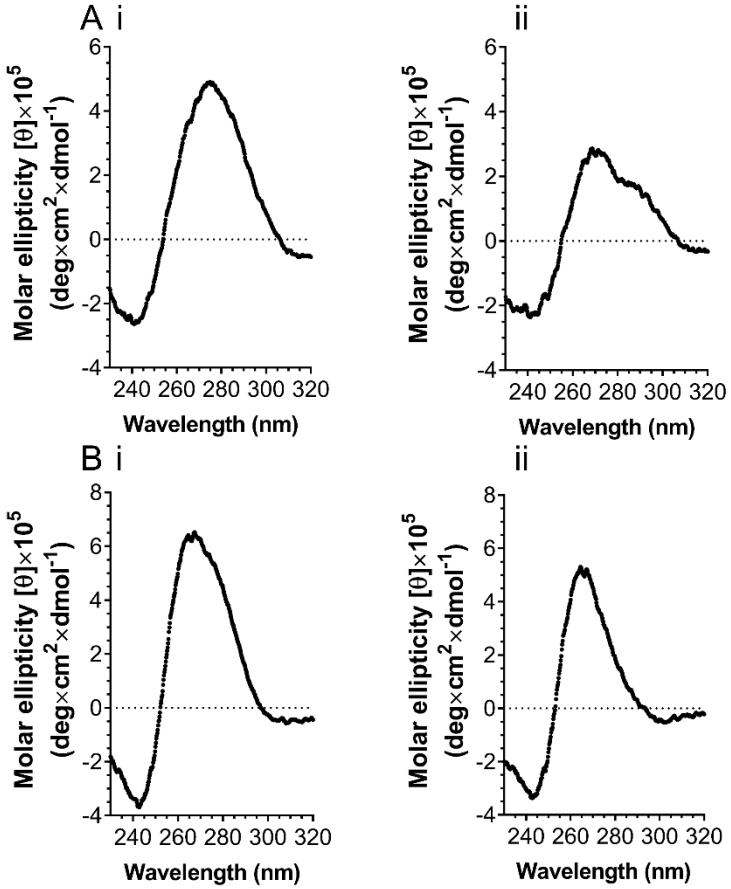

Figure 4.3 Circular dichroism (CD) of GD3 in the complex with G4 ligands at R = $n_{G4\text{-}ligand}$:n_{GD3} = 4 . CD spectra of (A) GD3/L2H2, and (B) GD3/L2G2. (i) CD spectra at 25 °C. (ii) CD spectra after subtracting to CD spectra of GD3 at 90 °C.

4.3.2. Effects of G4 ligands on thermodynamic stability of GD3

UV melting curves were determined by recording UV absorbance at 295 nm during heating process to examine thermodynamic stability of GD3/L2H2 and GD3/L2G2 (**Fig. 4.4**). The melting temperatures of G4 CpG ODNs are presented in **Table 4.3**. GD3/L2H2 showed melting temperature at 77 °C calculated based on the melting curves by the baseline method[103], while the melting curve of GD3/L2G2 did not show transition in the temperature range of 20-90 °C, suggesting that GD3/L2G2 may have melting temperature higher than 90 °C. Therefore,

melting temperature of GD3 in complex with L2H2 and L2G2 increased compared with GD3 (T_m = 41 °C).

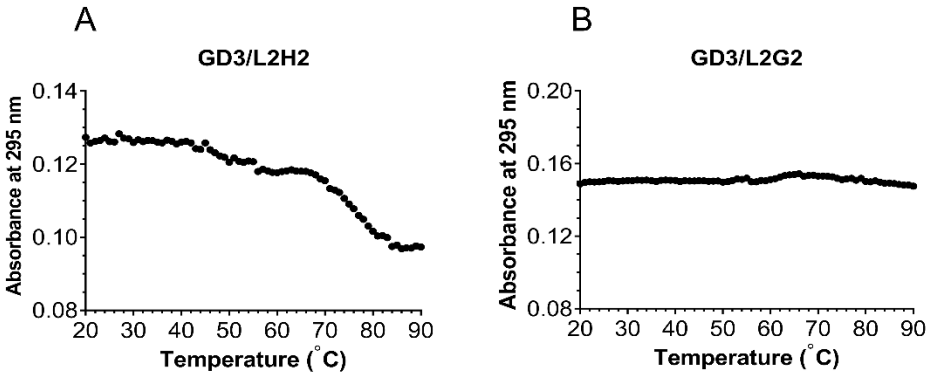

Figure 4.4 Ultraviolet (UV) melting curves of GD3 in the complex with G4 ligands at R = $n_{G4\text{-}ligand}$:n_{GD3} = 4. UV absorbance at 295 nm was monitored during the heating process of (A) GD3/L2H2 and (B) GD3/L2G2.

Table 4.3 Melting temperature of GD3 and GD3 in the complex with G4 ligands [a]

ODNs	G4 Topology	Melting temperature (°C)[b]	References
GD3	Hybrid	41	Chapter 2
GD3/L2H2	Hybrid	77	In this chapter
GD3/L2G2	Parallel	> 90	In this chapter

[a]GD3, GD3/L2H2, and GD3/L2G2 were prepared at concentration of 2 μM in D-PBS with about 4 μM K^+, and 150 μM Na^+. Molar ratio R = $n_{G4ligand}$:n_{GD3} = 4.

[b] The melting temperatures of GD3, GD3/L2H2, and GD3/L2G2 were determined from the UV melting curves at 295 nm by the baseline method.

In addition to UV melting curves, CD melting curves were conducted. Based on the subtraction of CD spectra at 90 °C (**Fig. 4.5A i and Fig. 4.5A ii**) from those at 25 °C (**Fig. 4.3A i and Fig. 4.3B i**), CD melting curves of GD3/L2H2 and GD3/L2G2 were monitored at 265 nm

and 270 nm, respectively, at which the largest difference in molar ellipticity between low and high temperature occurred. The molar ellipticity of GD3/L2H2 (**Fig. 4.5C i**) started to decrease from 70 °C, while that of GD3/L2G2 (**Fig. 4.5C ii**) was stable up to 90 °C. This tendency is consistent with the results of UV melting curves. The UV and CD melting curves revealed that L2H2 and L2G2 increased thermodynamic stability of GD3. Stabilizing abilities of these G4 ligands were observed in previous study of Ma et al.[99], who reported that L2H2 and L2G2 increase melting temperature of telomeric sequence named telo21 by 19.1 and 25.3 °C, respectively.

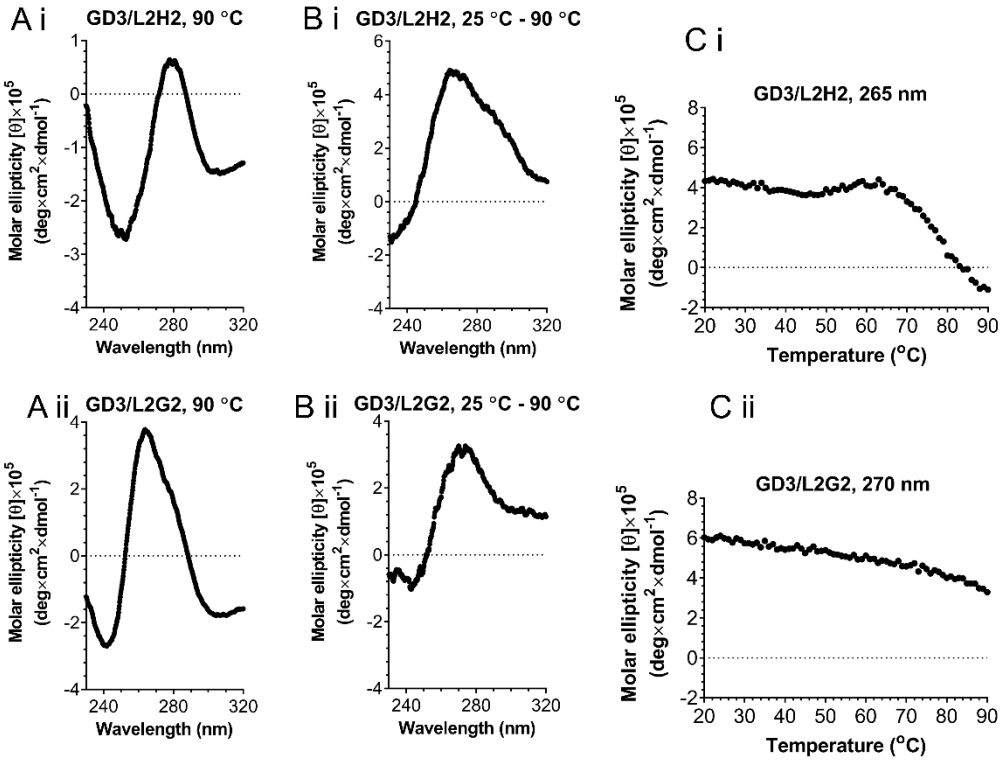

Figure 4.5 Circular dichroism (CD) melting profiles of GD3 in the complex with G4 ligands at R = $n_{G4\text{-}ligand}$:n_{GD3} = 4. (A) CD spectra of (i) GD3/L2H2, and (ii) GD3/L2G2 at 90 °C. (B) CD-thermal difference spectra of (i) GD3/L2H2, and (ii) GD3/L2G2 at 90 °C. CD-thermal difference spectra showed that the largest difference in molar ellipticity between low and high temperature occurred at 265 nm and 270 nm for GD3/L2H2 and GD3/L2G2, respectively. The (C) The molar ellipticity values were monitored during the heating from 20°C to 90°C of (i) GD3/L2H2 at 265 nm, and (ii) GD3/L2G2 at 270 nm.

4.3.3. Effects of G4 ligands on stability in serum of GD3

Figure 4.6 shows nuclease resistance of GD3 alone and GD3 in the complexes with G4 ligands at R = 4. PAGE was used to evaluate remaining ODNs after incubating in 18% FBS for indicated time (**Fig. 4.6 A-C**). The processing ODNs showed two bands with different migration speed in PAGE analysis. The upper bands with lower migration speed correspond to molecules with random coiled structures, while the lower bands with faster migration speed correspond to more compact molecules forming G4. The relative percentages of whole remaining ODNs to the amount of ODNs at the beginning were evaluated based on the total intensity of both these bands. In addition, contribution of the intensities of the upper and lower bands into these percentage were presented as a stacked column chart showed in **Figure 4.6D**. Contribution of G4-forming molecules into the remaining amount of ODNs was always higher than that of random coiled molecules over the examined incubation time indicated that the remaining ODNs were mainly in G4 conformation. This result is compatible with the previous findings that G4 have higher nuclease resistance than linear structure (**Fig. 2.8**). An increase in intensity of the upper band after 1 h-incubation compared with 0 h-incubation of GD3 may because some broken molecules, generated during the first hour incubation, were not able to form G4 structure still long enough to be observed on PAGE.

Figure 4.6E illustrates percentages of remaining G4-forming molecules relative to G4-forming molecules quantity at the beginning of incubation, which calculated based on only the intensity of lower bands. Accordingly, after 1 h of incubation, GD3, GD3/L2H2, and GD3/L2G2 remained 82%, 85%, and 96%, respectively. After 2-h incubation, 78%, and 96% GD3/L2H2 and GD3/L2G2 respectively were not degraded, while only 67% GD3 remained. The difference in percentage of remaining ODN between GD3 alone and GD3 coordinating with G4 ligands were observed more clearly after 4 h of incubation with a dramatic decrease in percentage of remaining

GD3 37%, while residual GD3/L2H2 and GD3/L2G2 only dropped to 68% and 84%, respectively. After 24 h, almost no GD3 remained, while GD3/L2H2 and GD3/L2G2 remain about 24% and 36% respectively. These results suggest that both G4 ligands increased nuclease resistance of GD3, and L2G2 was more effective in increase stability of GD3 than L2H2. To our knowledge, this is the first report about ability of G4 ligands on increase nuclease stability of G4 ODNs. The previous studies reported that G4 ligands increase mechanical strength G4 ODNs against the forces causing unfold form, and this may further prevent from elongation by telomerases.[101] The reinforcement of G4 CpG ODNs by G4 ligands may enable them are more difficult to be degraded by nucleases.

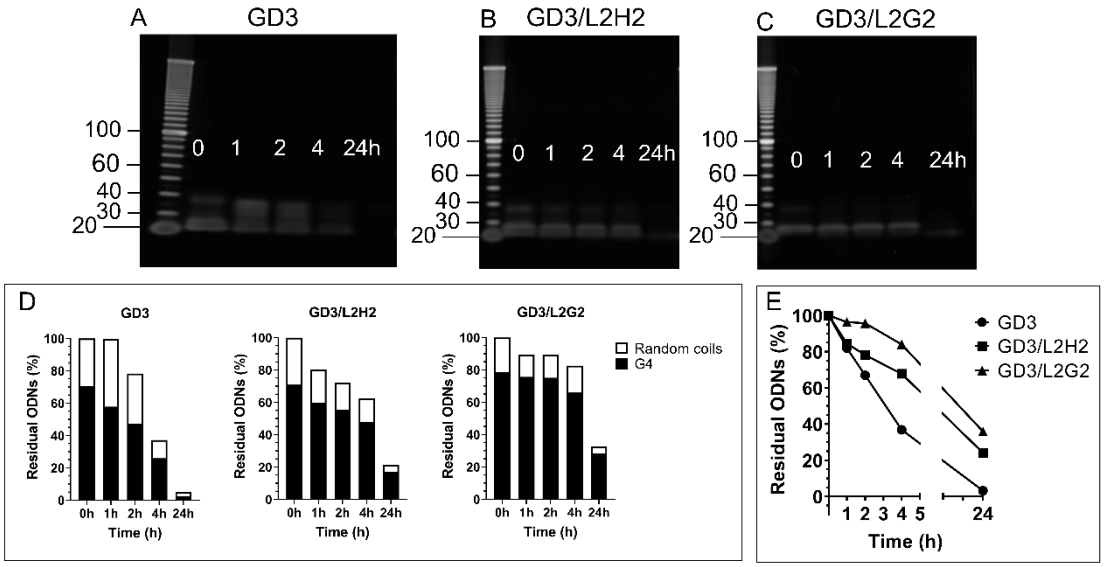

Figure 4.6 G4 ligands enhanced stability of GD3 in 18% serum. Polyacrylamide gel electrophoresis analysis of (A) GD3, (B) GD3/L2H2, and (C) GD3/L2G2 after incubation for 1, 2, 4, and 24 h with 18% fetal bovine serum (FBS). (D) Percentages of residual ODNs relative to ODN quantity at the start of incubation; (E) Percentages of remaining ODNs relative to ODN quantity at the start of incubation. Black segment: contribution of G4 ODNs in to the remaining ODNs; White segment: contribution of linear ODNs into the remaining ODNs.

4.3.4. Effects of G4 ligands on intracellular uptake of GD3

The cellular uptake of $GD3^{5'Cy5}$, $GD3^{5'Cy5}$/L2H2, $GD3^{5'Cy5}$/L2G2 and $2006\_PD^{5'Cy5}$ were examined in RAW264 cells. At 4 °C, receptor-mediated uptake is remarkably suppressed, so we can only observe the ligand-receptor binding at the cellular surface. At 37 °C, receptor-mediated uptake become active, so the observed fluorescent signals represent for both cell surface bound ODNs and cellular internalized ODN. Histograms showing fluorescence of the cells treated with G4 CpG ODN at 4 °C and 37 °C are displayed in **Figure 4.7A i and Figure 4.7A ii**, respectively. The gray bars in **Figure 4.7B** represent for the amount of Cy5-lablled ODNs bound on the surface, and the black bars in **Figure 4.7B** represent for the amount of both cell-surface bound ODNs and internalized ODNs. The difference between the black and gray bars, which are presented in **Figure 4.7C**, can be related to the net amount of labelled ODNs taken up into the cells. **Figure 4.7B** shows that at 4 °C the MFI values of cells treated with $GD3^{5'Cy5}$/L2G2 was 10 times higher than that of cells incubated with GD3 or $GD3^{5'Cy5}$/L2H2, suggesting that more GD3/L2G2 bound on cell surface compared with GD3 or GD3/L2H2. This result is consistent with the fact that parallel G4 have a stronger cellular binding than anti-parallel or hybrid G4.[84] At 37 °C the MFI values of cells treated with $GD3^{5'Cy5}$/L2G2 was also higher than that of cells incubated with GD3 (**Figure 4.7B**), but $\Delta MFI_{37°C - 4°C}$ for $GD3^{5'Cy5}$/L2G2 was lower than for $GD3^{5'Cy5}$ (**Figure 4.7C)**. This implies that the amount of internalized $GD3^{5'Cy5}$/L2G2 was lower than that of $GD3^{5'Cy5}$ regardless of its increase in cellular binding. Cell-surface bound amount of $GD3^{5'Cy5}$/L2H2 was not too much larger than $GD3^{5'Cy5}$, which may because both of them form hybrid G4, not parallel G4. However, the small change in conformation caused by L2H2 probably effected on the endocytosis of GD3, as we can observe a slight decrease in amount of internalized $GD3^{5'Cy5}$/L2H2.

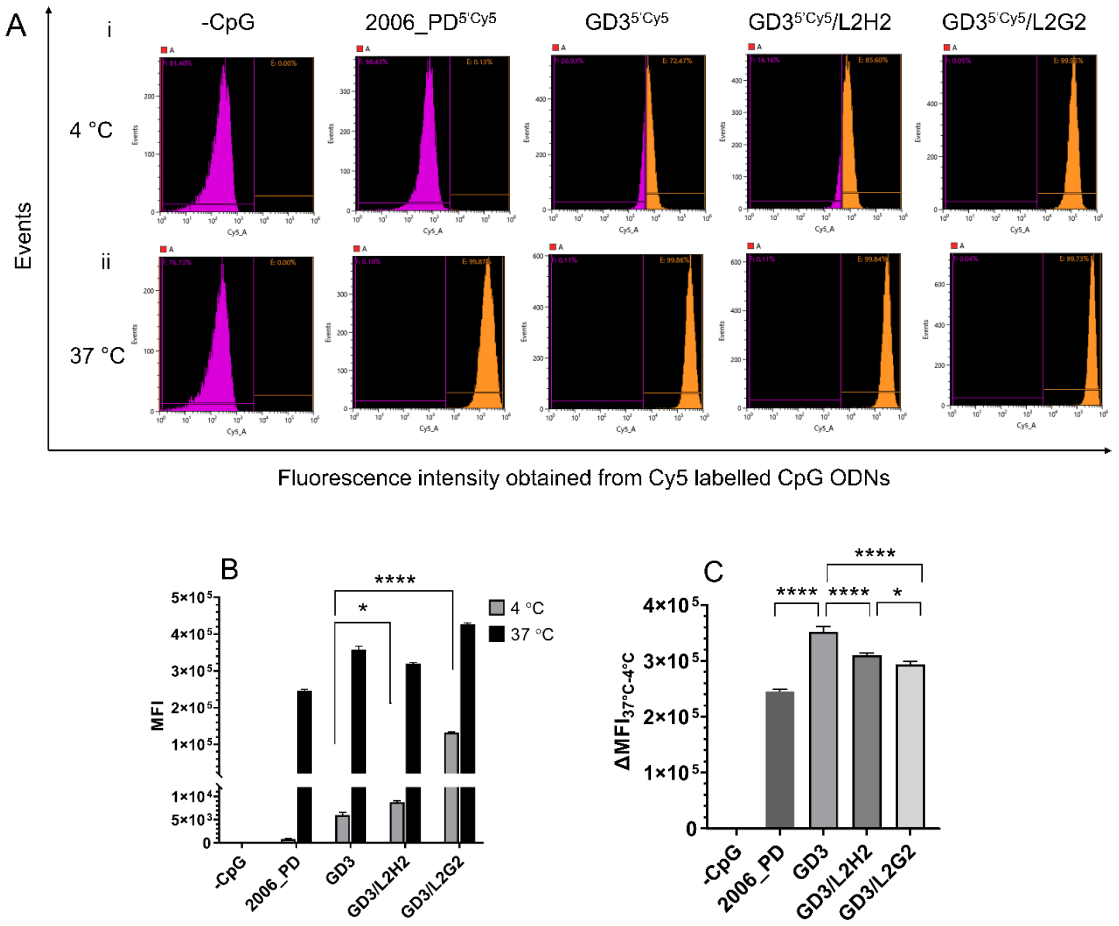

Figure 4.7 Uptake of Cy5 labelled CpG ODNs in RAW264 cells. (A) Histogram analysis of fluorescence intensity at (i) 4 °C and (ii) 37 °C. (B) Mean fluorescence intensity (MFI) of the cells incubated at 37 °C and 4 °C; (C) Internalized Cy5 labelled CpG ODNs were measured by $\Delta MFI_{37°C-4°C}$. RAW264 cells were incubated with 5 μM $GD3^{5'Cy5}$, $GD3^{5'Cy5}$/L2H2, $GD3^{5'Cy5}$/L2G2 or $2006\_PD^{5'Cy5}$ for 2 h. Data represent mean ± SD (n = 3). ****p < 0.0001, ***p < 0.001, *p < 0.05, p > 0.05, One-way ANOVA, Tukey's multiple comparisons test.

4.3.5. Immunoprecipitation assay

Immunoprecipitation assay was conducted to examine the binding between TLR9 ectodomain and GD3 without and with presence of G4 ligands (**Fig. 4.8**). In SDS-PAGE, we observed the comparable quantity of mTLR9Fc bound to protein-G-conjugated beads in all samples were confirmed by similar intensity of the TLR9 bands. In PAGE, the bands

corresponding to GD3, GD3/L2H2, and GD3/L2G2 were observed, suggesting that GD3 alone and GD3 in complex with L2H2 and L2G2 can bind to ectodomain of mTLR9.

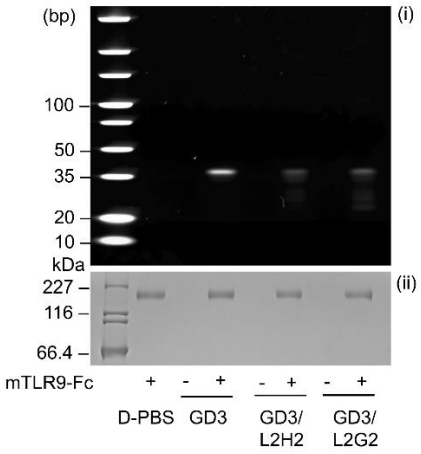

Figure 4.8 Immunoprecipitation binding assay of the binding between mouse TLR9 and GD3 or GD3 in the complex with G4 ligands at R = $n_{G4\text{-}ligand}$:n_{GD3} = 4. The assay was conducted at pH 6.5. GD3, GD3/L2H2, or GD3/L2G2 (250 pmol) was mixed with the protein-G-conjugated beads with and without bound mTLR9Fc. The DNA bound to the beads was examined by (i) polyacrylamide gel electrophoresis (PAGE) using a 10-20% polyacrylamide gel and 1× Tris-Glycine running buffer and were visualized by SYBR Gold staining. (ii) mTLR9Fc bound to protein-G-beads was detected by SDS-PAGE using a 15% polyacrylamide gel, 1× Tris-Glycine-SDS running buffer, and Coomassie brilliant blue staining.

4.3.6. Effects of G4 ligands on immunostimulatory properties of GD3

L2H2 was able to increase *IL-6* and *IL-12* mRNA production in mouse macrophage-like RAW264 cells expressing TLR9 treated by GD3 (**Fig. 4.9A i, ii**). Meanwhile, L2G2 decrease *IL-6* and *IL-12* mRNA production (**Fig. 4.9A i, ii**). We also observed that the transcript level of IL-6 was correlate with its secretion level in RAW264 cells (**Fig. 4.9B**). However, L2H2 and L2G2 did not change the *IFN-β* mRNA production induced by GD3 (**Fig. 4.9A iii**).

In addition, L2H2 and L2G2 themselves did not activate cytokine production in RAW264 cells (**Fig. 4.9 C i and ii**), indicated that the cytokine induction only depends on the ODN. Tera

et al.[98] demonstrate that L2H2 selectively binds and stabilizes telomere sequence. L2H2 inhibits activity of telomerase, an enzyme elongating telomere regions in chromosomes and leading to development of cancer cells.[104] In accordance with the telomerase inhibitory activity, L2H2 inhibits growth of cancer cell line such as Hela cells.[104] These results suggest that L2H2 is taken up into the cells, binds and stabilizes telomeres in chromosome of Hela cells, so inhibits activity of telomerase. This is an indirect evidence that L2H2 alone can be taken up into cells. Therefore, in my study, L2H2 was taken up into cells but did not induce cytokines.

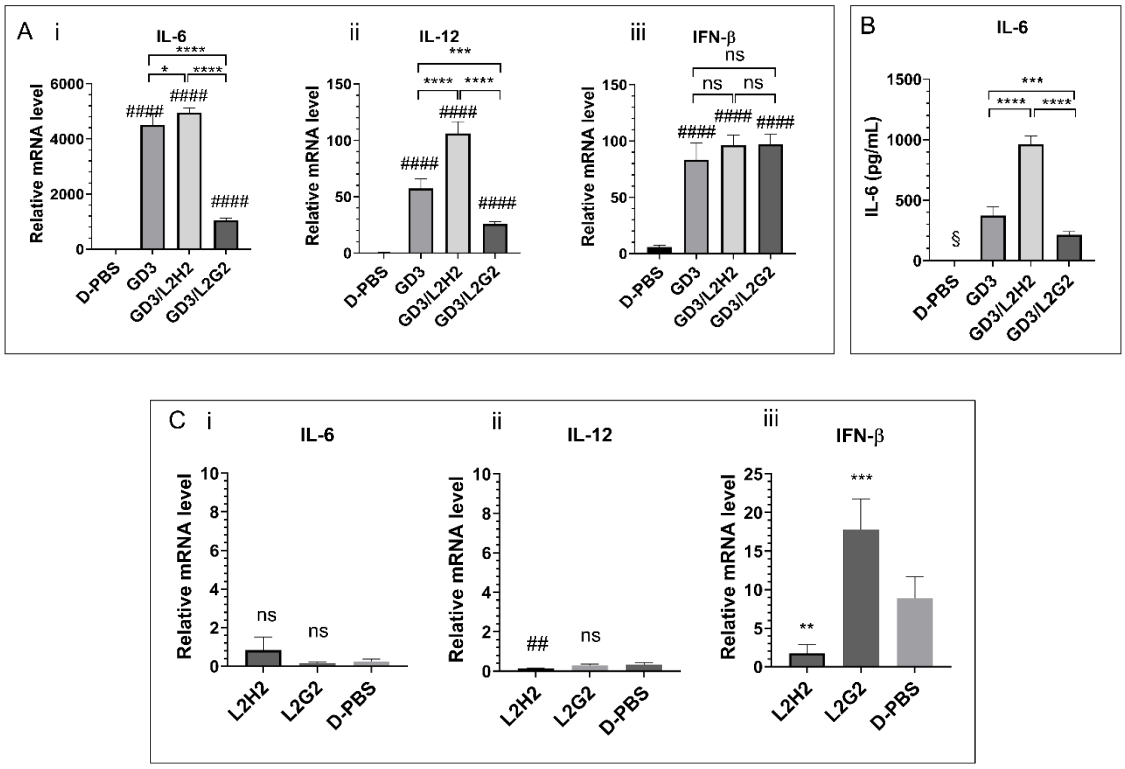

Figure 4.9 Cytokine induction in mouse macrophage-like RAW264 cells stimulated with GD3 and GD3 in the complex with G4-ligands at R = $n_{G4\text{-}ligand}$:n_{GD3} = 4. (A) Relative mRNA levels of (i) *IL-6*, (ii) *IL-12*, and (iii) *IFN-β* in mouse macrophage-like RAW264 cells after 24 h of stimulation with 4 μM GD3, GD3/L2H2, or GD3/L2G2. (B) The level of IL-6 secreted into the culture medium. Supernatants from RAW264 cells incubated with 4 μM GD3, or GD3 in complex with G4 ligands for 24 h were assayed by enzyme-linked immunosorbent assay for IL-6. (C) Relative mRNA levels of (i) *IL-6* and (ii) *IL-12*, and (iii) *IFN-β* in mouse macrophage-like RAW264 cells after 24 h of stimulation with L2H2 and L2G2. Data represent mean ± SD (n = 5). ****p < 0.0001, ***p < 0.001, **p < 0.01, *p < 0.05, ns (not significantly different from D-PBS)

$p > 0.05$ (*, one-way ANOVA, Tukey's multiple comparisons test for comparison with other groups; #, Dunnett's multiple comparisons test for comparison with the D-PBS control group); §: lower detection limit of ELISA (3.9 pg/mL).

The cellular uptake of GD3/L2H2 was lower than GD3, but it can induce higher cytokine induction than did GD3, suggesting that cellular uptake is not the reason for the differences in the immunostimulatory activities between GD3 and GD3/L2H2. Higher nuclease stability is a critical factor contribute to immunostimulatory efficiency of GD3/L2H2, as more CpG motifs in GD3/L2H2 are protected from degradation by nuclease and approach TLR9 in endosome.

Despite possessing higher nuclease resistance, GD3/L2G2 was less effective in cytokine induction than did GD3, indicating that nuclease resistance may not be a determining factor of immunostimulatory effect of GD3/L2G2. The extent of decrease in cellular uptake of GD3/L2G2 is not as much as to the extent of decrease in IL-6 and IL-12 production induced by GD3/L2G2, suggesting that there is another factor preventing TLR9 activation of GD3/L2G2 in addition to the poor internalization efficiency. The immunostimulatory properties of G4 CpG ODNs were revealed to relate to the binding between CpG ODNs and TLR9. The G4 topology may play a key role in making the binding. In this regard, L2H2 stabilizes and keeps hybrid form of GD3, while L2G2 facilitates parallel-type G4 formation of GD3, which is significantly different from the original hybrid structure of GD3. Concerning charge distribution, in the hybrid G4, the negative charges of phosphate backbone are distributed in whole of structure. Meanwhile, in the parallel case, negative charges only locate at the side parts, as the top and bottom of G4 are π-π stacking interaction with G4 ligands.[99] This difference in charge distribution of G4 leads to a difference in binding mode between G4 ODNs and TLR9. TLR9 dimerization resulting from the interaction between TLR9 and CpG ODNs is an important step in the TLR9-initiated intracellular signaling cascade and cytokine production.[6] We assume that the binding mode made by parallel GD3/L2G2 is less effective to induce dimerization of TLR9 compared with the one made by hybrid GD3 or

GD3/L2H2. The effects of G4 ligands on structures and properties of GD3 were demonstrated in **Figure 4.10**.

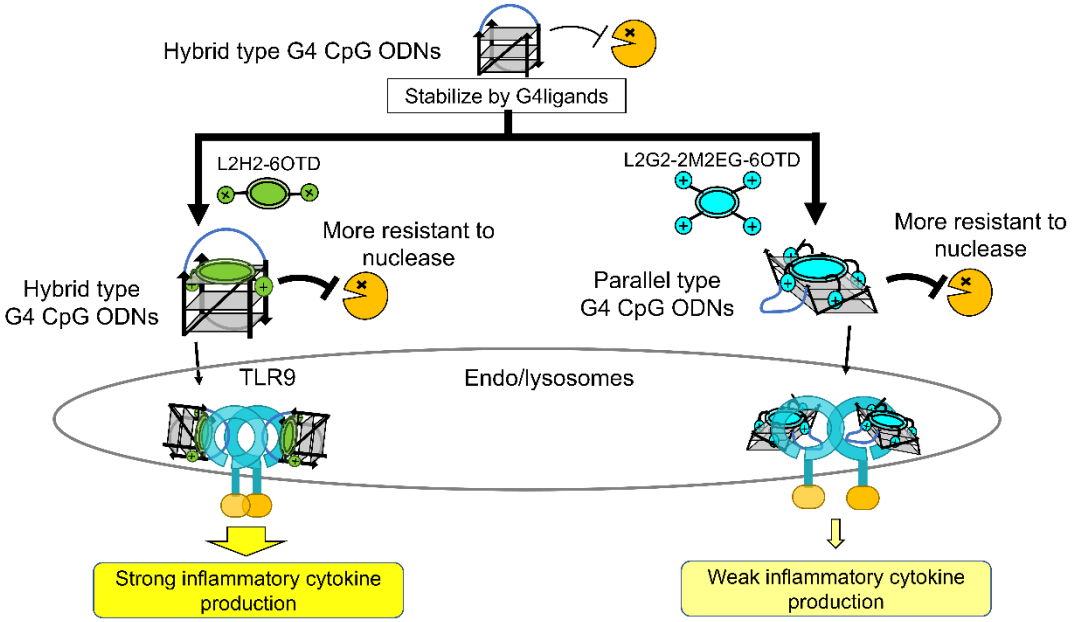

Figure 4.10 Schematic illustration of effects of G4 ligands on G4 topology and properties of G4 CpG ODNs. A hybrid-type monomeric G4 CpG ODN named GD3 was coordinated with G4 ligands, L2H2-6OTD and L2G2-2M2EG-6OTD which are mentioned as GD3/L2H2 and GD3/L2G2, respectively. L2H2 and L2G2 induced hybrid and parallel G4 of GD3, respectively. Both of G4 ligands enable a remarkable increase in nuclease resistance of GD3. Binding between GD3/L2H2 and TLR9 is more effective to induce dimerization of TLR9. Consequently, GD3/L2H2 induced higher cytokine production than GD3, but GD3/L2G2 was less effective in cytokine induction.

Besides the binding efficiency between CpG ODNs and TLR9, CpG ODN trafficking to endosomal compartments may be responsible for the hypo-response to GD3/L2G2 in RAW264 cells. GD3/L2G2 with parallel G4 topology have a stronger cellular binding than GD3 and GD3/L2H2 with hybrid G4 topology (**Fig. 4.7**). The increase in cell-surface binding of parallel G4 ODNs was revealed to involve to cell membrane proteins such as cell-surface nucleolin.[84] We doubt if GD3/L2G2 targets a cell membrane protein, while GD3 and L2H2 did not. Then, whether

the uptake GD3/L2G2, mediated by that cell membrane protein, leads to an improper delivery of GD3/L2G2 into cytosol, not into endo/lysosomes, and results in the poor response of RAW264 cells. Therefore, additional experiments should be done to examine intracellular localization of GD3, GD3/L2H2, and GD3/L2G2 in the cells.

4.3.7. Ability of GD3 and GD3/L2H2 to induce of Th1-biased immune milieu

T cell is one of two main types of lymphocytes and essential for adaptive immune responses. T helper cells are classified into two types called T-helper 1 (Th1) and 2 (Th2) cells, which have a mutually exclusive cytokine secretion. Differentiation of Th1 cells is initiated by IL-12 and IFN-γ. Th1 cells express cytokines including IFN-γ, IL-2, and lymphotoxin.[21] Meanwhile, differentiation of Th2 cells, which produce IL-4, IL-5, IL-10, and IL-13, is IL-4–dependent.[21] Concerning function, a certain infection requires a distinctive induction of Th1 or Th2 responses. Clearance of intracellular infections necessitates Th1 response, while Th2 responses eliminate helminth infection. Induction of inappropriate Th cell responses is often the cause of chronic infectious diseases.[105] Therefore, it is crucial to elucidate the type of Th immune milieu generated by GD3 and GD3/L2H2.

As shown in **Figure 4.11A**, GD3 and GD3/L2H2 induced IL-6 production in hPBMCs. In addition, GD3 and GD3/L2H2 induced IFN-γ, which is the characteristic Th1 cytokine (**Fig. 4.11B**). Furthermore, as shown in **Figure 4.12**, addition of IL-4 leads to increase of IL-13 production, because IL-4 activates differentiation of naïve T helper (Th0) cells to T helper type 2 (Th2) cells, which produce IL-13.[105] In the presence of GD3, and GD3/L2H2, the production of induced IL-13 significantly decreased with the level of IL-13 lower than the limit of detection (12.5 pg/mL) (**Fig. 4.12**). This may be resulted from their ability to induce IFN-γ production, as it is known that IFN-γ inhibits IL-4 secretion as well as differentiation of naive Th0 cells into Th2 cells.[106] These results indicate that GD3 and GD3/L2H2 suppresses Th2 response, so induces Th1-biased immune response.

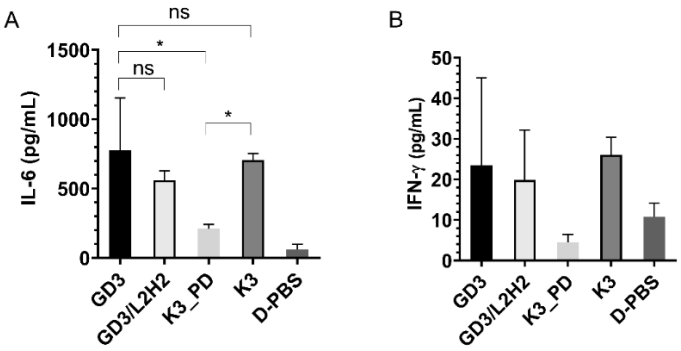

Figure 4.11 Cytokine production by human peripheral blood mononuclear cells stimulated by GD3/L2H2. Data represent mean ± SD (n = 2-3). *p < 0.05, ns (not significantly different) p > 0.05 (one-way ANOVA, Tukey's multiple comparisons test for comparison with other groups).

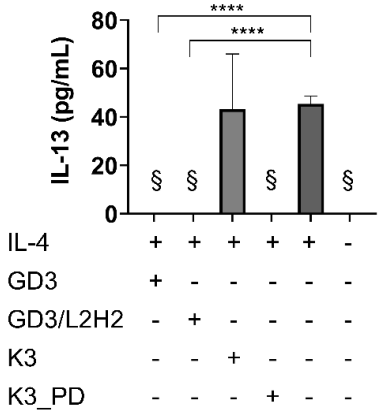

Figure 4.12 IL-13 production by human peripheral blood mononuclear cells stimulated by IL-4 with and without the presence of G4 CpG oligodeoxynucleotides (8μM). Data represent mean ± SD (n = 3 - 4). In the graphs, the section mark (§) indicates the lower detection limit (12.5 pg/mL). ****p < 0.0001 (one-way ANOVA, Tukey's multiple comparisons test for comparison with other groups).

4.3.8. Immunostimulatory properties of GD3/L2H2 in mice

Because L2H2 increases the immunostimulatory activity of G4 CpG ODNs, the immunostimulatory properties of GD3/L2H2 *in vivo* were evaluated in mice (**Fig. 4.13**). Blood samples were collected 2 h after intraperitoneal injection from the facial veins of the mice, then plasma concentration of IL-6, IL-12p70, and IFN-γ was determined by ELISA. The plasma IL-

12p70 and IFN-γ induced by GD3, GD3/L2H2, GD3-DOTAP, and K3 at 2 h-post injection were lower than the detection limit (7.8 pg/mL). Meanwhile, as shown in **Figure 4.13**, GD3, GD3/L2H2, GD3-DOTAP induced plasma IL-6 production at 2h-post stimulation, while the plasma IL-6 induced by K3 and D-PBS were lower than limit of detection (3.9 pg/mL). Notably, GD3/L2H2 induced higher plasma IL-6 compared with GD3. This may because of a higher nuclease resistance of GD3/L2H2. The increase of immunostimulatory activity of G4 CpG ODNs by L2H2 via intraperitoneal injections in mice indicates the potential application of GD3/L2H2 *in vivo*.

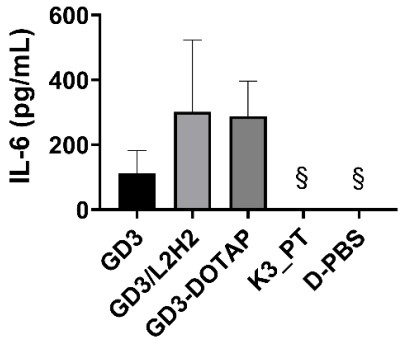

Figure 4.13 Plasma IL-6 production in mice at 2 h-post intraperitoneal injection of GD3, GD3/L2H2, GD3-DOTAP, and K3. Data represent mean ± SD of 3-5 mice. The section mark (§) indicates the lower detection limit (3.9 pg/mL).

4.4. Conclusion

In conclusion, we demonstrated that G4 ligands increased thermodynamic stability and nuclease resistance of G4 CpG ODNs. Our results show that the ability to enhance cytokine induction depends on type of G4 ligand. Indeed, L2H2, a parallel-inducing G4 ligand, may not be suitable for increase of immunostimulatory properties of G4 CpG ODNs. Meanwhile, L2H2 is a potential G4 ligand to promote the immune response to G4 CpG ODNs. These findings may facilitate a step forward for development of a more effective vaccine adjuvant based on G4 CpG ODNs.

Chapter 5 Cationic lipid DOTAP for enhanced immunostimulatory properties of G4 CpG ODNs

5.1. Introduction

Synthetic oligodeoxynucleotides (ODNs) containing unmethylated cytosine-phosphate-guanine (CpG) motifs activate innate immune system by stimulating Toll-like receptor 9 (TLR9).[4] Natural linear ODNs are susceptible to nuclease degradation, which limits their clinical applications. The chemical modification of backbone of CpG ODNs enhances stability against nucleases, but it is reported to cause some undesired effects. This has risen a concern about safety of modified CpG ODNs and suggested CpG ODNs with entirely phosphodiester backbone are more suitable for clinical application.[4] In Chapter 1, we exploited a G-quadruplex (G4) structure, which is a non-canonical, four-stranded structure, forming spontaneously in ODNs containing guanine-rich sequence, to increase nuclease stability of CpG ODNs. The obtained monomeric G-quadruplex-based CpG ODNs (G4 CpG ODNs) induced the production of IL-6, IL-12, and IFN-β in mouse macrophage-like RAW264 cells. Human peripheral blood mononuclear cells responded to G4 CpG ODNs by a promotion in IL-6 and IFN-γ production. This confirms their stimulatory effects on human immune cells. In addition, plasma IL-6 in mice given the intraperitoneal injection of G4 CpG ODNs was 4-fold higher than that in mice injected with linear ODNs. These results suggest potential as vaccine adjuvants of G4 CpG ODNs.

In vaccine adjuvant application, CpG ODN and antigen (Ag) should be delivered to the antigen presenting cells (APCs) simultaneously to obtained an optimized vaccine responses.[29] Co-encapsulation in liposomes is one of delivery strategies to insure that CpG ODN and Ag are co-delivered to the same APCs.[29] Cationic lipids such as 1,2-dioleoyl-3-trimethylammonium-propane (DOTAP) have been widely studied for as carrier for Ag and CpG ODNs. Recent advances have shown that the association of DOTAP and CpG ODN increase CpG-induced immunostimulatory activities *in vivo*.[107] Therefore, CpG ODNs associated to DOTAP also

possess the advantage in reducing the amount of adjuvant and antigen required to induce protective immunity. Furthermore, DOTAP has been exploited as a carrier for CpG ODNs to the endosomal compartment, where TLR9 locates.[108] B cells and conventional dendritic cells do not produce type I IFNs upon stimulation by class A CpG ODNs (CpG-A), but incorporation of DOTAP with an CpG-A induced a type I IFN response in these cell types[10914] *in vitro* and *in vivo*. Combination of DOTAP enables a class B CpG ODN (CpG-B) to activate endosomal TLR9 and produce type I IFN in plasmacytoid dendritic cells, although CpG-B alone hardly activates the MyD88–IRF-7 pathway and induces type I IFN.[14]

Despite that the effect of DOTAP on immunostimulatory properties of linear CpG ODNs have been demonstrated, the influence of DOTAP on immune response to G4 CpG ODNs has not been clarified. The G4-CpG-ODNs mediated immunomodulatory activity may not be derived from those of linear CpG ODNs, since G4-CpG-ODNs have distinct and unique characteristics such as 3-dimension overall shape, charge distribution, and topology diversity.[110] Understanding about immunostimulatory properties of lipoplex of G4 CpG ODNs and DOTAP is an important step toward application of G4 CpG ODNs in vaccine adjuvant field. Therefore, in this chapter, we evaluated cytokine induction of G4 CpG ODNs combined with DOTAP in various type of immune cells including mouse macrophage, human B cell, and dendritic cell line in addition to human peripheral blood mononuclear cells (PBMCs).

5.2. Materials and Methods

5.2.1. Chemicals, oligodeoxynucleotides

All ODNs with phosphodiester backbones (sequences are shown in the **Table 5.1**) were HPLC-grade and purchased from Eurofins Genomics (Tokyo, Japan).

Table 5.1 Sequences of oligodeoxynucleotides used in this chapter

Name	Sequence from 5' to 3'[a]	Length (mer)
GD2	GGGTTGGG**GTCGTT**TT**GTCGTT**GGGTTGGG	30
GD3	GGGTTGGG**GTCGTT**TT**GTCGTT**TT**GTCGTT**GGGTTGGG	38
GD2-Met	GGGTTGGGGTC$_{Met}$GTTTTGTC$_{Met}$GTTGGGTTGGG	30
GD3-Met	GGGTTGGGGTC$_{Met}$GTTTTGTC$_{Met}$GTTTTGTC$_{Met}$GTTGGGTTGGG	38
GD2	GGGTTGGGGTGCTTTTGTGCTTGGGTTGGG	30
GD3-GC123	GGGTTGGGGTGCTTTTGTGCTTTTGTGCTTGGGTTGGG	38
GD3-GC3	GGGTTGGG**GTCGTT**TT**GTCGTT**TTGTGCTTGGGTTGGG	38
2006_PT	tc**gtcgtt**tt**gtcgtt**tt**gtcgtt**	24
K3	at**cg**actct**cg**ag**cg**ttctc	20
ODN2216	ggGG*GA**CG**A:T**CG**TC*gggggg	20

[a] Capital letters, phosphodiester nucleotides; Lowercase letters, phosphorohiotate nucleotides; bold letters, human-specific immunostimulatory unmethylated CpG motif; C_{Met}, cytosine methylation; underline, G-tract; italic, palindrome.

5.2.2. Preparation of G4 CpG ODNs

The purchased ODNs were dissolved in sterile Mili-Q water to prepare stock solutions. The stock solutions were stored at -30 °C until use. To form the G4 structure, ODNs were diluted from the stock solution using Dulbecco's phosphate-buffered saline (D-PBS, DS Pharma Biomedical, Osaka, Japan) containing 2.68 mM KCl, 137 mM NaCl, 1.47 mM KH_2PO_4, and 8.10 mM Na_2HPO_4. For example, to prepare 20 μL of 10 μM G4 CpG ODN solution from a stock ODN solution at 100 μM, 2 μL of 10× D-PBS, 2 μL of 100 μM ODNs, and 16 μL of sterile Mili-Q water were added into a PCR tube. The ODN solutions were heated to 95 °C for 5 min, then cooled gradually to 30 °C for 30 min, followed by cooling to 4 °C using a thermal cycler (PCR

Thermal Cycler Dice Standard TP650, Takara, Kyoto, Japan). The folded ODN solutions were stored at 4 °C until use.

5.2.3. Preparation of complex of G4 CpG ODNs and DOTAP

Reconstructed CpG ODNs were prepared in D-PBS to make a certain concentration of CpG ODNs. The same volume of CpG ODN solutions and DOTAP were mixed together (1 μg/μL, Roche Diagnostics) and incubated for 15 min at room temperature. This means that a constant volume of DOTAP was used for preparing any concentration of CpG ODN/DOTAP mixture.

5.2.4. Stability in serum

For preparation of complex of G4 CpG ODNs and DOTAP, the reconstructed G4 CpG ODN solutions (15 μL) at 20 μM were mixed with 15 μL DOTAP (1μg/μL), then the mixtures were incubated for 15 min at 25 °C. The concentration of G4 CpG ODNs in the mixture is 10 μM. For stability in serum assay, 15 μL of GD2, GD3 or their complex with DOTAP were added into 135 μL of 55.6% (v/v) FBS in D-PBS. The final concentration of FBS and G4 CpG ODN in the assay is 50% (v/v) and 1 μM, respectively. The solution was divided into 5 tube of 30 μL for each tube and incubated at 37 °C for 0, 1, 2, 4, and 24 h. After indicated time, the reaction was stopped by adding 3 μL of 250 mM ethylenediaminetetraacetic acid solution and heating to 80 °C for 2 min before storing at 4°C for further PAGE analysis. The gel electrophoresis was performed using 10-20% polyacrylamide gels with thickness of 1 mm (ATTO, Tokyo, Japan) in Tris-Glycine (TG) buffer (25mM Tris, 192mM Glycine), under the constant current at 21 mA for 55 min, at 4 °C. The ultra-low range DNA ladder (Invitrogen) was used as a marker. The bands in gel were stained by SYBR ® Gold Nucleic Acid Gel Stain (Thermo Fisher Scientific, USA) for 20 min.

5.2.5. Cell Cultures

The mouse macrophage-like RAW264 cell line (RCB0535), purchased from RIKEN BioResource Center (Tsukuba, Japan), was cultured in Minimum Essential Medium (MEM) (Gibco, Carlsbad, CA, USA) containing 10% (v/v) fetal bovine serum (FBS) (Sigma-Aldrich, St

Louis, MO, USA) and 1% (v/v) MEM non-essential amino acid solution (100×, Wako Pure Chemical Industries, Osaka, Japan). Dulbecco's Modified Eagle Medium (DMEM; Sigma-Aldrich) supplemented with 4.5 g/L glucose, 2 mM L-glutamine, 10% (v/v) heat-inactivated FBS, and 0.5% (v/v) penicillin/streptomycin (100×, P/S; Thermo Fisher Scientific) was used for culturing the 293XL-hTLR9A and 293XL/null cells (the control cell line) (InvivoGen, San Diego, CA, USA). Roswell Park Memorial Institute 1640 medium RPMI1640 (#11875-093; Thermo Fisher Scientific) supplemented with 10 mM 4-(2-hydroxyethyl)-1-piperazineethanesulfonic acid (HEPES), 10% heat inactivated FBS, and 50U/ml Penicillin, 50 μg/ml Streptomycin was used to cultured Namalwa cell, a human B lymphocyte cell line, (IFO50040; Japanese Collection of Research Bioresources Cell Bank). PMDC05 cells, blastic plasmacytoid dendritic cell neoplasm, (gifted by Prof. Narita, Niigata University, Japan; [RRID: CVCL_5G47]), were maintained in Iscove's Modified Dulbecco's Medium (IMDM) containing 4 mM L-glutamine, and 25 mM HEPES, 10% heat-inactivated FBS, 100U/ml Penicillin, 100μg/ml Streptomycin. The cells were incubated at 37 °C in a humidified incubator with 5% CO_2.

5.2.6. Intracellular uptake

GD2, and GD3 were labelled at the 5' end by Cy5 ($GD2^{5'Cy5}$ and $GD3^{5'Cy5}$). For preparation of complex of G4 CpG ODNs and DOTAP, the reconstructed G4 CpG ODN solutions (65 μL) at 100 μM were mixed with 65 μL DOTAP (1 μg/μL), then the mixtures were incubated for 15 min at 25 °C. The concentration of G4 CpG ODNs in the mixture with DOTAP is 50 μM. Then G4 CpG ODNs alone or in the mixture with DOTAP were diluted by Opti-MEM (Thermo Fisher Scientific) to get the final concentration is 5 μM. RAW264 cells were seeded in a 48-well plate at 2×10^5 cells per well and then incubated for 18 h at 37 °C in a humidified incubator with 5% CO_2. Then, culture medium was replaced by 200 μL of Opti-MEM (Thermo Fisher Scientific) containing 5 μM $GD2^{5'Cy5}$, $GD3^{5'Cy5}$, $GD2^{5'Cy5}$-DOTAP, or $GD3^{5'Cy5}$-DOTAP. After 2 h-incubation at 37 °C or 4 °C, the cells were washed with 500 μL phosphate-buffered saline (PBS; Wako Pure Chemical Corporation) twice. The cells were harvested by adding 500 μL of

0.05%Tripsin-EDTA and incubating at 37 °C for 30 min. Afterwards, the cells were centrifuge at 500×g for 10 min and washed with 500 μL PBS before being resuspended in 500 μL PBS. Then, flow cytometric analyses were conducted using a flow cytometer (SP6800; Sony, Tokyo, Japan). Mean fluorescence intensity (MFI) was measured, and $\Delta MFI_{37°C\text{-}4°C}$ ($MFI_{37°C} - MFI_{4°C}$) was calculated. Error bars represent the SD obtained from three experimental replicates.

5.2.7. NF-κB reporter assay

293XL-hTLR9 cells and 293XL/null cells were seeded at 2.5×10^5 cells per well. Next, pNiFty-Luc (InvivoGen) containing the firefly luciferase gene under the NF-κB-inducible element and an expression control plasmid, pGL4.74 (Promega, WI, US) expressing a Renilla reniformis luciferase gene under the HSK-TK promoter, were transfected into the cells using the LyoVec (InvivoGen) transfection reagent. The cells were incubated for 20 h, and then complexes of G4 CpG ODN and DOTAP were added to a ODN final concentration of 0.5 μM. A passive lysis buffer was used to lyse cells after 24 h of stimulation, and then the luciferase signals from the lysates were measured using a luminometer TD-20/20 (Promega) based on the manufacturer's instructions. The data were presented as the NF-κB activity of G4 ODN-stimulated cells relative to that of the control cells (no ODN stimulation).

5.2.8. Stimulation of cells

RAW264 cells in culture medium supplemented with 1 (v/v) P/S (100×) were seeded into a 96-well plate at a density of 1×10^5 cells/well (5.3×10^5 cells/mL, 190 μL). After incubation for 18 h, 10 μL of 10 μM ODN in the mixture with DOTAP was added to the culture medium to a final ODN concentration of 0.5 μM. Then, the cells were incubated for 24 h at 37 °C in a humidified incubator containing 5% CO_2 before evaluation of the relative transcript levels.

Namalwa cells were seeded in a 96-well plate at a density of 1×10^5 cells/well and maintained for 18 h. Afterwards, 10 μL ODN in the mixture with DOTAP was added to the culture

medium to get a final ODN concentration of 1 μM. Next, the cells were incubated for 4 h at 37 °C in a humidified incubator containing 5% CO_2 before evaluation of the relative transcript levels.

PMDC05 cells were seeded in a 96-well plate at a density of 1×10^6 cells/well and maintained for 18 h. Afterwards, 10 μL ODN in the mixture with DOTAP was added to the culture medium to get a final ODN concentration of 1 μM. Next, the cells were incubated for 4 h at 37 °C in a humidified incubator containing 5% CO_2 before evaluation of the relative transcript levels.

5.2.9. Reverse transcription/real-time quantitative-polymerase chain reaction (RT/RQ-PCR)

The relative transcript levels of cytokines in the cells were determined by reverse transcription/real-time quantitative-polymerase chain reaction (RT/RQ-PCR). Total RNA was extracted from the cells using ISOGEN (Nippon Gene, Tokyo, Japan) following the manufacturer's instructions. The extracted RNA was treated with DNase I (RNase-free) (Takara Bio, Shiga, Japan) prior to reverse transcription into cDNA (Takara Bio). IL-6, IL-12, and IFN-β transcript levels were measured by quantitative real-time PCR using a LightCycler 480 System (Roche, Basel, Switzerland) with LightCycler®480 SYBR Green I Master (Roche) and the primers (FASMAC, Kanagawa, Japan) listed in **Table 2.2**. Amplification was performed using 50 ng cDNA in a total volume of 15 μL for 45 cycles of 10 s each at 95 °C, 10 s at 60 °C, and 10 s at 72 °C. After PCR, the crossing point value, the cycle at which the fluorescence starts to become significantly higher than the background fluorescence, was determined. The mRNA levels were normalized against that of glyceraldehyde 3-phosphate dehydrogenase (*GAPDH*), a housekeeping gene. In addition, the specificity of the amplified products was verified by analyzing the melt curves.

5.2.10. Stimulation of human peripheral blood mononuclear cells (PBMCs)

Human PBMCs (Sample ID: 20110727; ethnicity: Hispanic; age: 29; gender: Female; ABO/Rh: O/Pos), purchased from Cellular Technology Limited (Shaker Heights, OH, USA),

were thawed according to the manufacturer's instructions and resuspended in Roswell Park Memorial Institute 1640 medium (Thermo Fisher Scientific) containing GlutaMAX, 4-(2-hydroxyethyl)-1-piperazineethanesulfonic acid), 1% (v/v) P/S (100×), and 10% (v/v) heat-inactivated FBS. The cells were seeded into a 96-well plate at a density of 1×10^6 cells/well and stimulated with complex of ODN and DOTAP at final ODN concentration at 0.5 μM. After incubation for 48 h, the cells were centrifuged (10,000 ×*g*) for 10 min at 4 °C to collect the supernatants. IL-6 Ready-Set-Go kits and Human IFN-α Module Set ELISA (Thermo Fisher Science) were used according to the manufacturer's instructions to evaluate cytokine expression levels in the supernatants.

5.2.11. Statistical analysis

Statistical comparisons of the data were conducted by one-way analysis of variance (ANOVA) followed by Tukey's multiple comparisons test for comparison with other groups or by Dunnett's multiple comparisons test for comparison with a control group. Two-way ANOVA followed by the Sidak's multiple comparisons test was used for comparison of the groups in the TLR9 reporter assay. All statistical analyses were performed using GraphPad Prism version 8.2.0 for Windows (GraphPad Software, La Jolla, CA, USA). A *p*-value < 0.05 was considered statistically significant.

5.3. Results and discussion

5.3.1. DOTAP increases stability in serum of G4 CpG ODNs

Figure 5.1A shows the stability in serum of GD2 and GD2-DOTAP, while **Figure 5.1B** shows the stability in serum of GD3 and GD3-DOTAP. PAGE was performed to evaluate relatively the amount of the remaining ODNs after incubation for 1, 2, 4, or 24 h. GD2, and GD3 bands faded after 4 h of incubation with 50% (v/v) FBS, while the bands of GD2-DOTAP and GD3-DOTAP were still observed clearly even after 24 h of incubation. This indicates that DOTAP protected ODNs from DNase degradation.

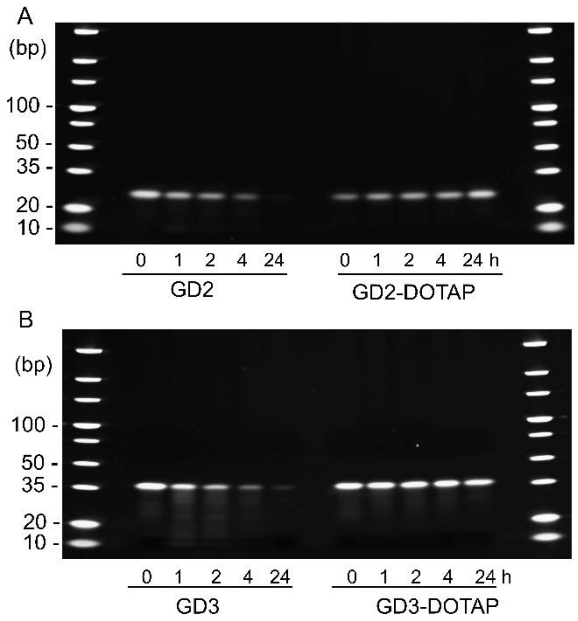

Figure 5.1 DOTAP increases stability in serum of G4 CpG ODNs. Polyacrylamide gel electrophoresis analysis of (A) GD2 and GD2-DOTAP (B) GD3 and GD3-DOTAP after incubation for 1, 2, 4, and 24 h with 50% fetal bovine serum.

5.3.2. DOTAP increases intracellular uptake of G4 CpG ODNs

The effects of DOTAP on intracellular uptake of G4 CpG ODNs were examined in RAW264 cells. **Figure 5.2A i** and **Figure 5.2A ii** display histograms showing fluorescence of the cells treated with $GD2^{5'Cy5}$, $GD3^{5'Cy5}$, alone or in combination with DOTAP at 4 °C and 37 °C, respectively. **Figure 5.2B** shows that, at 4 °C, the MFI values of cells treated with G4 CpG ODNs associated with DOTAP were higher than those of cells incubated with G4 CpG ODNs alone, suggesting that G4 CpG ODN-DOTAP conjugates bound on cell surfaces. This may be facilitated by the electrostatic interaction of positive charges of liposome and negative charges of cell membrane. The difference between MFI at 37 °C and that at 4 °C ($\Delta MFI_{37°C-4°C}$) was calculated as measure of internalized Cy5 labelled ODN. As shown in **Figure 5.2C**, the $\Delta MFI_{37°C-4°C}$ of cells

incubated with GD2$^{5'Cy5}$-DOTAP were 6-fold higher than the $\Delta MFI_{37°C-4°C}$ of those incubated with GD2$^{5'Cy5}$. Meanwhile, the combination with DOTAP leads to 4-time increase in $\Delta MFI_{37°C-4°C}$ of the cells incubated with GD3$^{5'Cy5}$. These results suggest that DOTAP enhances cellular uptake of G4 CpG ODNs. The effect of DOTAP on cellular uptake of GD2 is larger than on that of GD3.

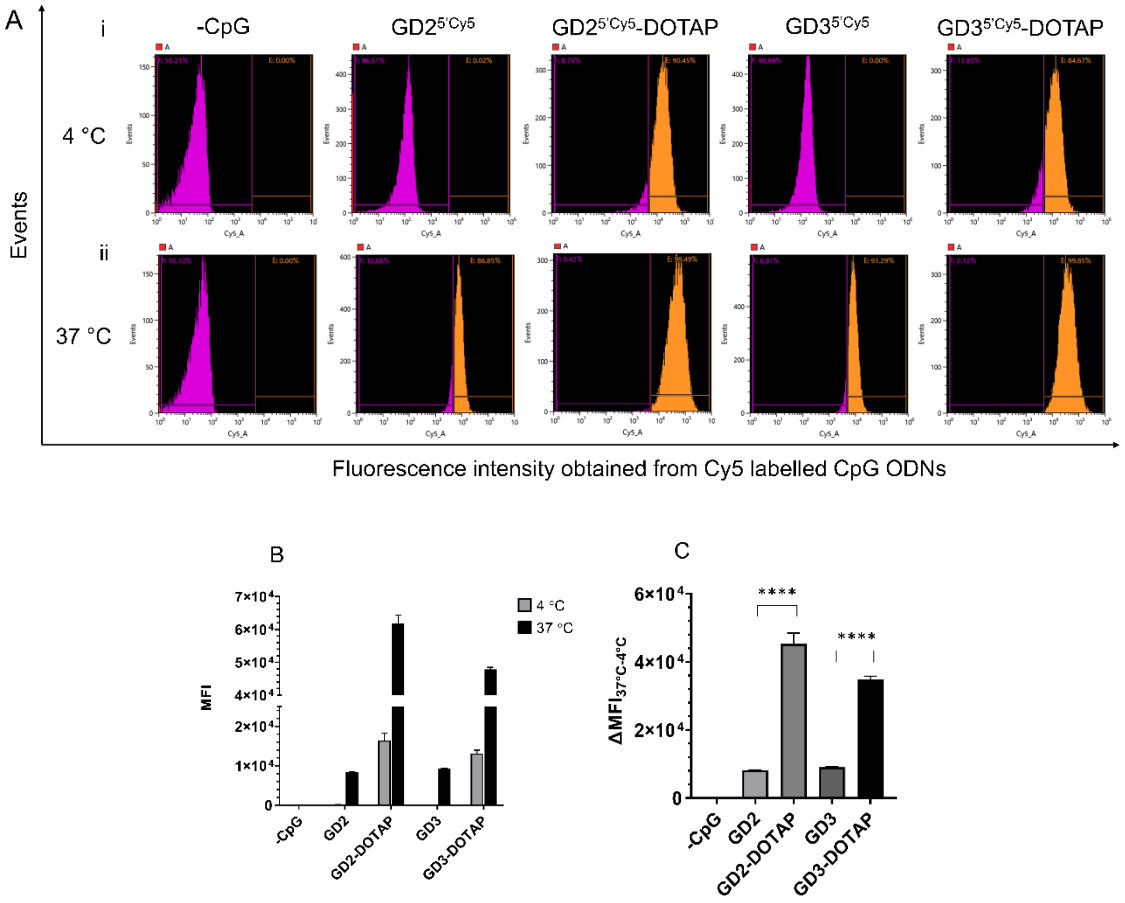

Figure 5.2 DOTAP increases intracellular uptake of G4 CpG ODNs in RAW264 cells. (A) Histogram analysis of fluorescence intensity at (i) 4 °C and (ii) 37 °C. (B) Mean fluorescence intensity (MFI) of the cells incubated at 37 °C and 4 °C; (C) Internalized Cy5 labelled CpG ODNs were measured by $\Delta MFI_{37°C-4°C}$. RAW264 cells were incubated with 5 μM GD2$^{5'Cy5}$, GD3$^{5'Cy5}$, GD2$^{5'Cy5}$-DOTAP, or GD3$^{5'Cy5}$-DOTAP for 2 h. Data represent mean ± SD (n = 3). ****p < 0.0001, ***p < 0.001, *p < 0.05, p > 0.05, One-way ANOVA, Tukey's multiple comparisons test.

5.3.3. DOTAP increases cytokine induction of G4 CpG ODNs

The relative transcript levels cytokines expressed by RAW264 cells exposed to free G4 CpG ODNs and the ODNs associated with DOTAP are shown in **Figure 5.3**. DOTAP alone did not show any cytokine induction. Combination with DOTAP leads to significant increase in *IL-6*, *IL-12*, and *IFN-β* mRNA production by RAW264 cell, this indicates that DOTAP has potential in enhancing activity of G4 CpG ODNs. This may because of the enhanced stability against nucleases and intracellular uptake of G4 CpG ODNs associated with DOTAP in comparison with G4 CpG ODNs alone. The immunostimulatory properties of lipoplexes of G4 CpG ODN and DOTAP is strongly dependent on the unmethylated CpG motifs, as their ability in cytokine induction significantly decreases when CpG motifs are methylated or replaced by GpC motifs (**Fig. 5.4**). This indicates that DOTAP does not have any role in activating TLR9, it may only work as carriers for delivery of CpG ODNs to the cells.

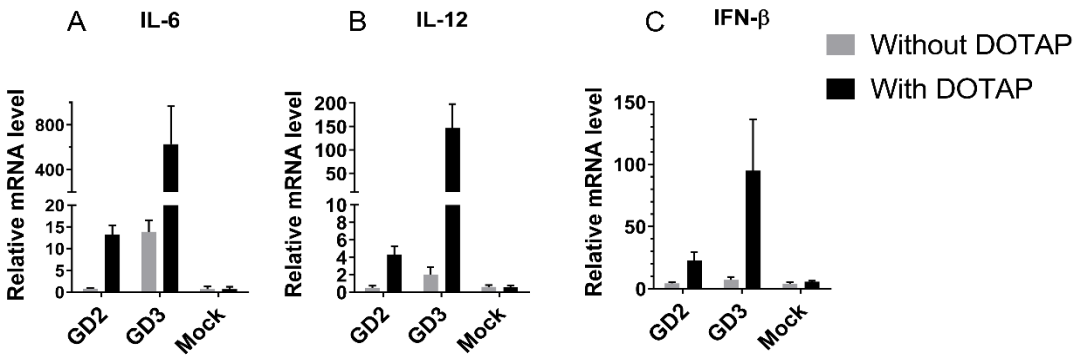

Figure 5.3 DOTAP increase cytokine production in mouse macrophage-like RAW264 cells stimulated by G4 CpG oligodeoxynucleotide. Relative mRNA levels of (A) *IL-6*, (B) *IL-12*, and (C) *IFN-β* in RAW264 cells were examined after 24 h of stimulation with 0.5 μM GD2, GD3 or their DOTAP conjugates. Data represent mean ± SD (n = 5).

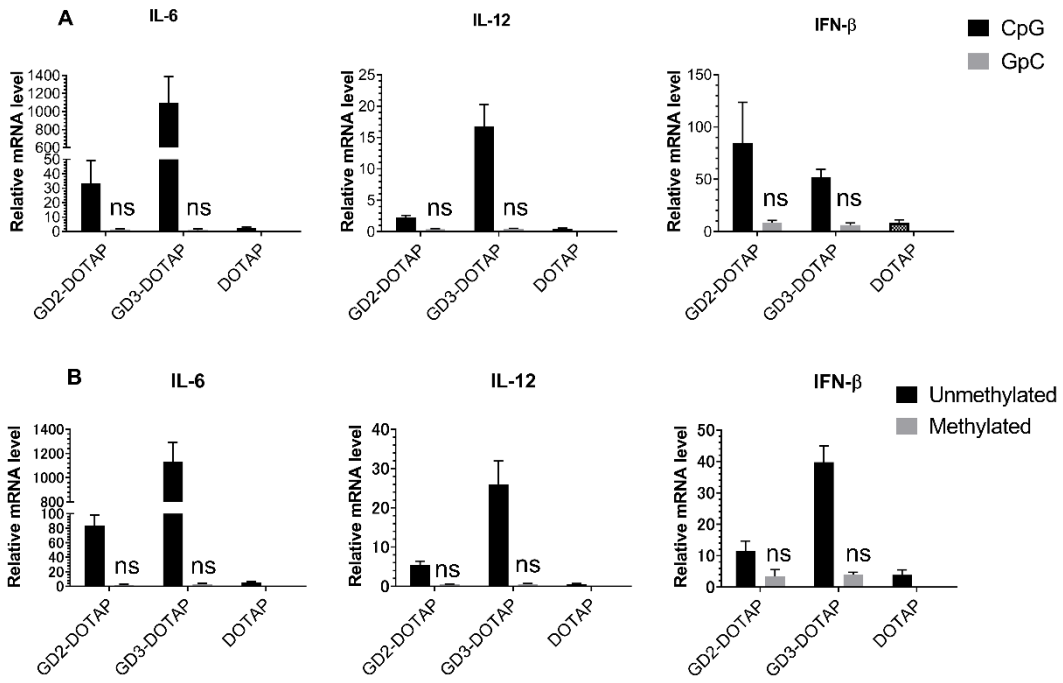

Figure 5.4 The immunostimulatory properties of lipoplexes of G4 CpG ODN and DOTAP are strongly dependent on the unmethylated CpG motifs. Relative mRNA levels of *IL-6*, *IL-12*, and *IFN-β* in RAW264 cells were examined after 24 h of stimulation with complex of DOTAP and GD2, GD3, or their variants. (A) Effects of GpC inversion; (B) Effects of methylation on cytokine production. Data represent mean ± SD (n = 5). $p > 0.05$ (one-way ANOVA, Sidak's multiple comparisons test).

GD2 and GD3 in complex with DOTAP induce NF-κB-regulated luciferase activities in cells expressing TLR9, but not in the control cells, which are not expressed TLR9 (**Fig. 5.5**). This result implies that GD2 and GD3 keep TLR9 agonistic properties when they are combined with DOTAP.

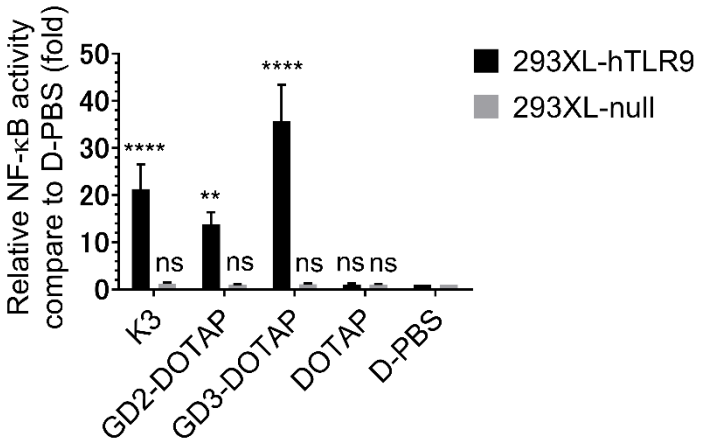

Figure 5.5 G4 CpG ODN-DOTAP conjugates stimulate TLR9-mediated NF-κB activity. NF-κB activation in human TLR9-expressing cells (293XL-hTLR9) and control cell line not expressing TLR9 (293XL-null) were analyzed 24 h after stimulation with 0.5 μM GD2, GD3 in complex with DOTAP. K3, a TLR9 agonist with linear phosphorothioate backbone was used as positive controls. Data represent mean ± SD ($n = 5$). ****$p < 0.0001$, ***$p < 0.001$, **$p < 0.01$, *$p < 0.05$, ns (not significantly different from D-PBS) $p > 0.05$, two-way ANOVA, Sidak's multiple comparisons test.

5.3.4. Cytokine induction of CpG ODN-DOTAP complexes in human cell lines

Human B cells bear TLR9 and respond to CpG by activation of NF-κB pathway and cytokine production.[111] In an *in vitro* assay, the Namalwa cell line is reported to behave as an appropriate, homogeneous, and stable B cell model[112], so we examined responses of Namalwa cells evoked by GD2, GD3 in complex with DOTAP, which are presented in **Figure 5.6A**. The levels of *IL-6*, *IL-12*, and *IFN-β* mRNAs induced by GD2-DOTAP were the same as those in the negative control. GD3-DOTAP showed significant higher cytokine induction than D-PBS, with the intensity comparable with the positive control, K3.

PMDC05 is a plasmacytoid dendritic cell (pDC) line, which expressed TLR9 and produce of type I IFN in response to stimulation of A-CpG.[113] GD-2 and GD3 possessed a remarkable

cytokine inducing ability in PMDC05, with IFN-β level considerably higher than CpG-A, ODN2216 (**Fig. 5.6B**).

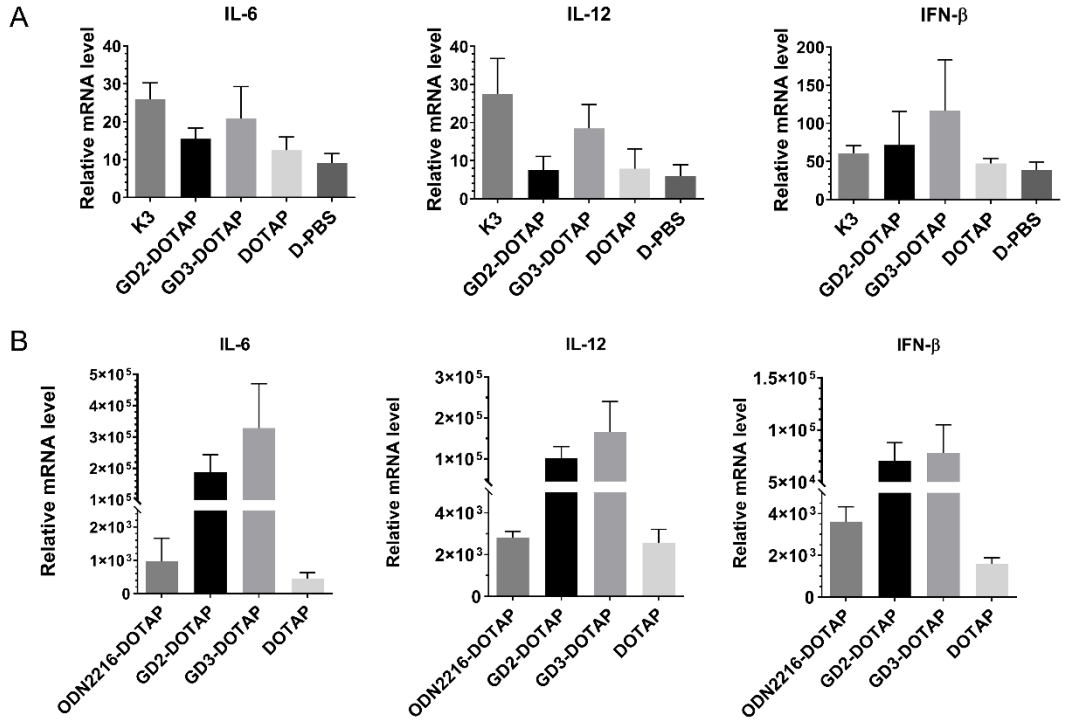

Figure 5.6. The immunostimulatory properties of lipoplexes of G4 CpG ODN and DOTAP in (A) Namalwa cells, a human B cell line and (B) PMDC05 cells, a human dendritic cell line. Relative mRNA levels of *IL-6*, *IL-12*, and *IFN-β* in the cells were examined after 4 h of stimulation with 1 μM. Data represent mean ± SD (n = 5).

5.3.5. Cytokine induction of CpG ODN-DOTAP complexes in human primary cells

The immunostimulatory responses of primary human immune cells to lipoplex of G4 CpG ODN and DOTAP were also examined. **Figure 5.7** shows the IL-6 and IFN-α production in human PBMCs exposed to GD2, GD3 in their complexes with DOTAP. Combination of GD2, GD3 with DOTAP magnified the production of IL-6 from human PBMCs. We also observed that GD3-DOTAP induced lower IL-6 than did GD2-DOTAP, while, in the free form, GD3 induced higher IL-6 than did GD2. Importantly, GD3 associated with DOTAP was able to induce IFN-α,

but GD3 alone was not. These results suggest that DOTAP not only enhances immunostimulatory properties, but also provides anti-viral response induction for G4 CpG ODNs.

However, the ability in inducing IFN-α of GD3-DOTAP was not observed in GD2-DOTAP, this indicates that there were some factors controlling the IFN-α production of G4 CpG ODN-DOTAP lipoplexes. The number of CpG motifs may not involve to IFN-α, as the complex with DOTAP of GD3-GC3, an ODN having the same length and similar G4 structure to GD3 (**Fig. 2.4**) but containing only two immunostimulatory CpG motifs, induced IFN-α at the same level compared with GD3-DOTAP.

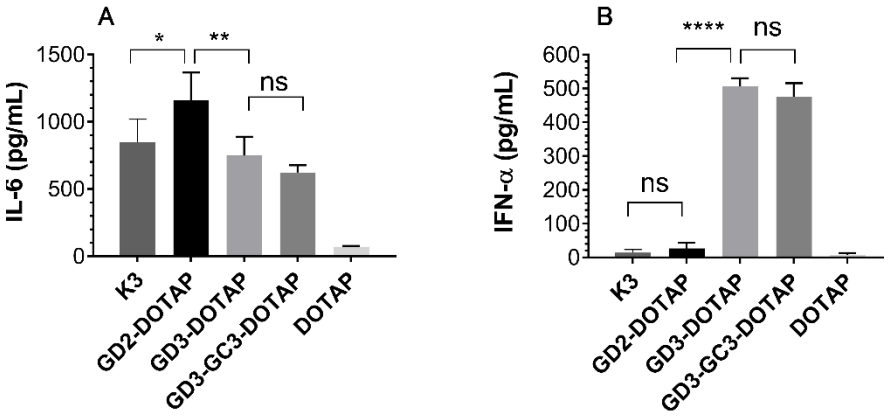

Figure 5.7 Cytokine induction of CpG ODN-DOTAP complexes in human peripheral mononuclear cells (PBMCs). Supernatants from PBMCs incubated with 0.5 μM G4 CpG ODNs in complex with DOTAP for 48 h were assayed by ELISA for (A) IL-6, and (B) IFN-α. Data represent mean ± SD (n = 5). ****p < 0.0001, ***p < 0.001, **p < 0.01, *p < 0.05, ns (not significantly different) p > 0.05 (one-way ANOVA, Tukey's multiple comparisons test).

Human PBMCs are cell populations containing different types of human immune cells including T cell, NK cells, B cells, monocytes, and dendritic cells.[114] Plasmacytoid dendritic cells (pDCs) are characterized by the ability to produce robustly type I IFN (IFN-α and IFN-β), which connects to TLR9 activation by CpG ODNs.[115] Honda et al.[14] reported that the spatiotemporal regulation of MyD88–IRF-7 signaling is important for a robust type I IFN production in response

to TLR9 stimulation.[14] Accordingly, TLR9 ligands induce type 1 IFN when they are retained for long time in the endosome. DOTAP was found to be able to prolong endosomal retention, so provided type I IFN induction ability for CpG ODNs.[14] In addition, multimeric CpG-A mediated TLR9 activation takes place in endosomes and offers an exclusive IFN-α production, while monomeric CpG-B is reported to rapidly translocate to lysosome and bring about the induction of proinflammatory cytokines such as IL-6.[116]

Referring our results and previous reports, we hypothesize that GD3-DOTAP may be restrained in endosomal compartments of pDCs and evoked IFN-α production, after a certain time which may be several hours[14], GD3-DOTAP translocated to lysosome and leads to IL-6 secretion. In case of GD2-DOTAP, one possibility that this lipoplex may not be retained in endosomes, and quickly merge with lysosome, where it activated TLR9 to produce IL-6. Another possibility is that both GD2-DOTAP and GD3-DOTAP were held back from translocating to lysosome, but during the period of endosomal retention, there is a factor preventing GD2-DOTAP not GD3-DOTAP from interaction with TLR9. Then, when GD2-DOTAP lipoplex translocated to lysosome, due to the changes in endosomal maturation, some factors including the factor interfering GD2-DOTAP-mediated TLR9 activation were lifted. However, a detailed mechanism by which DOTAP offers the type I IFN induction to GD3, and reasons for difference in IFN-α between GD2-DOTAP and GD3-DOTAP remain unknown, and additional investigation is in progress.

5.4. Conclusion

In this chapter, we examined the effects of cationic lipid DOTAP on the immunostimulatory properties of G4 CpG ODNs. Combination with DOTAP enhanced cytokine induction of GD2 and GD3 in mouse macrophage cell line, as well as human B cell, and plasmacytoid dendritic cell lines. DOTAP did not involve in TLR9 activation and may only function as carriers for delivery of CpG ODNs into the cells. TLR9 agonistic properties of GD2

and GD3 were maintained when they are associated with DOTAP. The enhanced cytokine induction by DOTAP was also observed in human PBMCs. Especially, GD3 in complex with DOTAP was able to provoke production of IFN-α, which is a critical cytokine in immune response against viral infection, while GD3 alone did not. Interestingly, the IFN-α production was not observed for the complex of GD2 with DOTAP. We anticipate that these findings are starting points for a systematic investigation to identify the mechanism that governs cytokine profile induced by G4 CpG ODN-DOTAP lipoplex, which offers an ability to control the immune response to G4 CpG ODN-based adjuvants.

Chapter 6 Summary

Toll-like receptor 9 activation by oligodeoxynucleotides (ODNs) containing unmethylated cytosine-phosphate-guanine (CpG) motifs triggers the innate immune system and establishes an adaptive immune response, and therefore these ODNs have been studied as vaccine adjuvants against infectious diseases. The phosphodiester backbone of ODNs is prone to degradation by nucleases; therefore, in clinical trials, phosphorothioate-modified CpG ODNs are used to increase DNase stability. However, phosphorothioate ODNs have been reported to cause thrombocytopenia, anemia, and neutropenia.[66] These data suggest that CpG ODNs with a phosphodiester backbone are more suitable for clinical applications. Self-assemble CpG ODNs forming high order structures gain increase in nuclease resistance without backbone chemical modification, so they possess major advantage in term of safety. Nevertheless, an assurance of precise self-association is required for some high order structured CpG ODNs, thereby leads to the high cost and complexity of the operations.[23] Therefore, self-assemble CpG ODNs with a simple folding process and a potent immunostimulatory activity are in high demand. Recently, our group was the first to report that the guanine-quadruplex (G4) structure enables higher nuclease stability, cellular uptake, and inflammatory cytokine induction compared to the linear phosphodiester CpG ODN.[68] As such, the use of G4 ODNs in immunotherapy is still in its infancy, and few knowledge about their immunomodulatory activities is known. Understanding the preclinical characteristics will make progress in studies of G4 CpG ODNs as vaccine adjuvants. Therefore, this dissertation focuses on further investigation of the immunostimulatory properties of CpG ODNs forming G4 structures, particularly monomeric G4.

In chapter one, we present a general background for this study with information about Innate and adaptive immunity, CpG ODNs, evaluation of CpG ODNs as vaccine adjuvants, CpG ODNs forming high order structures, as well as G-quadruplex structures.

In chapter two, the new monomeric G-quadruplex-based CpG ODNs (G4 CpG ODNs) named GD1, GD2, and GD3, with different lengths and numbers of CpG sequences, are designed with CpG motifs in the central loop region of the G4 structure. Success in controlling the G4 molecularity into a monomer in this chapter facilitates further investigation of intrinsic factors governing the efficiency of G4 CpG ODNs, which is presented in Chapter 3. We also confirm that the immunostimulatory properties of monomeric G4 CpG ODNs are mediated by TLR9 activation. In addition, we reveal the advantages of monomeric G4 in increasing nuclease resistance, intracellular uptake, and cytokine induction *in vitro* and *in vivo* of a phosphodiester CpG ODNs.

In chapter three, the effects of intrinsic factors, including the position of the loop containing the CpG motif, the position of the CpG motif within a loop, spaces between a CpG motif and G-tracts, and the number of CpG ODNs on immunostimulatory activity, are examined. Adding CpG motifs into the second loop rather than the first or third loop satisfies the requirement of a stable and potent monomeric G4 CpG ODNs. An increase in the length of the loop containing the CpG motifs is necessary but not adequate for effective TLR9 stimulation. The number of CpG motifs and the spaces between CpG motifs and G-tracts are critical factors governing immunostimulatory efficiency of G4 CpG ODNs, probably because of improved flexibility in the loop region. The findings we report in this chapter provide further understanding of the mechanisms underlying the immunostimulatory activities of G4 CpG ODNs and provide hints for the rational design of G4 CpG ODNs for vaccine adjuvant applications.

In chapter four, we evaluate the influences of G4 ligands on the immunostimulatory properties of G4 CpG ODNs. G4 ligands are small molecules developed to stabilize G4 through binding to G4 ODNs with high affinity. Some G4 ligands have been developed to induce a specific G4 topology, such as parallel or anti-parallel. With the ability to stabilize G4 ODNs, we expect that G4 ligands may also stabilize G4 CpG ODNs, which may further increase their

immunostimulatory activity. We examine the effects of two types of G4 ligands named L2H2-6OTD and L2G2-2M2EG-6OTD on a G4 CpG ODN, GD3. We find that both ligands increase the thermodynamic stability and nuclease resistance of GD3. Furthermore, the ability to enhance cytokine induction depends on the type of G4 ligand. Indeed, L2G2-2M2EG-6OTD, a parallel-inducing G4 ligand, may not be suitable for increasing the immunostimulatory properties of G4 CpG ODNs. Meanwhile, L2H2-6OTD is a potential G4 ligand that promotes an immune response to G4 CpG ODNs. These findings may represent a step forward towards development of a more effective vaccine adjuvant based on G4 CpG ODNs.

In chapter five, the effects of 1,2-dioleoyl-3-trimethylammonium-propane (DOTAP) on the immunostimulatory properties of G4 CpG ODNs are demonstrated. Cationic lipids such as DOTAP have been widely studied as carriers for antigen and CpG ODNs in vaccine adjuvant applications. Therefore, understanding the immunostimulatory properties of the lipoplex of G4 CpG ODNs and DOTAP is an important step toward the application of G4 CpG ODNs in the field of vaccine adjuvant. Association with DOTAP enhances cytokine induction of GD2 and GD3 in mouse macrophage cell lines, as well as human B cell, and plasmacytoid dendritic cell lines. GD2 and GD3 function as TLR9 agonists when they are combined with DOTAP. Combination with DOTAP enhances G4 CpG ODN-induced interleukin (IL)-6 production in human PBMCs. Notably, the GD3-DOTAP lipoplex is able to induce IFN-α production, which is an important cytokine for anti-viral immune response, while GD3 alone does not. Surprisingly, GD2 in a complex with DOTAP does not induce IFN-α production. These results suggest that G4 CpG ODN-DOTAP is a potential Th1-inducing adjuvant system for human vaccines against infectious diseases. In addition, the provoked adaptive immune response by G4 CpG ODN DOTAP lipoplexes can be tailored by controlling lipoplex preparation.

Chapter six summarizes the concluding remarks of this study. In conclusion, we successfully developed monomeric G4 CpG ODNs, and for the first time, we investigated the

parameters affecting their immunostimulatory activities. The monomeric G4 CpG ODNs developed in this study are not only effective, safe, and nuclease resistant, but also do not require a complicated conformation process. Therefore, G4 CpG ODNs are promising potent vaccine adjuvants that can be produced on a large scale without high costs. In future, the work improving the efficiency of G4 CpG ODNs based on hints given by this study and clarifying the mechanism by which G4 CpG ODN-DOTAP lipoplexes regulate IFN-α production will be conducted.

Publications

Papers published in journals

1. Anh Thi Tram TU, Kazuaki HOSHI, Kazunori IKEBUKURO, Nobutaka HANAGATA, Tomohiko YAMAZAKI, Monomeric G - Quadruplex-Based CpG Oligodeoxynucleotides as Potent Toll-Like Receptor 9 Agonists. *Biomacromolecules* **2020**, *21* (9), 3644–3657. https://doi.org/10.1021/acs.biomac.0c00679.

Presentations in conferences

1. Anh Thi Tram TU, Kazuaki HOSHI, Kazunori IKEBUKURO, Tomohiko YAMAZAKI, Forming Monomeric Guanine-Quadruplex Structure for Enhancing CpG Oligodeoxynucleotides-mediated Immunostimulatory Properties, 15th Nano Biomedical Annual Meeting (**2020** November, Tsukuba, Japan, online).
2. Anh Thi Tram TU, Kazuaki HOSHI, Kazunori IKEBUKURO, Nobutaka HANAGATA, Tomohiko YAMAZAKI, Enhanced Immunostimulatory Activity of CpG Oligodeoxynucleotides by Forming Monomeric Guanine-Quadruplesx Structure, 16th Annual Meeting of the Oligonucleotide Therapeutics Society (**2020** September, US, online).
3. Anh Thi Tram TU, Kazuaki HOSHI, Kazunori IKEBUKURO, Tomohiko YAMAZAKI, Tuning of the Immunostimulatory Effect of G-quadruplex Based CpG Oligodeoxynucleotides, MANA International Symposium 2020 jointly with ICYS (**2020** March, Tsukuba, Japan).
4. Anh Thi Tram TU, Kazuaki HOSHI, Kazunori IKEBUKURO, Tomohiko YAMAZAKI, Immunostimulatory Properties of CpG ODNs Forming G-quadruplex Structure, 46th International Symposium on Nucleic Acids Chemistry (**2019** October, Tokyo, Japan).

Acknowledgements

I would like to express my gratitude to all those who helped me during my doctoral course.

I would like to express my deepest gratitude to my main supervisor, Associate Professor Dr. Tomohiko Yamazaki for his knowledge, academic advices, kindness, and patience. He is an outstanding, conscientious, and gentle supervisor. I am absolutely grateful to him for giving me an opportunity to do research in his group as a doctoral student and for his encouragement during the course.

I especially would like to express my gratitude to Professor Dr. Nobutaka Hanagata for his kindness and scientific guidance during my doctoral course.

I am deeply grateful to Professor Dr. Kazunori Ikebukuro for his knowledge, academic advices, and gentleness.

I would like to express my gratitude to Professor Dr. Kazuo Nagasawa for supplying the G4 ligands, as well as the support during my study.

I am deeply grateful to Dr. Kazuaki Hoshi for his instruction in experiments, academic discussion, sharing practical experiences and continuous encouragement.

I am grateful to Ms. Akemi Hoshikawa, for her kindness in helping me completing Japanese documents and in helping me in daily life.

I would like to thank Ms. Satomi Kohara, Ms. Satomi Magae, Ms. Tomoyo Umezawa for their technical assistance. I am deeply grateful to Dr. Miwako Shobo, who has excellent skills in handling with mice, for her technical assistance in the animal experiment.

I deeply thank to Dr. Takashi Minowa, and Dr. Taro Takemura for creating the most favorable conditions for me to conduct my research at the NIMS Molecule and Material Synthesis platform, supported by the Nanotechnology Platform Program of the Ministry of Education, Culture, Sports, Science and Technology (MEXT), Japan. I really thank to Dr. Xianglan Li, Dr. Hiromi Morita, Dr. Shinya Hattori, Dr. Jie Li, as well as the other members of the NIMS Molecule and Material Synthesis platform for technical support.

I am deeply grateful to Dr. Masayuki Takeuchi, Dr. Aimi Junko, Mr. Akira Nagai, Mr. Haruki Sanematsu for their technical suggestions for the CD and UV analyses.

We would like to thank Dr. Satoko.Suzuki and Dr. Kenichi.Akao (JASCO Corporation) for their technical assistance in the peak fitting and deconvolution to the CD spectra.

I deeply thank Hokkaido university, and National Institute for Materials Science (NIMS) for creating outstanding conditions for me to conduct my research.

I would like to thank you all of my friends in Vietnam and Japan, who support my daily life, and explore wonderful Japanese scenery with me.

Last but not least, from the bottom of my heart, I extremely thank my family, and family in law because of their great love and quiet support. Especially, I would like to thank my husband, who always listens, encourages, and supports me.

References

(1) Bonam, S. R.; Partidos, C. D.; Halmuthur, S. K. M.; Muller, S. An Overview of Novel Adjuvants Designed for Improving Vaccine Efficacy. *Trends Pharmacol. Sci.* **2017**, *38* (9), 771–793. https://doi.org/10.1016/j.tips.2017.06.002.

(2) Krieg, A. M. Toll-like Receptor 9 (TLR9) Agonists in the Treatment of Cancer. *Oncogene* **2008**, *27* (2), 161–167. https://doi.org/10.1038/sj.onc.1210911.

(3) Klinman, D. M. Immunotherapeutic Uses of CpG Oligodeoxynucleotides. *Nat. Rev. Immunol.* **2004**, *4* (4), 249–259. https://doi.org/10.1038/nri1329.

(4) Hanagata, N. CpG Oligodeoxynucleotide Nanomedicines for the Prophylaxis or Treatment of Cancers, Infectious Diseases, and Allergies. *Int. J. Nanomedicine* **2017**, *12*, 515–531. https://doi.org/10.2147/IJN.S114477.

(5) Kaisho, T.; Akira, S. Toll-like Receptor Function and Signaling. *J. Allergy Clin. Immunol.* **2006**, *117* (5), 979–987. https://doi.org/10.1016/j.jaci.2006.02.023.

(6) Melisi, D.; Frizziero, M.; Tamburrino, A.; Zanotto, M.; Carbone, C.; Piro, G.; Tortora, G. Toll-like Receptor 9 Agonists for Cancer Therapy. *Biomedicines* **2014**, *2* (3), 211–228. https://doi.org/10.3390/biomedicines2030211.

(7) Leifer, C. A.; Kennedy, M. N.; Mazzoni, A.; Lee, C.; Kruhlak, M. J.; Segal, D. M. TLR9 Is Localized in the Endoplasmic Reticulum Prior to Stimulation. *J. Immunol.* **2004**, *173* (2), 1179–1183. https://doi.org/10.4049/jimmunol.173.2.1179.

(8) Latz, E.; Schoenemeyer, A.; Visintin, A.; Fitzgerald, K. A.; Monks, B. G.; Knetter, C. F.; Lien, E.; Nilsen, N. J.; Espevik, T.; Golenbock, D. T. TLR9 Signals after Translocating from the ER to CpG DNA in the Lysosome. *Nat. Immunol.* **2004**, *5* (2), 190–198. https://doi.org/10.1038/ni1028.

(9) Wittig, B.; Schmidt, M.; Scheithauer, W.; Schmoll, H. J. MGN1703, an Immunomodulator and Toll-like Receptor 9 (TLR-9) Agonist: From Bench to Bedside. *Critical Reviews in Oncology/Hematology*. Elsevier April 1, 2015, pp 31–44. https://doi.org/10.1016/j.critrevonc.2014.12.002.

(10) Goulopoulou, S.; McCarthy, C. G.; Clinton Webb, R. Toll-like Receptors in the Vascular System: Sensing the Dangers Within. *Pharmacol. Rev.* **2016**, *68* (1), 142–167. https://doi.org/10.1124/pr.114.010090.

(11) Eicke Latz, Anjali Verma, Alberto Visintin, Mei Gong, Cherilyn M Sirois, Dionne C G Klein, Brian G Monks, C James McKnight, Marc S Lamphier, W Paul Duprex, T. E. & D. T. G. Ligand-Induced Conformational Changes Allosterically Activate Toll-like Receptor 9. *Nat. Immunol.* **2007**, *8* (7), 772–779. https://doi.org/10.1038/ni1479.

(12) Zannetti, C.; Parroche, P.; Panaye, M.; Roblot, G.; Gruffat, H.; Manet, E.; Debaud, A. L.; Plumas, J.; Vey, N.; Caux, C.; et al. TLR9 Transcriptional Regulation in Response to Double-Stranded DNA Viruses. *J. Immunol.* **2014**, *193* (7), 3398–3408. https://doi.org/10.4049/jimmunol.1400249.

(13) Ohba, Y.; Yanai, H.; Negishi, H.; Mizutani, T.; Takaoka, A.; Taya, C.; Taniguchi, T. Spatiotemporal Regulation of MyD88 – IRF-7 Signalling for Robust Type-I Interferon Induction. *Nature* **2005**, *2*, 1–6. https://doi.org/10.1038/nature03487.1.

(14) Kenya Honda, Yusuke Ohba, Hideyuki Yanai, Hideo Negishi, Tatsuaki Mizutani, Akinori Takaoka, Choji Taya, T. T. Spatiotemporal Regulation of MyD88 – IRF-7 Signalling for Robust Type-I Interferon Induction. *Nature* **2005**, *2*, 1–6. https://doi.org/10.1038/nature03487.1.

(15) Collins, B.; Wilson, I. A. Crystal Structure of the C-Terminal Domain of Mouse TLR9. *Proteins* **2014**, *82* (10), 2874–2878. https://doi.org/10.1002/prot.24616.

(16) Peter, M. E.; Kubarenko, A. V.; Weber, A. N. R.; Dalpke, A. H. Identification of an N-Terminal Recognition Site in TLR9 That Contributes to CpG-DNA-Mediated Receptor Activation. *J. Immunol.* **2009**, *182* (12), 7690–7697. https://doi.org/10.4049/jimmunol.0900819.

(17) Ohto, U.; Shibata, T.; Tanji, H.; Ishida, H.; Krayukhina, E.; Uchiyama, S.; Miyake, K.; Shimizu, T. Structural Basis of CpG and Inhibitory DNA Recognition by Toll-like Receptor 9. *Nature* **2015**, *520* (7549), 702–705. https://doi.org/10.1038/nature14138.

(18) Hanagata, N. Structure-Dependent Immunostimulatory Effect of CpG Oligodeoxynucleotides and Their Delivery System. *Int. J. Nanomedicine* **2012**, *7*, 2181–2195. https://doi.org/10.2147/IJN.S30197.

(19) Bode, C.; Zhao, G.; Steinhagen, F.; Kinjo, T.; Klinman, D. M. CpG DNA as a Vaccine Adjuvant. *Expert Review of Vaccines*. NIH Public Access April 2011, pp 499–511. https://doi.org/10.1586/erv.10.174.

(20) Bhat, P.; Leggatt, G.; Waterhouse, N.; Frazer, I. H. Interferon-γ Derived from Cytotoxic Lymphocytes Directly Enhances Their Motility and Cytotoxicity. *Cell Death Dis.* **2017**, *8* (6), e2836. https://doi.org/10.1038/cddis.2017.67.

(21) Chu, R. S.; Targoni, O. S.; Krieg, A. M.; Lehmann, P. V.; Harding, C. V. CpG Oligodeoxynucleotides Act as Adjuvants That Switch on T Helper 1 (Th1) Immunity. *J. Exp. Med.* **1997**, *186* (10), 1623–1631. https://doi.org/10.1084/jem.186.10.1623.

(22) Mutwiri, G. K.; Nichani, A. K.; Babiuk, S.; Babiuk, L. A. Strategies for Enhancing the Immunostimulatory Effects of CpG Oligodeoxynucleotides. *J. Control. Release* **2004**, *97* (1), 1–17. https://doi.org/10.1016/j.jconrel.2004.02.022.

(23) Hanagata, N. CpG Oligodeoxynucleotide Nanomedicines for the Prophylaxis or Treatment of Cancers, Infectious Diseases, and Allergies. *Int. J. Nanomedicine* **2017**, *12*,

515–531. https://doi.org/10.2147/IJN.S114477.

(24) Dalpke, A. H.; Zimmermann, S.; Albrecht, I.; Heeg, K. Phosphodiester CpG Oligonucleotides as Adjuvants: Polyguanosine Runs Enhance Cellular Uptake and Improve Immunostimulative Activity of Phosphodiester CpG Oligonucleotides in Vitro and in Vivo. *Immunology* **2002**, *106* (1), 102–112. https://doi.org/10.1046/j.1365-2567.2002.01410.x.

(25) Kramer, K.; Young, S. L.; Walker, G. F. Comparative Study of 5′- and 3′-Linked CpG–Antigen Conjugates for the Induction of Cellular Immune Responses. *ACS Omega* **2017**, *2* (1), 227–235. https://doi.org/10.1021/acsomega.6b00368.

(26) Samulowitz, U.; Weber, M.; Weeratna, R.; Uhlmann, E.; Noll, B.; Krieg, A. M.; Vollmer, J. A Novel Class of Immune-Stimulatory Cpg Oligodeoxynucleotides Unifies High Potency in Type i Interferon Induction with Preferred Structural Properties. *Oligonucleotides* **2010**, *20* (2), 93–101. https://doi.org/10.1089/oli.2009.0210.

(27) Mount, A.; Koernig, S.; Silva, A.; Drane, D.; Maraskovsky, E.; Morelli, A. B. Combination of Adjuvants: The Future of Vaccine Design. *Expert Rev. Vaccines* **2013**, *12* (7), 733–746. https://doi.org/10.1586/14760584.2013.811185.

(28) Bode, C.; Zhao, G.; Steinhagen, F.; Kinjo, T.; Klinman, D. M. CpG DNA as a Vaccine Adjuvant. *Expert Review of Vaccines*. NIH Public Access April 2011, pp 499–511. https://doi.org/10.1586/erv.10.174.

(29) Shirota, H.; Klinman, D. M. Recent Progress Concerning CpG DNA and Its Use as a Vaccine Adjuvant. *Expert Rev. Vaccines* **2014**, *13* (2), 299–312. https://doi.org/10.1586/14760584.2014.863715.

(30) Jackson, S.; Lentino, J.; Kopp, J.; Murray, L.; Ellison, W.; Rhee, M.; Shockey, G.; Akella, L.; Erby, K.; Heyward, W. L.; et al. Immunogenicity of a Two-Dose Investigational

Hepatitis B Vaccine, HBsAg-1018, Using a Toll-like Receptor 9 Agonist Adjuvant Compared with a Licensed Hepatitis B Vaccine in Adults. *Vaccine* **2018**, *36* (5), 668–674. https://doi.org/10.1016/j.vaccine.2017.12.038.

(31) Scheiermann, J.; Klinman, D. M. Clinical Evaluation of CpG Oligonucleotides as Adjuvants for Vaccines Targeting Infectious Diseases and Cancer. *Vaccine*. NIH Public Access November 12, 2014, pp 6377–6389. https://doi.org/10.1016/j.vaccine.2014.06.065.

(32) Schmidt, M.; Hagner, N.; Marco, A.; König-Merediz, S. A.; Schroff, M.; Wittig, B. Design and Structural Requirements of the Potent and Safe TLR-9 Agonistic Immunomodulator MGN1703. *Nucleic Acid Ther.* **2015**, *25* (3), 130–140. https://doi.org/10.1089/nat.2015.0533.

(33) Nishikawa, M.; Matono, M.; Rattanakiat, S.; Matsuoka, N.; Takakura, Y. Enhanced Immunostimulatory Activity of Oligodeoxynucleotides by Y-Shape Formation. *Immunology* **2008**, *124* (2), 247–255. https://doi.org/10.1111/j.1365-2567.2007.02762.x.

(34) Rattanakiat, S.; Nishikawa, M.; Funabashi, H.; Luo, D.; Takakura, Y. The Assembly of a Short Linear Natural Cytosine-Phosphate-Guanine DNA into Dendritic Structures and Its Effect on Immunostimulatory Activity. *Biomaterials* **2009**, *30* (29), 5701–5706. https://doi.org/10.1016/j.biomaterials.2009.06.053.

(35) Nishikawa, M.; Matono, M.; Rattanakiat, S.; Matsuoka, N.; Takakura, Y. Enhanced Immunostimulatory Activity of Oligodeoxynucleotides by Y-Shape Formation. *Immunology* **2008**, *124* (2), 247–255. https://doi.org/10.1111/j.1365-2567.2007.02762.x.

(36) Matsuoka, N.; Nishikawa, M.; Mohri, K.; Rattanakiat, S.; Takakura, Y. Structural and Immunostimulatory Properties of Y-Shaped DNA Consisting of Phosphodiester and Phosphorothioate Oligodeoxynucleotides. *J. Control. Release* **2010**, *148* (3), 311–316. https://doi.org/10.1016/j.jconrel.2010.09.019.

(37) Yang, G.; Koo, J. E.; Lee, H. E.; Shin, S. W.; Um, S. H.; Lee, J. Y. Immunostimulatory Activity of Y-Shaped DNA Nanostructures Mediated through the Activation of TLR9. *Biomed. Pharmacother.* **2019**, *112* (August 2018), 108657. https://doi.org/10.1016/j.biopha.2019.108657.

(38) Rattanakiat, S.; Nishikawa, M.; Funabashi, H.; Luo, D.; Takakura, Y. The Assembly of a Short Linear Natural Cytosine-Phosphate-Guanine DNA into Dendritic Structures and Its Effect on Immunostimulatory Activity. *Biomaterials* **2009**, *30* (29), 5701–5706. https://doi.org/10.1016/j.biomaterials.2009.06.053.

(39) Koo, J. E.; Shin, S. W.; Um, S. H.; Lee, J. Y. X-Shaped DNA Potentiates Therapeutic Efficacy in Colitis-Associated Colon Cancer through Dual Activation of TLR9 and Inflammasomes. *Mol. Cancer* **2015**, *14* (1), 1–12. https://doi.org/10.1186/s12943-015-0369-2.

(40) Nishikawa, M.; Mizuno, Y.; Mohri, K.; Matsuoka, N.; Rattanakiat, S.; Takahashi, Y.; Funabashi, H.; Luo, D.; Takakura, Y. Biodegradable CpG DNA Hydrogels for Sustained Delivery of Doxorubicin and Immunostimulatory Signals in Tumor-Bearing Mice. *Biomaterials* **2011**, *32* (2), 488–494. https://doi.org/10.1016/j.biomaterials.2010.09.013.

(41) Mohri, K.; Nishikawa, M.; Takahashi, N.; Shiomi, T.; Matsuoka, N.; Ogawa, K.; Endo, M.; Hidaka, K.; Sugiyama, H.; Takahashi, Y.; et al. Design and Development of Nanosized DNA Assemblies in Polypod-like Structures as Efficient Vehicles for Immunostimulatory Cpg Motifs to Immune Cells. *ACS Nano* **2012**, *6* (7), 5931–5940. https://doi.org/10.1021/nn300727j.

(42) Uno, S.; Nishikawa, M.; Mohri, K.; Umeki, Y.; Matsuzaki, N.; Takahashi, Y.; Fujita, H.; Kadowaki, N.; Takakura, Y. Efficient Delivery of Immunostimulatory DNA to Mouse and Human Immune Cells through the Construction of Polypod-like Structured DNA.

Nanomedicine Nanotechnology, Biol. Med. **2014**, *10* (4), 765–774. https://doi.org/10.1016/j.nano.2013.11.017.

(43) Schmidt, M.; Hagner, N.; Marco, A.; König-Merediz, S. A.; Schroff, M.; Wittig, B. Design and Structural Requirements of the Potent and Safe TLR-9 Agonistic Immunomodulator MGN1703. *Nucleic Acid Ther.* **2015**, *25* (3), 130–140. https://doi.org/10.1089/nat.2015.0533.

(44) Goodman, R. P.; Berry, R. M.; Turberfield, A. J. The Single-Step Synthesis of a DNA Tetrahedron. *Chem. Commun. (Camb).* **2004**, *44* (April), 1372–1373. https://doi.org/10.1039/b402293a.

(45) Li, J.; Pei, H.; Zhu, B.; Liang, L.; Wei, M.; He, Y.; Chen, N.; Li, D.; Huang, Q.; Fan, C. Self-Assembled Multivalent DNA Nanostructures for Noninvasive Intracellular Delivery of Immunostimulatory CpG Oligonucleotides. *ACS Nano* **2011**, *5* (11), 8783–8789. https://doi.org/10.1021/nn202774x.

(46) Koo, J. E.; Shin, S. W.; Um, S. H.; Lee, J. Y. X-Shaped DNA Potentiates Therapeutic Efficacy in Colitis-Associated Colon Cancer through Dual Activation of TLR9 and Inflammasomes. *Mol. Cancer* **2015**, *14* (1), 1–12. https://doi.org/10.1186/s12943-015-0369-2.

(47) Chu, B. C. F.; Orgel, L. E. The Stability of Different Forms of Double-Stranded Decoy DNA in Serum and Nuclear Extracts. *Nucleic Acids Res.* **1992**, *20* (21), 5857–5858. https://doi.org/10.1093/nar/20.21.5857.

(48) Spiegel, J.; Adhikari, S.; Balasubramanian, S. The Structure and Function of DNA G-Quadruplexes. *Trends Chem.* **2020**, *2* (2), 123–136. https://doi.org/10.1016/j.trechm.2019.07.002.

(49) Sun, Z. Y.; Wang, X. N.; Cheng, S. Q.; Su, X. X.; Ou, T. M. Developing Novel G-

Quadruplex Ligands: From Interaction with Nucleic Acids to Interfering with Nucleic Acid–Protein Interaction. *Molecules* **2019**, *24* (3), 396. https://doi.org/10.3390/molecules24030396.

(50) Baumann, P. *G-Quadruplex DNA*; Baumann, P., Ed.; Methods in Molecular Biology; Humana Press: Totowa, NJ, 2010; Vol. 608. https://doi.org/10.1007/978-1-59745-363-9.

(51) Kwok, C. K.; Merrick, C. J. G-Quadruplexes: Prediction, Characterization, and Biological Application. *Trends Biotechnol.* **2017**, *35* (10), 997–1013. https://doi.org/10.1016/j.tibtech.2017.06.012.

(52) Bochman, M. L.; Paeschke, K.; Zakian, V. A. DNA Secondary Structures: Stability and Function of G-Quadruplex Structures. *Nat. Rev. Genet.* **2012**, *13* (11), 770–780. https://doi.org/10.1038/nrg3296.

(53) Largy, E.; Marchand, A.; Amrane, S.; Gabelica, V.; Mergny, J. L. Quadruplex Turncoats: Cation-Dependent Folding and Stability of Quadruplex-DNA Double Switches. *J. Am. Chem. Soc.* **2016**, *138* (8), 2780–2792. https://doi.org/10.1021/jacs.5b13130.

(54) Smirnov, I.; Shafer, R. H. Effect of Loop Sequence and Size on DNA Aptamer Stability. *Biochemistry* **2000**, *39* (6), 1462–1468. https://doi.org/10.1021/bi9919044.

(55) Guédin, A.; Gros, J.; Alberti, P.; Mergny, J. L. How Long Is Too Long? Effects of Loop Size on G-Quadruplex Stability. *Nucleic Acids Res.* **2010**, *38* (21), 7858–7868. https://doi.org/10.1093/nar/gkq639.

(56) Cheng, M.; Cheng, Y.; Hao, J.; Jia, G.; Zhou, J.; Mergny, J. L.; Li, C. Loop Permutation Affects the Topology and Stability of G-Quadruplexes. *Nucleic Acids Res.* **2018**, *46* (18), 9264–9275. https://doi.org/10.1093/nar/gky757.

(57) Vorlíčková, M.; Kejnovská, I.; Sagi, J.; Renčiuk, D.; Bednářová, K.; Motlová, J.; Kypr, J.

Circular Dichroism and Guanine Quadruplexes. *Methods* **2012**, *57* (1), 64–75. https://doi.org/10.1016/j.ymeth.2012.03.011.

(58) Yang, D.; Okamoto, K. Structural Insights into G-Quadruplexes: Towards New Anticancer Drugs. *Future Med. Chem.* **2010**, *2* (4), 619–646. https://doi.org/10.4155/fmc.09.172.

(59) Zahler, A. M.; Williamson, J. R.; Cech, T. R.; Prescott, D. M. Inhibition of Telomerase by G-Quartet DNA Structures. *Nature* **1991**, *350* (6320), 718–720. https://doi.org/10.1038/350718a0.

(60) Rhodes, D.; Lipps, H. J. Survey and Summary G-Quadruplexes and Their Regulatory Roles in Biology. *Nucleic Acids Research*. October 15, 2015, pp 8627–8637. https://doi.org/10.1093/nar/gkv862.

(61) Yuwei Chen and Danzhou Yang. Sequence, Stability, Structure of G-Quadruplexes and Their Drug Interactions. *Curr Protoc Nucleic Acid Chem* **2012**, *23* (1), 1–7. https://doi.org/10.1002/0471142700.nc1705s50.

(62) Zhu, Q.; Liu, G.; Kai, M.; Miller, A. O. A. DNA Aptamers in the Diagnosis and Treatment of Human Diseases. *Molecules* **2015**, *20* (12), 20979–90997. https://doi.org/10.3390/molecules201219739.

(63) Platella, C.; Riccardi, C.; Montesarchio, D.; Roviello, G. N.; Musumeci, D. G-Quadruplex-Based Aptamers against Protein Targets in Therapy and Diagnostics. *Biochim. Biophys. Acta - Gen. Subj.* **2017**, *1861* (5), 1429–1447. https://doi.org/10.1016/j.bbagen.2016.11.027.

(64) Carolina Roxo, W. K. and A. P. G-Quadruplex-Forming Aptamers—Characteristics, Applications, and Perspectives. *Molecules* **2019**, *24* (20), 3781. https://doi.org/https://doi.org/10.3390/molecules24203781.

(65) Lane, A. N.; Chaires, J. B.; Gray, R. D.; Trent, J. O. Stability and Kinetics of G-Quadruplex Structures. *Nucleic Acids Res.* **2008**, *36* (17), 5482–5515. https://doi.org/10.1093/nar/gkn517.

(66) Hanagata, N. Structure-Dependent Immunostimulatory Effect of CpG Oligodeoxynucleotides and Their Delivery System. *Int. J. Nanomedicine* **2012**, *7*, 2181–2195. https://doi.org/10.2147/IJN.S30197.

(67) Chu, B. C. F.; Orgel, L. E. The Stability of Different Forms of Double-Stranded Decoy DNA in Serum and Nuclear Extracts. *Nucleic Acids Res.* **1992**, *20* (21), 5857–5858. https://doi.org/10.1093/nar/20.21.5857.

(68) Hoshi, K.; Yamazaki, T.; Sugiyama, Y.; Tsukakoshi, K.; Tsugawa, W.; Sode, K.; Ikebukuro, K. G-Quadruplex Structure Improves the Immunostimulatory Effects of CpG Oligonucleotides. *Nucleic Acid Ther.* **2019**, *29* (4), 224–229. https://doi.org/10.1089/nat.2018.0761.

(69) Mergny, J. L.; Lacroix, L. UV Melting of G-Quadruplexes. *Curr. Protoc. Nucleic Acid Chem.* **2009**, No. SUPPL. 37, 1–15. https://doi.org/10.1002/0471142700.nc1701s37.

(70) Bugaut, A.; Alberti, P. Understanding the Stability of DNA G-Quadruplex Units in Long Human Telomeric Strands. *Biochimie* **2015**, *113*, 125–133. https://doi.org/10.1016/j.biochi.2015.04.003.

(71) Pohar, J.; Lainšček, D.; Ivičak-Kocjan, K.; Cajnko, M.-M. M.; Jerala, R.; Benčina, M. Short Single-Stranded DNA Degradation Products Augment the Activation of Toll-like Receptor 9. *Nat. Commun.* **2017**, *8* (May), 15363. https://doi.org/10.1038/ncomms15363.

(72) Mergny, J. L.; Li, J.; Lacroix, L.; Amrane, S.; Chaires, J. B. Thermal Difference Spectra: A Specific Signature for Nucleic Acid Structures. *Nucleic Acids Res.* **2005**, *33* (16), 1–6. https://doi.org/10.1093/nar/gni134.

(73) del Villar-Guerra, R.; Trent, J. O.; Chaires, J. B. G-Quadruplex Secondary Structure Obtained from Circular Dichroism Spectroscopy. *Angew. Chemie - Int. Ed.* **2018**, *57* (24), 7171–7175. https://doi.org/10.1002/anie.201709184.

(74) Li, Q. J.; Tong, X. J.; Duan, Y. M.; Zhou, J. Q. Characterization of the Intramolecular G-Quadruplex Promoting Activity of Est1. *FEBS Lett.* **2013**, *587* (6), 659–665. https://doi.org/10.1016/j.febslet.2013.01.024.

(75) Burge, S.; Parkinson, G. N.; Hazel, P.; Todd, A. K.; Neidle, S. Quadruplex DNA: Sequence, Topology and Structure. *Nucleic Acids Res.* **2006**, *34* (19), 5402–5415. https://doi.org/10.1093/nar/gkl655.

(76) Gibbs, S.; Miller, A. DNA Quadruplex Folding Formalism – A Tutorial on Quadruplex Topologies. *Methods* **2013**, *64* (1), 28–35. https://doi.org/10.1080/13540602.2013.844408.

(77) Zhang, A. Y. Q.; Bugaut, A.; Balasubramanian, S. A Sequence-Independent Analysis of the Loop Length Dependence of Intramolecular RNA G-Quadruplex Stability and Topology. *Biochemistry* **2011**, *50* (33), 7251–7258. https://doi.org/10.1021/bi200805j.

(78) Mergny, J. L.; Phan, A. T.; Lacroix, L. Following G-Quartet Formation by UV-Spectroscopy. *FEBS Lett.* **1998**, *435* (1), 74–78. https://doi.org/10.1016/S0014-5793(98)01043-6.

(79) Dapić, V.; Abdomerović, V.; Marrington, R.; Peberdy, J.; Rodger, A.; Trent, J. O.; Bates, P. J. Biophysical and Biological Properties of Quadruplex Oligodeoxyribonucleotides. *Nucleic Acids Res.* **2003**, *31* (8), 2097–2107. https://doi.org/10.1093/nar/gkg316.

(80) Xiong, J.; Zhu, M. X.; Biology, R. Regulation of Lysosomal Ion Homeostatsis by Channels and Transporters. *Sci China Life Sci.* **2016**, *59* (8), 777–791. https://doi.org/10.1007/s11427-016-5090-x.Regulation.

(81) Scott, C. C.; Gruenberg, J. Ion Flux and the Function of Endosomes and Lysosomes: PH Is Just the Start: The Flux of Ions across Endosomal Membranes Influences Endosome Function Not Only through Regulation of the Luminal PH. *BioEssays* **2011**, *33* (2), 103–110. https://doi.org/10.1002/bies.201000108.

(82) Hu, Y. B.; Dammer, E. B.; Ren, R. J.; Wang, G. The Endosomal-Lysosomal System: From Acidification and Cargo Sorting to Neurodegeneration. *Transl. Neurodegener.* **2015**, *4* (1), 1–10. https://doi.org/10.1186/s40035-015-0041-1.

(83) Lodish H, Berk A, Zipursky SL, et al. Intracellular Ion Environment and Membrane Electric Potential. In *Molecular Cell Biology*; 2000.

(84) Chang, T.; Qi, C.; Meng, J.; Zhang, N.; Bing, T.; Yang, X.; Cao, Z.; Shangguan, D. General Cell-Binding Activity of Intramolecular G-Quadruplexes with Parallel Structure. *PLoS One* **2013**, *8* (4), 1–10. https://doi.org/10.1371/journal.pone.0062348.

(85) Minari, J.; Mochizuki, S.; Matsuzaki, T.; Adachi, Y.; Ohno, N.; Sakurai, K. Enhanced Cytokine Secretion from Primary Macrophages Due to Dectin-1 Mediated Uptake of CpG DNA/??-1,3-Glucan Complex. *Bioconjug. Chem.* **2011**, *22* (1), 9–15. https://doi.org/10.1021/bc1001196.

(86) Ivanov, S.; Dragoi, A.-M.; Wang, X.; Dallacosta, C.; Louten, J.; Musco, G.; Sitia, G.; Yap, G. S.; Wan, Y.; Biron, C. A.; et al. A Novel Role for HMGB1 in TLR9-Mediated Inflammatory Responses to CpG-DNA. *Blood* **2007**, *110* (6), 1970–1981. https://doi.org/10.1182/blood-2006-09-044776.

(87) Cornélie, S.; Hoebeke, J.; Schacht, A. M.; Bertin, B.; Vicogne, J.; Capron, M.; Riveau, G. Direct Evidence That Toll-like Receptor 9 (TLR9) Functionally Binds Plasmid DNA by Specific Cytosine-Phosphate-Guanine Motif Recognition. *J. Biol. Chem.* **2004**, *279* (15), 15124–15129. https://doi.org/10.1074/jbc.M313406200.

(88) Ishida, H.; Ohto, U.; Shibata, T.; Miyake, K.; Shimizu, T. Structural Basis for Species-specific Activation of Mouse Toll-like Receptor 9. *FEBS Lett.* **2018**, *592* (15), 2636–2646. https://doi.org/10.1002/1873-3468.13176.

(89) Chu, R. S.; Targoni, O. S.; Krieg, A. M.; Lehmann, P. V; Harding, C. V. CpG Oligodeoxynucleotides Act as Adjuvants That Switch on T Helper 1 (Th1) Immunity. *J. Exp. Med.* **1997**, *186* (10), 1623–1631.

(90) Mitchell, W. A.; Aspinall, R. *The Immune System*, fourth ed.; Garland Science: New York, 2015.

(91) Mohri, K.; Nagata, K.; Ohtsuki, S.; Toyama, S.; Nonomura, M.; Takahashi, Y.; Takakura, Y.; Nishikawa, M.; Sakuma, S. Elucidation of the Mechanism of Increased Activity of Immunostimulatory DNA by the Formation of Polypod-like Structure. *Pharm. Res.* **2017**, *34* (11), 2362–2370. https://doi.org/10.1007/s11095-017-2243-y.

(92) Cheng, M.; Cheng, Y.; Hao, J.; Jia, G.; Zhou, J.; Mergny, J. L.; Li, C. Loop Permutation Affects the Topology and Stability of G-Quadruplexes. *Nucleic Acids Res.* **2018**, *46* (18), 9264–9275. https://doi.org/10.1093/nar/gky757.

(93) Ohto, U.; Shibata, T.; Tanji, H.; Ishida, H.; Krayukhina, E.; Uchiyama, S.; Miyake, K.; Shimizu, T. Structural Basis of CpG and Inhibitory DNA Recognition by Toll-like Receptor 9. *Nature* **2015**, *520* (7549), 702–705. https://doi.org/10.1038/nature14138.

(94) Sanada, Y.; Shiomi, T.; Okobira, T.; Tan, M.; Nishikawa, M.; Akiba, I.; Takakura, Y.; Sakurai, K. Polypod-Shaped DNAs: Small-Angle X-Ray Scattering and Immunostimulatory Activity. *Langmuir* **2016**, *32* (15), 3760–3765. https://doi.org/10.1021/acs.langmuir.6b00398.

(95) Klinman, D. M.; Currie, D. Hierarchical Recognition of CpG Motifs Expressed by Immunostimulatory Oligodeoxynucleotides. *Clin. Exp. Immunol.* **2003**, *133* (2), 227–232.

https://doi.org/10.1046/j.1365-2249.2003.02216.x.

(96) Meng, W.; Yamazaki, T.; Nishida, Y.; Hanagata, N. Nuclease-Resistant Immunostimulatory Phosphodiester CpG Oligodeoxynucleotides as Human Toll-like Receptor 9 Agonists. *BMC Biotechnol.* **2011**, *11* (1), 88. https://doi.org/10.1186/1472-6750-11-88.

(97) Largy, E.; Marchand, A.; Amrane, S.; Gabelica, V.; Mergny, J. L. Quadruplex Turncoats: Cation-Dependent Folding and Stability of Quadruplex-DNA Double Switches. *J. Am. Chem. Soc.* **2016**, *138* (8), 2780–2792. https://doi.org/10.1021/jacs.5b13130.

(98) Tera, M.; Ishizuka, H.; Takagi, M.; Suganuma, M.; Shin-Ya, K.; Nagasawa, K. Macrocyclic Hexaoxazoles as Sequence- and Mode-Selective G-Quadruplex Binders. *Angew. Chemie - Int. Ed.* **2008**, *47* (30), 5557–5560. https://doi.org/10.1002/anie.200801235.

(99) Ma, Y.; Tsushima, Y.; Sakuma, M.; Sasaki, S.; Iida, K.; Okabe, S.; Seimiya, H.; Hirokawa, T.; Nagasawa, K. Development of G-Quadruplex Ligands for Selective Induction of a Parallel-Type Topology. *Org. Biomol. Chem.* **2018**, *16* (40), 7375–7382. https://doi.org/10.1039/C8OB01702F.

(100) Tsukakoshi, K.; Ikuta, Y.; Abe, K.; Yoshida, W.; Iida, K.; Ma, Y.; Nagasawa, K.; Sode, K.; Ikebukuro, K. Structural Regulation by a G-Quadruplex Ligand Increases Binding Abilities of G-Quadruplex-Forming Aptamers. *Chem. Commun.* **2016**, *52* (85), 12646–12649. https://doi.org/10.1039/c6cc07552e.

(101) Koirala, D.; Dhakal, S.; Ashbridge, B.; Sannohe, Y.; Rodriguez, R.; Sugiyama, H.; Balasubramanian, S.; Mao, H. A Single-Molecule Platform for Investigation of Interactions between G-Quadruplexes and Small-Molecule Ligands. *Nat. Chem.* **2011**, *3* (10), 782–787. https://doi.org/10.1038/nchem.1126.

(102) O'Hagan, M. P.; Morales, J. C.; Galan, M. C. Binding and Beyond: What Else Can G-Quadruplex Ligands Do? *European J. Org. Chem.* **2019**, *2019* (31–32), 4995–5017. https://doi.org/10.1002/ejoc.201900692.

(103) Mergny, J. L.; Lacroix, L. UV Melting of G-Quadruplexes. *Curr. Protoc. Nucleic Acid Chem.* **2009**, No. SUPPL. 37, 1–15. https://doi.org/10.1002/0471142700.nc1701s37.

(104) Tera, M.; Ishizuka, H.; Takagi, M.; Suganuma, M.; Shin-Ya, K.; Nagasawa, K. Macrocyclic Hexaoxazoles as Sequence- and Mode-Selective G-Quadruplex Binders. *Angew. Chemie - Int. Ed.* **2008**, *47* (30), 5557–5560. https://doi.org/10.1002/anie.200801235.

(105) Mikhalkevich, N.; Becknell, B.; Caligiuri, M. A.; Bates, M. D.; Harvey, R.; Zheng, W. Responsiveness of Naive CD4 T Cells to Polarizing Cytokine Determines the Ratio of Th1 and Th2 Cell Differentiation. *J. Immunol.* **2006**, *176* (3), 1553–1560. https://doi.org/10.4049/jimmunol.176.3.1553.

(106) Spellberg, B.; Edwards, J. E. Type 1/Type 2 Immunity in Infectious Diseases. *Clin. Infect. Dis.* **2002**, *32* (1), 76–102. https://doi.org/10.1086/317537.

(107) Munir Akkaya, Billur Akkaya, Patrick W. Sheehan, Pietro Miozzo, Mirna Pena, Chen-Feng Qi, Javier Manzella-Lapeira, Silvia Bolland, and S. K. P. Immunization with a T Cell-Dependent Protein Antigen Adjuvanted with DOTAP-CpG-B but Not DOTAP-CpG-A Induces Robust Germinal Center Responses and High Affinity Antibodies. *Eur J Immunol.* **2017**, *47* (11), 1890–1899. https://doi.org/10.1002/eji.201747113.

(108) Yasuda, K.; Yu, P.; Kirschning, C. J.; Schlatter, B.; Schmitz, F.; Heit, A.; Bauer, S.; Hochrein, H.; Wagner, H. Endosomal Translocation of Vertebrate DNA Activates Dendritic Cells via TLR9-Dependent and -Independent Pathways. *J. Immunol.* **2005**, *174* (10), 6129–6136. https://doi.org/10.4049/jimmunol.174.10.6129.

(109) Akkaya, M.; Akkaya, B.; Miozzo, P.; Rawat, M.; Pena, M.; Sheehan, P. W.; Kim, A. S.; Kamenyeva, O.; Kabat, J.; Bolland, S.; et al. B Cells Produce Type 1 IFNs in Response to the TLR9 Agonist CpG-A Conjugated to Cationic Lipids. *J. Immunol.* **2017**, *199* (3), 931–940. https://doi.org/10.4049/jimmunol.1700348.

(110) Umar, M. I.; Ji, D.; Chan, C. Y.; Kwok, C. K. *G-Quadruplex-Based Fluorescent Turn-on Ligands and Aptamers: From Development to Applications*; 2019; Vol. 24. https://doi.org/10.3390/molecules24132416.

(111) Henault, M.; Lee, L. N.; Evans, G. F.; Zuckerman, S. H. The Human Burkitt Lymphoma Cell Line Namalwa Represents a Homogenous Cell System Characterized by High Levels of Toll-like Receptor 9 and Activation by CpG Oligonucleotides. *J. Immunol. Methods* **2005**, *300* (1–2), 93–99. https://doi.org/10.1016/j.jim.2005.02.012.

(112) Van Belle, K.; Herman, J.; Boon, L.; Waer, M.; Sprangers, B.; Louat, T. Comparative In Vitro Immune Stimulation Analysis of Primary Human B Cells and B Cell Lines. *J. Immunol. Res.* **2016**, *2016*, 5281823. https://doi.org/10.1155/2016/5281823.

(113) Narita, M.; Watanabe, N.; Yamahira, A.; Hashimoto, S.; Tochiki, N.; Saitoh, A.; Kaji, M.; Nakamura, T.; Furukawa, T.; Toba, K.; et al. A Leukemic Plasmacytoid Dendritic Cell Line, PMDC05, with the Ability to Secrete IFN-α by Stimulation via Toll-like Receptors and Present Antigens to Naïve T Cells. *Leuk. Res.* **2009**, *33* (9), 1224–1232. https://doi.org/10.1016/j.leukres.2009.03.047.

(114) C.R., K. Peripheral Blood Mononuclear Cells. In *The Impact of Food Bioactives on Health*; Al., V. K. et, Ed.; Springer, Cham, 2015; pp 161–167. https://doi.org/https://doi.org/10.1007/978-3-319-16104-4_15.

(115) Rothenfusser, S.; Tuma, E.; Endres, S.; Hartmann, G. Plasmacytoid Dendritic Cells: The Key to CpG. *Hum. Immunol.* **2002**, *63* (12), 1111–1119. https://doi.org/10.1016/S0198-

8859(02)00749-8.

(116) Guiducci, C.; Ott, G.; Chan, J. H.; Damon, E.; Calacsan, C.; Matray, T.; Lee, K.-D.; Coffman, R. L.; Barrat, F. J. Properties Regulating the Nature of the Plasmacytoid Dendritic Cell Response to Toll-like Receptor 9 Activation. *J. Exp. Med.* **2006**, *203* (8), 1999–2008. https://doi.org/10.1084/jem.20060401.